creative commons
COMMONS DEED

저작자표시-비영리-변경금지 2.0 대한민국

이용자는 아래의 조건을 따르는 경우에 한하여 자유롭게

- 이 저작물을 복제, 배포, 전송, 전시, 공연 및 방송할 수 있습니다.

다음과 같은 조건을 따라야 합니다:

저작자표시. 귀하는 원저작자를 표시하여야 합니다.

비영리. 귀하는 이 저작물을 영리 목적으로 이용할 수 없습니다.

변경금지. 귀하는 이 저작물을 개작, 변형 또는 가공할 수 없습니다.

- 귀하는, 이 저작물의 재이용이나 배포의 경우, 이 저작물에 적용된 이용허락조건을 명확하게 나타내어야 합니다.
- 저작권자로부터 별도의 허가를 받으면 이러한 조건들은 적용되지 않습니다.

저작권법에 따른 이용자의 권리는 위의 내용에 의하여 영향을 받지 않습니다.

이것은 이용허락규약(Legal Code)을 이해하기 쉽게 요약한 것입니다.

Disclaimer

dCollection

치의과학박사 학위논문

Effects of pentoxifylline on the protein expression of macrophage and the bone healing in an osteoradionecrosis rat model

펜톡시필린의 대식세포에서 단백질 발현 양상과 백서 방사선골괴사증 모델에서 골 치유에 대한 효과

2019년 2월

서울대학교 대학원

치의과학과 구강악안면외과학 전공

서 미 현

Effects of pentoxifylline on the protein expression of macrophage and the bone healing in an osteoradionecrosis rat model

지도교수 김 성 민

이 논문을 치의과학박사 학위논문으로 제출함

2018년 11월

서울대학교 대학원

치의과학과 구강악안면외과학 전공

서 미 현

서미현의 박사학위논문을 인준함

2019년 1월

위 원 장 이 종 호 (인)

부위원장 김 성 민 (인)

위 원 명 훈 (인)

위 원 양 형 철 (인)

위 원 이 석 근 (인)

Abstract

Effects of pentoxifylline on the protein expression of macrophage and the bone healing in an osteoradionecrosis rat model

Mi Hyun Seo

Program in Oral and Maxillofacial Surgery, Department of Dental Science, Graduate School, Seoul National University

(Directed by Professor Soung Min Kim)

Background and purpose

Radiation therapy has long been an established treatment modality for the head and neck cancer. Osteoradionecrosis (ORN) of the jaws is one of the serious complications of radiotherapy. Since the radiation-induced fibrosis theory was introduced, pentoxifylline (PTX) have been used to treat or prevent of ORN. The purpose of this study was to investigate the effects of PTX through both *in vivo* animal experiment using rat ORN model and *in vitro* experiment using RAW 264. 7 cells.

Materials and methods

1. Protein expression profiles in macrophage treated with PTX

To understand the cellular effects of PTX, protein expression in PTX-treated RAW 264.7 cells was analyzed by using immunoprecipitation high performance liquid chromatography (IP-HPLC).

2. Animal study: the effects of PTX on the bone healing in a rat ORN model

A total of 48 Sprague-Dawley rats were used in this experimental animal study: 40 received a single irradiation dose of 35 Gy on the left mandible, and eight were used as the nonirradiated control group. The rats were treated with pentoxifylline (T1, C1), tocopherol (T2, C2), a combination of pentoxifylline and tocopherol (T3, C3), or normal saline (T4, C4). Three weeks after irradiation, the mandibular posterior teeth were extracted. The drugs were administered daily from the irradiation to the end of study. The rats were sacrificed at 4 weeks after extraction, and were evaluated clinically, and using micro-CT, histology, immunohistochemistry, and quantitative reverse transcription PCR (RT-qPCR). Statistical analyses were performed using SPSS 25.0® (SPSS Inc., Chicago, IL, USA). The Kruskal-Wallis test was performed, and the Mann-Whitney U test was used for post-hoc testing. $p < 0.05$ was considered to indicate statistical significance.

Results

1. Protein expression profiles in macrophage treated with PTX

RAW 264.7 cells treated with PTX for 12, 24, 48 hours showed gradual increases in the expressions of immunity-, and osteogenesis-related proteins and concurrent decreases in the expressions of proliferation-, matrix inflammation-, cellular apoptosis-related proteins.

2. Animal study: the effects of PTX on the bone healing in a rat ORN model

The areas of skin alopecia and intraoral bony exposure and the changes in body weight showed no statistically significant differences among the experimental groups. In the laboratory analysis, statistically significant differences were observed seven weeks after irradiation: WBC, neutrophil count, lymphocyte count, monocyte count, and the neutrophil to lymphocyte ratio differed significantly between test groups. The T4 control group had lower hemoglobin values than the other groups ($p < 0.05$). In the micro-CT analysis, significant differences between experimental groups occurred in the bone volume/tissue volume ratio, trabecular number, trabecular spaces, and bone mineral density ($p < 0.05$). In the histological observation, T3 group which received both PTX and tocopherol showed the most prominent bone remodeling and viable osteocytes in significantly higher number than the other groups ($p < 0.05$). In the immunohistochemical staining, the expression of TNF-α was lower in the T3 group (PTX and tocopherol) than in the control (T4) and tocopherol alone (T2) groups. In the RT-qPCR, mRNA expressions of PECAM, VEGF-A, osteocalcin were increased in the group treated with PTX and tocopherol (T3).

Conclusions

IP-HPLC results indicate that PTX plays wound healing roles by regulating cellular proliferation-, immunity-, anti-inflammation-, apoptosis-, and osteogenesis-related proteins in RAW 264.7 cells. In animal studies, PTX has been shown to promote bone healing when combined with tocopherol. These data suggest that PTX is effective in the treatment of ORN when combined with tocopherol.

……..

Keywords: Osteoradionecrosis (ORN), Pentoxifylline (PTX), Immunoprecipitation-high performance liquid chromatography (IP-HPLC)

Student Number: 2011-31179

Contents

I. Introduction

Radiation therapy is an established treatment modality in the management of malignant disease in the head and neck area. Radiotherapy targets all cells with a high turnover rate, whether malignant or normal tissue (1). Tolerance of radiation is site specific, and is modified by volume, fraction size, total dose, and possibly by dose rate. The ideal radiation treatment would deliver the total dose within the tumor in healthy tissue. Most patients treated with radiation will develop some degree of fibrosis of atrophy in the irradiated normal tissue. This varies in clinical significance depending on site, dose, and individual tolerance. Fibrosis predominates in breast, skin, small bowel, lung, kidney, and liver. Atrophy and necrosis can occur following radiation and surgery and local trauma to bone, nerve, and brain (2). The term osteoradionecrosis (ORN) indicates radiation-induced bone death, histologically defined as empty bone lacunae resulting from osteocyte death (3). Diagnosis of ORN is based on clinical signs of mucosal ulceration with exposure of necrotic bone, without healing for 3-6 months. The ORN can be clinically defined by 1) exposed bone for at least 2 to 6 months, 2) a history of radiation therapy (RT) on the region of exposed bone, 3) the presence of necrotic or devitalized bone, and 4) no evidence of tumor recurrence. The incidence of ORN varies from 5% to 15%, with over 70% of the cases occurring within the first 3 years after RT (4). The time elapsed between the exposure to RT and the evidence of ORN differs significantly across the literature. There are clinical reports in which ORN developed after short periods of a few months (range, 3-7 months) and others only after many years (range, 38-45 years) (5).

Most patients with oropharyngeal cancer, treated with curative intent, receive a total does between 50 and 70 Gy. Acute effects are observed during

or within a few weeks after treatment. Consequential effects are defined as persistent acute damage, late effects are defined as persistent acute damage. ORN is a serious late complication of radiation therapy and has been defined as a condition in which irradiated bone becomes devascularized and exposed through the overlying skin or mucosa, persistent without healing for at least 3 months (6).

Radiation related risk factors of ORN have been identified, total dose, photon energy, brachytherapy, field size, and fractionation are included (7). Intensity-modulated radiotherapy (IMRT) is used to deliver precise radiation dose to the tumor and areas within the tumor, as a result, minimizing the dose delivered to surrounding normal tissues. IMRT has resulted in a decrease in incidence and severity of ORN (8). A radiation dose higher than 60 Gy represents the higher risk for developing ORN, and it is more common when brachytherapy is used (1, 9, 10). Dental extractions performed before and after irradiation can increase the risk of ORN, and chemotherapy combined with radiotherapy can also increase the risk of ORN (10).

The purpose of this study was to investigate the effects of pentoxifylline (PTX) on the ORN of the jaw. To evaluate cellular effects of PTX on RAW 264.7 cells, the expressions of different proteins were analyzed using immunoprecipitation-high performance liquid chromatography (IP-HPLC). In animal study, we used a rat ORN model to evaluate the effects of PTX.

II. Review of literature

II-1. Osteoradionecrosis (ORN)

II-1.1. Pathophysiology of ORN

The pathophysiology of ORN has been a controversial. Regaude first described the pathophysiology of ORN in 1922, Meyer (11) defined the classic triad in the pathophysiology of ORN as radiation, trauma, and infection. He proposed that trauma, such as tooth removal, provided access for oral bacteria to enter the underlying bone, and the infection could then rapidly progress because the radiated bone had lost its resistance to bacterial infection. This process then resulted in radiation osteomyelitis.

In 1983, Marx (12) changed Meyer`s theory, based on the observation that ORN did not have the clinical signs of infection, nor did it progress to sepsis in the same way osteomyelitis can, and occurred in cases without trauma. He studied 26 cases of ORN and noted bacteria to only be on the surface of the bone and not in the necrotic area, indicating that microorganisms played a very minor role in the pathophysiology. The histologic findings noted by Marx showed fibrosis of the mucosa, skin, and marrow space; hyalinization and thrombosis of vessels with loss of osteocytes and osteoblasts; and decreased vascularity of the connective tissue. He proposed the hypoxic-hypocellular-hypovascular theory, describing a 4-part sequence of: (1) radiation; (2) formation of hypoxic-hypovascular-hypocellular tissue; (3) tissue breakdown whereby collagen lysis and cellular death exceeds the synthesis and cellular replication; and (4) chronic nonhealing wounds in which energy, oxygen, and structural precursor demand exceeds supply (13). Marx observed that ORN is

not a primary infection of the irradiated bone but that metabolic and homeostatic tissue alterations cause cell death as a result of persistent hypoxia and chronic injury. The theory developed by Marx is currently the most widely accepted. However, the importance of hypoxia in tissues affected by ORN has not been proven (14).

Recent advances in cellular and microbiology have allowed for new fibroatrophic theory. The fibroatrophic theory supposes that the bony changes that brings about these processes are similar to those that occur when other forms of physical injury affect tissues such as lungs and liver. There are three distinct phases. The first is a prefibrotic phase in which changes in endothelial cells predominate with an acute inflammatory response. The second is a constitutive organized phase in which abnormal fibroblastic activity predominates and there is disorganization of the extracellular matrix. During the third, the late fibroatrophic phase, attempts at tissue remodeling result in the formation of fragile healed tissues that carry a serious inherent risk of late reactivated inflammation in the event of local injury, which in bone can result in necrosis (15, 16). The molecular mechanism of radiation fibrosis has features in common with the normal wound healing response (17). In the final remodeling phase, cells either undergo apoptosis or exit the wound and this phase becomes less active with time. In radiation fibrosis, the process is dysregulated and has been linked to “a wound that does not heal (18).”

II-1.2. Staging

Several staging or scoring systems of ORN have been proposed. These systems are based on response to hyperbaric oxygen (HBO) therapy, degree of bone damage, clinical-radiological findings, duration of bone exposure and

treatment required. Coffin (19) divided cases of ORN into major and minor groups. Morton and Simpson (20) subdivided ORN into three groups – 'minor', 'moderate' and 'major'. In 1983, Marx (12) proposed a three-stage system for ORN. According to his protocol, patients are categorized as stage I if they exhibit exposed bone in a field of radiation that has failed to heal for at least 6 months and do not have a pathological fracture, cutaneous fistula or osteolysis to the inferior border. In stage I if they exhibit exposed bone in a field of radiation that has failed to heal for at least 6 months and do not have a pathological fracture, cutaneous fistula or osteolysis to the inferior border. In stage I, all patients receive 30 sessions of HBO at 2.4 atmospheres absolute for 90 minutes. Patients who respond to HBO alone demonstrate a softening of the radiated tissue and spontaneous sequestration of exposed bone with formation of granulation tissue. Stage II patients are those who do not respond to the 30 sessions of HBO. This group is characterized by a large amount of non-viable bone that makes resorption and sequestration from HBO-induced angiogenesis alone impossible. Consequently, careful surgical debridement is required. Stage III patients are characterized by having a large quantity of non-viable bone and/or soft tissue unable to be managed by HBO-induced angiogenesis alone or HBO combined with local sequestrectomy. These patients require resection, stabilization and 10 postoperative sessions of HBO, and are scheduled for later reconstruction.

Glanzmann and Gratz (21) proposed a system based on the duration of bone exposure and necessity of treatment. Clayman (22) introduced a classification of ORN related to the integrity of the overlying mucosa. According to this classification, type I includes cases of ORN in which bone lysis occurs under intact gingiva or mucosa. Type II includes more aggressive

cases of ORN in which soft tissues breakdown and the bone is exposed to saliva, causing secondary contamination. The systems of Schwartz and Kagan (23) is based on clinical and radiological findings. Notani et al. (24) divided the cases into three grades based on the extent of the ORN lesion. Grade I is defined as ORN confined to the alveolar bone. Grade II is defined as ORN limited to the alveolar bone and/or the mandible above the level of the mandibular alveolar canal. In grade III the ORN extends to the mandible under the level of the mandibular alveolar canal and a skin fistula and/or a pathological fracture is present.

II-2. Pentoxifylline (PTX)

PTX [1-(5-oxohexyl)-3,7-dimethylxanthine] (Fig.2.1) is a methylxanthine derivatives developed and indicated for use against symptoms associated with impaired microcirculation (25). The closest methylated xanthines include caffeine, theophylline and aminophylline, which have been discovered in plants and have several similar pharmacological actions (26). PTX improves blood perfusion through multiple processes. PTX is a non-selective inhibitor of cyclic nucleotide phosphodiesterases (PDEs), that inhibits cyclic adenosine monophosphate (cAMP) PDEs, increasing cAMP and adenosine-5′-triphosphate in erythrocytes and increasing red blood cell deformability. The PDEs are large group of enzymes consisting of at least nine groups of isoenzymes (PDE1 through PDE9) encoded by distinctive genes and expressed in various tissues in a tissue-specific manner. The primary enzymatic action of PDEs is the degradation of the intracellular second messengers cyclic AMP and/or cyclic guanosine monophosphate (GMP), which are generated by activated adenylyl cyclases or guanylyl cyclases responding to the binding of

ligands to specific receptors on cytoplasmic membrane. PTX reduces leukocyte adhesion to endothelial cells, increases production of prostacyclin, and inhibits platelets aggregation. These effects lead to capillary dilatation, to reduce blood viscosity and increase peripheral blood flow (27).

II-2.1. Anti-inflammatory effect of PTX

Recently, attention has been paid to the possibility of treating PTX as an immunomodulatory, anti-inflammatory and antitumor agent. PTX has been shown to down-regulate the production of proinflammatory cytokines, particularly tumor necrosis factor-α (TNF-α). PTX inhibits TNF-α synthesis by blocking transcriptional activity (28). In a study of radiation-induced lung injury in mice model, TNF-α mRNA and protein production were significantly reduced in the PTX-treated group (29). Zein et al. (30) conducted a placebo-controlled randomized clinical trial with 55 patients with biopsy-proven nonalcoholic steatoheapatitis (NASH) to determine the effects of PTX. After 1 year, PTX significantly improved steatosis, lobular inflammation and liver fibrosis in comparison with placebo. In a study of neonatal sepsis, PTX inhibited the production of inflammatory cytokines by microorganisms, particularly when used in combination with antimicrobial agents (31). In a randomized controlled trial including 120 newborns with late onset sepsis and mean gestational age of 30 weeks, PTX administration reduced TNF-α and C-reactive protein (CRP) levels, shorter duration of respiratory support and antibiotic treatment, shorter hospital stay, lower incidence of disseminated intravascular coagulopathy, metabolic acidosis, and thrombocytopenia (32). However, there was no differences in mortality and short-term morbidity between PTX treated and untreated newborn sepsis (32-34).

II-2.2. Anti-fibrotic effect of PTX

PTX inhibits the proliferation of human dermal fibroblasts and the production of extracellular matrix (35, 36), and increases collagenase activity (37). PTX has been shown to reduce fibrosis caused by external stress such as irradiation. The mechanisms by which PTX inhibits development of fibrosis, or maybe even reverses fibrosis, are not exactly known. Interestingly, PTX inhibits intracellular signaling in response to transforming growth factor-β (TGF-β), and connective tissue growth factor (CTGF), two growth factors that are considered to play an important role in radiation-induced fibrosis. Lin et al. (38) reported that PTX suppresses CTGF expression as well as the promoter effects of CTGF on kidney cells. However, in the study of the effects of PTX in combination with α-tocopherol on cardiac structure and function after localized fractionated heart irradiation in the rat model, no significant changes were found in TGF-β expression at either the mRNA or protein level (39). In postoperative peritoneal adhesion studies, PTX may reduce intraperitoneal adhesion formation by increasing peritoneal fibrinolysis activity and inhibiting angiogenesis and collagen synthesis (40). In a model of radiation induced lung fibrosis, western analysis revealed PTX treatment reduced expression of plasminogen activator inhibitor-1 (PAI-1) and fibronectin by restoring protein kinase A (PKA) phosphorylation but not TGF-β/Smad in both irradiated lung tissues and epithelial cells (41). Delanian et al. conducted a study involving 22 breast cancer patients with radiation induced fibrosis (RIF); significant surface regression was observed for the combination of PTX and vitamin E (42). In a subsequent study, they reported that long-term treatment with PTX and tocopherol is effective and curative for refractory ORN (43).

Extended-release tablet form of PTX is 400 mg, three times a day with meals. While the effect of PTX may be seen within 2 to 4 weeks, it is recommended that treatment be continued for at least 8 weeks. Dose related central nervous system and digestive tract side effects may occur, if so it is advised to lower the dosage to one tablet bid, 800 mg/day.

II-3. Tocopherol

Vitamin E can be classified into tocopherols and tocotrienols, resulting in a total of eight isoforms: namely α-, β-, γ-, and δ-tocopherols, and α-, β-, γ-, and δ- tocotrienols (Fig. 2.2) (44). Tocopherols are a group of fat soluble organic chemical compounds consisting of various methylated phenols. Each tocopherol consists of chromanol ring and 16-carbone phytyl chain (45). Depending on the number and position of methyl groups on the chromanol ring, tocopherols are designated α, β, γ, and δ (46). The unmethylated carbons at the 5- and 7-positions are electrophilic centers that can effectively trap reactive oxygen and nitrogen species (46). Free radicals attack on cell membrane result in peroxyl radicals and lipid peroxidation which is responsible for hypercholesterolemia and cardiovascular disease (44). Reactive oxygen species (ROS) are generated during the inflammatory reactions induced by radiation injury. If these are not efficiently scavenged, the resulting oxidative stress can lead to cell necrosis or apoptosis. These compounds have potent antioxidant properties that help protect cell membranes against lipid peroxidation. However, the effect of tocopherol supplementation on bone are inconsistent and somehow controversial (47). High doses of α-tocopherol were shown to exert negative effect on bone in normal animals but was protective in stressed animals (48, 49). Fujita et al.

(50) showed that there was increased bone resorption and decreased bone mass in mice fed with high-dose α-tocopherol, probably due to increased osteoclast fusion and differentiation. Combined PTX and vitamin E decreases protein expression of the TGF-β1 target molecule PAI-1 more effectively than either drug alone (51). The combination was more potent than the individual drugs, which is the definition of drug synergy, but the mechanism of action of both is unclear (16).

II-4. Immunoprecipitation-high performance liquid chromatography (IP-HPLC)

IP-HPLC is a type of protein detection methods, that is based on real antigen-antibody reaction in a PBS buffer solution, followed by purification using protein A/G- conjugated agarose beads. Although its procedures are simple and easy to apply to most biological samples, IP-HPLC can yield a minimum error range by using micro-beads instead of small wells to mimic the enzyme-linked immunosorbent assay (ELISA) (52, 53).

IP-HPLC is used to determine protein expression levels versus reference controls. Generally, IP-HPLC is comparable to ELISA; the former uses protein A/G agarose beads in buffer solution and UV spectroscopy to determine whole areas of protein peaks, and the latter uses fluorescence-conjugated antibody fixed in plastic wells and fluoroscopy to measure the highest intensity of fluorescence excitation (52, 54). In IP-HPLC procedures, the mixtures of protein sample and antibody-bound protein A/G agarose beads are incubated in a chaotic state by stirring, and after multiple washes of agarose beads, the target protein is eluted and analyzed by the automatic HPLC system using stable UV spectroscopy (Fig. 2.3). Multiple trials have

shown that IP-HPLC can detect protein expression changes accurately and reproducibly (± 5% standard deviation).

III. Materials and methods

III-1. Protein expression profiles in macrophage treated with PTX

III-1.1. Cell culture

Unstimulated RAW 264.7 cells derived from murine macrophages (ATCC, Manassas, Virginia, USA) were used. Cells were cultured using Dulbecco`s Modified Eagles Medium (WelGene Inc., Korea) with 10% fetal bovine serum (WelGene Inc., Korea), 100 units/ml penicillin, 100 μg/ml streptomycin, 250 ng/ml amphotericin B (WelGene Inc., Korea) in a humidified incubator at 5% CO_2 and 37℃. PTX (10 μg/ml) was added to the media in the test group. Cells were cultured for 12, 24, and 48 hours with PTX.

III-1.2. Protein extraction

After treating RAW 264.7 cell with PTX at 10 μg/ml for 12, 24, and 48 hours, the RAW 264.7 cells were harvested with protein lysis buffer (0.3% SDS, 50 mM Tris-HCl pH 8.0, 0.3% β-mercaptoethanol, 1 mL PMSF, 1 mL EDTA) containing protein inhibitor cocktail (Sigma, USA). Protein extracts were kept in a -70℃ deep freezer until use to prevent further protein degradation (53).

III-1.3. IP-HPLC

For IP-HPLC, 100 μg of each protein extract to the immunoprecipitation procedure using a protein A/G agarose column (Amicogen Co., Korea). The protein A/G agarose columns were separately pre-

incubated with 1 μg of each of the different antisera, including Ki-67, PCNA, CDK4, cMyc, MAX, MAD, MPM2, PLK4, cyclin D2, p14, p16, p21, p27, Rb-1, E2F-1, histone H1, KDM4D, HDAC-10, MBD4, DMAP1, DNMT1, DOHH, DHS, elF5A1, HER1, HER2, TGF-β1, Met, FGF-1, FGF-2, IGF-1, CTGF, ERβ, NRAS, KRAS, HRAS, JNK-1, ERK-1, Rab, pAKT, mTOR, PKC, MEKK, NFκB, IKK, NFATS, p38, GADD-45, GADD-153, MDR, PGC-1α, AP-1, SP-1, SP-3, PLC-β2, TGase-2, HXKII, Jagged-2, Notch-1, GLI-1, p53, MDM2, BAX, caspase 9, BAK, APAF-1, PARP, FASL, FAS, FADD, FLIP, caspase 8, 14-3-3, YAP, HSP-70, HSP-90, SOD-1, LC3, GST, NOS1, AMPK, TERT, TNF-α, IL-1, IL-6, IL-10, IL-28, LTA4H, CXCR4, MMP-1, MMP-2, MMP-3, MMP-9, MMP-10, MMP-12, MCP-1, TLR3, cathepsin K, lysozyme, M-CSF, CD3, CD4, CD20, CD28, CD31, CD 68, COX-2, CRP-1, hepcidin, angiogenin, HIF, ET-1, VEGF-A, VEGF-C, vWF, VCAM, CMG-2, BMP-2, OPG, RANKL, osteopontin, osteonectin, osterix, osteocalcin, ALP, RUNX2, β-actin (Supplement 1).

Briefly, the protein samples were mixed with 5 ml of binding buffer (150 mM NaCl, 10 mM Tris pH 7.4, 1 mM EDTA, 1 mM EGTA, 0.2 mM sodium vanadate, 0.2 mM PMSF, and 0.5% NP-40) and incubated in the protein A/G agarose columns at 10℃ for 3 hours. The columns were placed on a rotary agitator during incubation. Each column was washed with a sufficient amount of PBS solution (pH 7.3, 137 mM NaCl, 2.7 mM KCl, 43 mM Na_2HPO_4-$7H_2O$, and 1.4 mM KH_2PO_4), and then 250 μl of IgG elution buffer (Pierce Co., USA) was added to elute the target protein. The immunoprecipitated proteins were identified by HPLC (1100 Series®, Agilent, USA) using a reverse-phase column and micro-analytical detector system (SG Hightech Co., Korea) processed with a 0.15 M NaCl, 20% acetonitrile solution at a rate of 0.4 mL/min for 30 min

and analyzed via UV spectroscopy at 280 nm. IP-HPLC analysis was performed simultaneously in both the control and experimental groups. The peak area of the antibody (mAU*s) of the sample obtained by HPLC analysis was removed by protein peak area on the negative control (52, 53). The data were then mathematically reduced to the square root value as the unit level for molecular concentration and subsequently compared between the experimental and control groups. All square root values of protein peak areas were graphed according to the protein groups of interest (55).

III-2. Animal study: the effects of PTX on the bone healing in a rat ORN model

III-2-1. Establishment of an ORN rat model

The present study's protocol was reviewed and approved by the Seoul National University Institutional Animal Care and Use Committee (SNU-121123-12-11). A total of 16 Sprague-Dawley male rats aged seven weeks with an average weight of 267.59 g (OrientBio Inc., Seongnam, Korea) were housed in the Laboratory Animal Center of the Korea Institute of Radiological and Medical Sciences with a 12-hour light/dark cycle and were given chow and water ad libitum. The animals were housed for at least seven days prior to being used for this experiment. All of the experimental procedures were carried out in accordance with the "Recommendations for Handling of Laboratory Animals for Biomedical Research" complied by the Committee on the Safety and Ethical Handling Regulations for Laboratory Experiments at Seoul National University and Korea Institute of Radiological and Medical Sciences.

III-2-1.1 Grouping and experimental design

Extractions of teeth were performed under general anesthesia with an intraperitoneal injection of a mixture of Ketamin® (90 mg/kg, ketamine hydrochloride, Yuhan Co., Seoul, Korea) and Rompun® (10 mg/kg, xylazine, Bayer Korea, Seoul, Korea). The surgical procedure proceeded as follows: dermal and oral disinfection was completed with betadine, the mouth was opened, the gingiva around the right first lower molar was detached, and atraumatic extraction of the tooth was performed. Under general anesthesia, the

animals were fixed in the supine position, with all extraction procedures gently performed with dental explorers and root forceps.

One week after the extraction, the extracted region was exposed to a graded single dose of radiation. 16 rats were divided into four groups following radiation doses. A single dose of 14, 16, 18 or 20 Gy were irradiated to the right mandible following experimental group (Table 3.1). A flow-chart of the study design is described in Fig. 3.1.

III-2-1.2. External irradiation

Radiation doses of 14, 16, 18, or 20 Gy were administered once to the right mandible of all experimental animals, with each animal under general anesthesia. We used the X-RAD 320 irradiator® (Precision X-ray Inc., North Branford, USA), which has a 320 kVp orthovoltage energy level with a 450 kV maximum output (tube limited to 320 kV) and 45 maximum mA (Figs. 3.2a, b). The field size was set at 10 × 10 mm^2, focusing on the right mandible, and the dose rate was 2.0 Gy/min.

III-2-1.3. Animal sacrifice and clinical evaluation

In each group, two animals were sacrificed two weeks after irradiation and the others were sacrificed three weeks after irradiation, respectively, via CO_2 inhalation. The occurrence of ORN was investigated during the harvest of the mandible. The harvested mandibles were fixed in 10% formalin for micro-CT analysis. The weight of the rats was assessed in this study. Moreover, the clinical manifestations of irradiation observed on gross pathologic evaluation of rat mandibles before and after irradiation including alopecia of the facial skin, mucosa coverage of the wound, and denuded necrotic bone.

III-2-1.4. Micro-CT analysis

Micro-CT images was taken with the SkyScan 1172® microfocus X-ray system (Bruker, Kontich, Belgium). This device is equipped with a microfocus X-ray tube with a focal spot of 2 mm and produces a cone beam that is detected by a 12-bit, cooled X-ray camera that was a charge-coupled device (CCD) fiber-optically coupled to a scintillator. The resulting images for two-dimensional (2D) and three-dimensional (3D) analyses were square 512 x 512 pixels images. An optimized 3D cone beam reconstruction algorithm with a cluster volumetric reconstruction (Feldkamp algorithm) was used. The scan parameters were 70 kV, 141 μA, 0.5 mm Al filter, and 360° rotations with 0.4° steps. A full 3D image containing the experimental area obtained with image pixel size of 17 μm, resulting in about 900 slices 2D images per specimen (Fig. 3.2c). Image analysis was done with the CTAn 1.8® application (Bruker, Kontich, Belgium), while 3D reconstruction was done with NRecon 1.6.9.8® (Bruker, Kontich, Belgium). Using 3D reconstructed images, regions demonstrating consistent bony necrosis and bone formation were designated as regions of interest (ROIs). Each ROI was defined as a volume of 50 pixels in width by 130 pixels in height by 132 pixels in length. Micro-CT image analysis was done by assessing the volume and quality of bone. Root rests within the ROI were excluded and only bone tissue was assessed. The specific thresholds for mineralized bone were defined by superimposing original segmented images over grayscale images. Equivalent thresholds were applied for every image to divide mineralized bone from the background. Within each ROI, bone mineral density (BMD, g/cm^3), bone volume (BV, mm^2), and bone volume/tissue volume (BV/TV, %) were measured and compared.

III-2-1.5 Histological evaluation

After micro-CT scanning, we resected and decalcified the surgical fields at the mandible using 0.5 M ethylenediaminetetraacetic acid solution (pH 8.0) for three to four days, with replacement of the acid solution done on the second day. The specimens were then dehydrated in 70% ethanol, fixed in 10% formalin-buffered solution, and embedded in paraffin wax (Fig. 3.2c). For histological staining, decalcified paraffin sections were cleaned with xylene for 10 minutes, and 5-μm thick slices were prepared and then stained with both hematoxyline and eosin (H&E) and Masson`s trichrome (MT). The interesting region was designated as that in the level of extraction of the first molar. The slides were examined using a BX41® Light Microscope (Olympus Co., Tokyo, Japan). The numbers of osteoclasts and osteoblasts were counted at a high-power field (HPF) (×200). Three HPFs were examined within the area of the extraction socket and the numbers of osteoclasts and osteoblasts were counted. The mean values were calculated and used in the statistical analysis.

III-2-1.6. Statistics

Statistical analyses were descriptive and done with the SPSS 22.0 program® (SPSS Inc., Chicago, IL, USA). The difference in radiation dose between osteoblast/ HPF and osteoclast/ HPF was analyzed statistically using ANOVA method, and the Bonferroni method was used for post-test. Results were considered statistically significant at $p < 0.05$.

III-2-2. The effects of PTX on the bone healing in a rat ORN model

The study protocol was reviewed and approved by the Seoul National University Institutional Animal Care and Use Committee (SNU-180213-1-1). All procedures were conducted in accordance with the "Recommendations for Handling of Laboratory Animals for Biomedical Research" complied by the Committee on the Safety and Ethical Handling Regulations for Laboratory Experiments at the School of Dentistry, Seoul National University. Forty-eight eight-week-old male Sprague-Dawley rats (Orientbio Inc., Korea; average weight of 369.6g) were used and housed in the Laboratory Animal Center of the Korea Institute of Radiological and Medical Sciences with a 12-hour light/dark cycle and chow and water available ad libitum. The animals were housed in those conditions for at least seven days before being used for this experiment. The rats were classified into 40 irradiated individuals and 8 nonirradiated individuals (control). The 40 irradiated rats were classified as PTX alone (T1), tocopherol alone (T2), PTX, tocopherol combination (T3), and normal saline group (T4). The nonirradiated rats were also classified into four groups according to drug administration (Table 3.2). Four of the irradiated animals died after the external radiation, so they were excluded from this study.

III-2-2.1 External radiation

The external radiation delivery was performed with an X-RAD 320 Irradiator® (Precision X-ray Inc., USA) at the Korea Institute of Radiological and Medical Sciences under general anesthesia. Anesthesia was performed with an intraperitoneal injection of a mixture of Ketamin® (90 mg/kg, ketamine

hydrochloride, Yuhan Co., Korea) and Rompun® (10 mg/kg, xylazine, Bayer Korea, Korea) after an overnight fast. The radiation dose was 35 Gy given in a single dose (dose rate 2.5 Gy/minute). Each animal was positioned on his left side in a window of radiation measuring 2 cm by 1 cm, allowing irradiation of only the mandible (Fig 3.3). Palpation and laser light were used to locate the isocenter.

III-2-2.1. PTX application with surgical procedure

The day after irradiation, drugs were administered according to the experimental protocol. PTX was administered at 50 mg/kg daily, and tocopherol was administered at 40 IU/kg daily by oral gavage. The rats were observed for 7 weeks after radiation and maintained on soft chow and water ad libitum. Tooth extractions were performed three weeks after irradiation under the same general anesthesia protocol used for the irradiation. Surgery was performed by disinfecting the skin and oral cavity with a betadine, then the first and second molar were removed using root forcep and elevator. The animals were sacrificed by CO_2 inhalation seven weeks after irradiation. Each mandible was removed, and intraoral bone exposure was observed. The timeline of this experiment is shown in Fig. 3.4.

III-2-2.2. Evaluations

III-2-2.2.1 Clinical analysis

After irradiation, the face, neck and whole body of the animal were photographed every week. Hair loss and the degree of skin inflammation were observed. The dimension of alopecia was calculated using ImageJ software® (NIH, Bethesda, Maryland, USA) (Fig. 3.5) and the photographs taken at three

weeks. The degree of bone exposure at the extraction site was measured after sacrifice.

III-2-2.2.2. Laboratory analysis

Blood sampling was performed from the tail before irradiation, before extraction (3 weeks after irradiation), and 4 weeks after extraction (7 weeks after irradiation) under general anesthesia. Analytic values were a complete blood count (CBC), neutrophil to lymphocyte ratio (NLR), and C-reactive protein (CRP).

III-2-2.2.3. Micro-CT analysis

Four weeks after extraction, experimental animals were sacrificed, and micro-CT was performed with a SkyScan 1172® (Bruker, Belgium). The resulting images, which were used in two-dimensional (2D) and three-dimensional (3D) analyses, were rectangular 1272 x 1050- pixel images. An optimized 3D cone beam reconstruction algorithm with a cluster volumetric reconstruction (Feldkamp algorithm) was used. The scan parameters were 70 kV, 141 μA, a 0.5 mm Al filter, and a 360° rotation with 0.4° steps. A full 3D image containing the experimental area and surrounding trabecular bone was obtained with a cubic voxel size of 16.94 μm, resulting in about 900 two-dimensional images per specimen. Image analysis was done with a CTAn 1.17® (Bruker, Belgium), and 3D reconstruction was done with NRecon 1.7.3.2® (Bruker, Belgium). Using the reconstructed 3D images, regions demonstrating consistent bony necrosis and bone formation were designated as the regions of interest (ROIs). The ROIs were set in two ways (Fig. 3.6): the first method defined each ROI as the whole inner marrow defect above the mandibular canal and root of the incisor, and the second method defined each ROI as a volume

of 50 pixels in width by 80 pixels in height by 200 pixels in length. Quantity and quality of bone was evaluated by the micro-CT image analysis. Root rests within each ROI were excluded; only bone tissue was assessed. Equivalent thresholds were applied to every image to divide mineralized bone from the background. Within each ROI, bone mineral density (BMD, g/cm^3), tissue volume (TV, mm^3), bone volume (BV, mm^3), percentage bone volume (BV/TV, %), trabecular thickness (Tb. Th., mm), trabecular number (Tb. N., 1/mm), and trabecular separation (Tb. Sp., mm) were measured and compared. The 3D images of mandibular bony defects were reconstructed with CT Vol software® (Bruker, Belgium).

III-2-2.2.4. Histological evaluation

After micro-CT reconstruction, we resected and decalcified the surgical fields at the mandible using 0.5 M ethylene diamine tetra-acetic acid (EDTA) solution (pH 8.0) for 3-4 days, replacing the acid solution on day 2-3. The specimens were then dehydrated in 70% ethanol, fixed in 10% formalin-buffered solution, and embedded in paraffin wax. For histological staining, decalcified paraffin sections were cleaned with xylene for 10 minutes, and 4-μm thick slices were prepared and then stained with both H&E and MT. The slides were examined using a BX41® Light Microscope (Olympus Co., Japan). For the quantitative analysis, viable osteocytes were counted. On a 400x magnification H&E slide, a square of 500 x 500 pixels was set on the inner surface of the alveolar sockets to measure the ratio of empty lacunae to the whole bony lacunae. The other part was measured three times and the average value was used for the statistical analysis (Fig. 3.7).

III-2-2.2.5. Immunohistochemical staining

For immunohistochemical staining, paraffin-embedded tissues were sectioned at 4 μm and collected in serial sections on slide glass. An automated BOND-MAX system® (Leica Microsystems, Mannheim, Germany) was used to for immunohistochemical staining. Briefly, antigen retrieval was performed by boiling the section for 20 minutes in Tris/EDTA (BOND Epitope Retrieval Solution 2, pH 9.0; Leica Biosystems). A peroxidase block was then applied for 10 minutes, and the sections were incubated for 15 minutes at room temperature with anti-alkaline phosphatase (1:100, sc-271431, Santa Cruz), anti-TNF-α (1:100, sc-52746, Santa Cruz), anti-TGF-β1 (1:100, sc-130348, Santa Cruz), anti-IL-6 (1:100, sc-28343, Santa Cruz), anti-osteocalcin (1:300, sc-30044, Santa Cruz), and anti-CD31 (1:100, sc-8306, Santa Cruz). The sections were then incubated for 8 minutes with a post-primary rabbit anti-mouse linker followed by incubation for 8 minutes with anti-rabbit horseradish-peroxidase labeled polymer. After incubation for 10 minutes with mixed DAB Refine, the slides were counterstained with hematoxylin for 5 minutes (BOND Polymer Refine Detention Kit; Leica Biosystems), dehydrated, cleared, and mounted. The slides were examined using a BX41® Light Microscope (Olympus Co., Japan). Quantitative analyses using IHC profiler software were performed for TNF-α, TGF-β1, IL-6, and CD31.

III-2-2.2.6. Quantitative reverse transcription-PCR (RT-qPCR)

Two animals in each experimental group were selected for the RT-qPCR analysis. Before studying the irradiated sample, RT-qPCR was performed on mandibular samples taken 0, 2, and 4 weeks after the extraction

of two molars on the left side of the mandible. The samples were acquired after sacrifice, and the resected mandible, including the extraction socket, were used for RNA extraction. Total RNA was extracted by adding 1 ml of Trizol™ Reagent (Thermo Fisher Scientific Co., Waltham, MA, USA) to the homogenized tissues. The RNA concentration was determined with a Nanodrop™ 2000 (Thermo Fisher Scientific, Inc., USA). The concentration and purity of the RNA was determined by measuring the absorbance of RNA at 230, 260, and 280 nm. The cDNA was synthesized from the total RNA with a reverse transcription kit (PrimeScripts™ RT reagent kit, Takara Korea Biomedical Inc., Seoul, Korea). qPCR was performed on a 7500 Real-Time PCR System (Applied Biosystems™, Carlsbad, CA, USA) with a SYBR® Premix Ex Taq™ kit (Takara Korea Biomedical Inc., Korea) according to the manufacturer's instructions. The primers used for the qPCR are listed in Table 3.3. The thermocycling conditions were as follows: initial denaturation at 95℃ for 30 seconds, annealing and extension for 40 cycles at 95℃ for 5 seconds, and 60℃ for 30 seconds, and a final dissociation stage at 95℃ for 15 seconds, 60℃ for 1 minute, and 95℃ for 15 seconds. Each mRNA expression was normalized against glyceraldehyde-3-phosphate dehydrogenase (GAPDH) mRNA expression.

III-2-2.2.7. Statistical analysis

All data are presented as the mean ± standard deviation for each group. Statistical analyses were performed using IBM SPSS software version 25® (SPSS Inc., Chicago, IL, USA). We performed the Kruskal-Wallis test, and used the Mann-Whitney U test for post-hoc testing. $p < 0.05$ was considered

statistically significant. Bonferroni correction was used to modify the alpha level.

IV. Results

IV-1. Protein expression profiles in macrophage treated with PTX

IV-1.1. Effects of PTX on the expression of proliferation-related proteins in macrophage

Cyclin dependent kinase 4 (CDK4) expression was reduced to 92.32% of baseline in 24-hour PTX-treated RAW 264.7 cells and elevated back to 99.91% of baseline in the 48-hour-treated sample. The expression level of Ki-67 was decreased to 92.0% of baseline in the 12-hour-treated sample and increased with time to 105.2%. RAW 264.7 cells treated with PTX demonstrated significantly lower expression of mitotic protein monoclonal 2 (MPM2, 93.9%), proliferation-inhibiting proteins, p21 (90.2%), p27 (90.9%), cyclin D2 (88.7%) than untreated controls. The expression levels of proliferating cell nuclear antigen (PCNA), polo-like kinase 4 (PLK4), p14, and p16 were measured to be within ± 5% in response to PTX, which was similar to control housekeeping protein; β-actin (Fig. 4.1a). These results suggest that PTX inhibits the proliferation of RAW 264.7 cells.

IV-1.2. Effects of PTX on the expression of cMyc/MAX/MAD signaling proteins in macrophage

PTX-treated RAW 264.7 cells showed slightly increased expression of V-Myc myelocytomatosis viral oncogene homolog (cMyc, 106.4%) and Myc-associated factor X (MAX, 108.8%) in samples treated for 24 hours. The

expression level of MAD (105.7%) also increased slight after treatment for 12 hours. These results suggested that PTX slightly enhanced cMyc/MAX signaling and participated in transcriptional control in RAW 264.7 cells (Fig. 4.1b).

IV-1.3. Effects of PTX on the expression of p53/Rb/E2F signaling proteins in macrophage

RAW 264.7 cells treated with PTX were found to express p53 (86.4%), retinoblastoma-1 (Rb-1, 91.7%), E2F-1 (88.3%), mouse double minute 2 homolog (MDM2, 85.1%), CDK4 (92.3%), and p21 (90.2%). These results indicate that PTX inhibits p53/Rb/E2F signaling leading to cellular proliferation (Fig. 4.1c).

IV-1.4. Effects of PTX on the expression of epigenetic modification-related proteins in macrophage

RAW 264.7 cells treated with PTX showed slightly increased expression of histone H1 (108.6%) and methyl-CpG-binding domain protein 4 (MBD4, 111.0%), but no significant change in the expression of lysine-specific demethylase 4D (KDM4D, 95.1-103.6%). RAW 264.7 cells treated with PTX demonstrated decreases in the expression of DNA methyltransferase 1-associated protein 1 (DMAP1, 88.0%), DNA (cytosine-5)-methyltransferase 1 (DNMT1, 94.5%), and histone deacetylase 10 (HDAC-10, 94.9%). These results suggested that PTX may reduce DNA methylation and activate DNA transcription in RAW 264.7 cells. Therefore, PTX can be associated with epigenetic modifications and regulation of gene expressions. MBD4 may function to mediate the biological consequences of the methylation signal.

MBD4 is similar in protein sequence to bacterial DNA repair enzymes, and it has been shown to perform some function in DNA repair (Fig. 4.2a).

IV-1.5. Effects of PTX on the expression of translation-related proteins in macrophage

RAW 264.7 cells treated with PTX slightly reduced expression of eukaryotic translation initiation factor 5A1 (eIF5A1, 92.5%) compared with untreated controls. The expression levels of deoxyhypusine synthase (DHS, 95%) and deoxyhypusine hydroxylase (DOHH, 95.2%) changed less than ± 5%, which is similar to control protein. Hypusination of lysine residues by DHS and DOHH can affect functions of eIF5A-1 related to translation (56). These results suggest that PTX may reduce the basal protein translation levels for cellular proliferation and other functions (Fig. 4.2b).

IV-1.6. Effects of PTX on the expression of cellular differentiation-related proteins in macrophage

RAW 264.7 cells treated with PTX demonstrated slightly reduced expression levels of the differentiation-related proteins, phosophoinositide phospholipase C (PLC-β2, 88.1%), transglutaminase-2 (TGase-2, 94.6%), hexokinase type II enzyme (HXK II, 92.4%), Jagged-2 (93.8%), and GLI-1 (94.5%). The expression of Notch-1 did not show significant changes remaining similar to those of the housekeeping protein. These findings showed that PTX treatment down-regulates cellular differentiation in RAW264.7 cells (Fig. 4.2c).

IV-1.7. Effects of PTX on the expression of RAS signaling proteins in macrophage

PTX slightly reduced the expressions levels of V-Ki-ras2 Kirsten rat sarcoma viral oncogene homolog (KRAS, 92.0%), neuroblastoma RAS viral oncogene homolog (NRAS, 94.2%), and GTPase HRas (HRAS, 94.3%). MAP kinase kinase kinase (MEKK, 107.6%) expression was increased in the 12-hour-treated group, but it decreased with time to similar to that of house keeping protein. Expression of extracellular signal-regulated protein kinases-1 (ERK-1, 108.9%) increased in the 24-hour-treated group. The expression level of mammalian target of Rapamycin (mTOR, 94.0%) was decreased in the 12-hour-treated sample, while that of pAKT1/2/3 (89.1%) markedly decreased with time. The expression levels of JNK-1, Rab, and protein kinase C (PKC) showed less then ± 5% changes in response to PTX, similar to house keeping protein. RAS signaling appeared to be reduced by PTX in RAW 264.7 cells (Fig. 4.3a).

IV-1.8. Effects of PTX on the expression of NFkB signaling proteins in macrophage

RAW 264.7 cells treated with PTX showed decreases in the expression of nuclear factor kappa-light-chain-enhancer of activated B cells (NFkB) signaling proteins. After PTX treatment, TNF-α, growth arrest and DNA damage 153 (GADD 153) decreased a minimum of ± 5%, but the expression levels of NFkB (84.9%), IκB kinase (IKK, 94.2%), pAKT (89.1%), peroxisome proliferation-activated receptor gamma coactivated 1-α (PGC-1α, 86.2%), and p38 (84.4%) were significantly reduced. RAW 264.7 cells treated with PTX

showed a slight decrease in the expression of multidrug resistance (MDR, 92.4%) and a slight increase in the expression of ERK1 (108.9%). The expression levels of GADD45 were slightly increased (105.0%) in the 12-hour-treated sample; however, levels decreased with time. These results indicated that NFkB signaling was affected by PTX treatment and that the cells were in a stress-free state (Fig. 4.3b).

IV-1.9. Effects of PTX on the expression of growth factor-related proteins in macrophage

RAW 264.7 cells treated with PTX showed slight increases in the expression of insulin-like growth factor 1 (IGF1, 107.2%), human epidermal growth factor receptor 1 (HER1, 107.5%), and HER2 (107.3%). Conversely, the expression levels of fibroblast growth factor 1 (FGF1, 88.8%), FGF2 (91.9%), and estrogen receptor beta (ERβ, 92.8%) decreased in RAW 264.7 cells treated with PTX. The expression of transforming growth factor- β1 (TGF-β1, 96.2-104.4%), connective tissue growth factor (CTGF, 95.2-105.1%), and Met (95.9-104.6%) changed only minimally to less than ± 5%, which was similar to the control housekeeping protein (Fig. 4.3c).

IV-1.10. Effects of PTX on the expression of immunity-related proteins in macrophage

RAW 264.7 cells treated with PTX showed significant increases in the expression of cluster of differentiation 4 (CD4, 112.1%) and CD20 (106.4%). The expression levels of CD31 and CD68 showed minimal changes of less than ± 5%, which was similar to that of the housekeeping proteins. The expression levels of CD3 and CD28 after treatment were 87.4% and 91.6%, respectively.

These results indicate that PTX can affect immunity-related proteins and, in turn, inhibit the T-cell associated immunity (Fig. 4.4a, b).

IV-1.11. Effects of PTX on the expression of inflammation-related proteins in macrophage

PTX-treated RAW 264.7 cells demonstrated a decrease in interleukin-6 (IL-6, 92.4%) and IL-1 (88.9%). IL-28 (97.7-105.9%) showed no significant change. IL-10, also known as human cytokine synthesis inhibitory factor, is an anti-inflammatory cytokine. The expression level of IL-10 was significantly increased to 123.5% by PTX treatment. The matrix metalloproteases (MMPs) expression levels after PTX treatment varied; MMP-1, MMP-2, MMP-3, and MMP-9 were increased to 108.4%, 109.1%, 117.0%, and 117.0%, respectively, while MMP-10 revealed a minimal change less than ± 5%, and MMP-12 decreased in the 12-hour-treated sample to 93.9%. The expression levels of leukotriene-A4 hydrolase (LTA4H), C-X-C chemokine receptor type 4 (CXCR4), macrophage-colony stimulating factor (M-CSF), monocyte chemoattractant protein-1 (MCP-1), hepcidin, and cathepsin K were dramatically reduced by PTX to 91.2%, 82.3%, 87.7%, 93.8%, 94.2%, and 92.7%, respectively, but TNF-α and Toll like receptor 3 (TOR3) showed minimal changes less than ± 5%. The expression level of cyclooxygenase (COX-2, 91.0%) was reduced by PTX; however, that of CRP-1 was slightly increased in the 12-hour-treated sample (109.9%), which decreased to 101.4% with time. These results suggest that PTX down-regulates LTA4H, CXCR4, interleukins, and matrix metalloproteases and induces anti-inflammatory signaling in RAW 264.7 cells without affecting the expression of TNF-α (Fig. 4.4a, b).

IV-1.12. Effects of PTX on the expression of p53-mediated apoptosis-related proteins in macrophage

PTX treatment on RAW 264.7 cells significantly reduced p53 expression (86.4%) with a concurrent decreased in MDM2 expression (85.1%), poly (ADP-ribose) polymerase (PARP, 92.2%), but it increased p53-mediated apoptosis-related proteins, such as BCL2-associated X (BAX, 111.1%) and apoptotic protease-activating factor 1 (APAF-1, 106.3%). The expression levels of BCL-2 homologous antagonist killer (BAK, 96.6%) and caspase 9 (97.5%) proteins showed slight decreases with time, but they were similar to housekeeping protein within 5%. These results suggested that PTX significantly inhibited p53 but did not show any significant changes in down-regulated proteins (Fig. 4.5a).

IV-1.13. Effects of PTX on the expression of FAS-mediated apoptosis-related proteins in macrophage

RAW 264.7 cells treated with PTX demonstrated decreased expression of FAS ligand (FASL, 90.9%), FAS-associated via death domain (FADD, 84.8%), and FLICE inhibitory protein (FLIP, 88.7%). Caspase 8 expression levels were consistently down-regulated by PTX to 89.0% of baseline. The expression of FAS (95.6%) showed only a slight change, but it was within 5% to the control housekeeping protein. The expression of poly-ADP ribose polymerase (PARP) was slightly decreased to 92.2% by PTX. These results suggested that PTX tends to inhibit FAS-mediated cell death in RAW 264.7 cells (Fig. 4.5b).

IV-1.14. Effects of PTX on the expression of cell protection-related proteins in macrophage

RAW 264.7 cells treated with PTX demonstrated significant induction of some kinds of cytoprotective protein: HSP-70 (110.2%), activating protein-1 (AP-1, 111.3%), specificity protein 1 (SP-1, 113.4%), and PKC (105.1%). The expression levels of HSP-90 (93.2%) slightly decreased in 24-hour-treated cells; however, they were increased in the samples treated for 48 hours. In the PTX treatment group, p38 (84.4% in the 12-hour-treated sample), pAKT (89.1%), telomerase reverse transcriptase (TERT, 93.7%), and SP-3 (88.9%) were significantly decreased. JNK-1 showed minimal changes less than ± 5% after PTX treatment (Fig. 4.6a). These finding suggested that the cytoprotective effect increased up to 12 hours but was down-regulated as time progressed.

IV-1.15. Effects of PTX on the expression of antioxidant-related proteins in macrophage

RAW 264.7 cells treated with PTX displayed a slight increase in AMP-activated protein kinase (AMPK, 106.6%) in samples treated for 24 hours. The expression of microtubule-associated protein 1A/1B light chain 3 (LC3, 90.4%) and superoxide dismutase-1 (SOD-1, 89.2%) were decreased in the samples treated for 12 hours and increased with time to 105.6% and 99.3% of baseline, respectively. Glutathione S-transferase (GST, 89.5%) was down-regulated by PTX treatment. However, the expression of NOS1 decreased to 88.0% in the sample treated for 48 hours. These results suggest that PTX inhibits NO synthesis and the action of other antioxidant enzymes (Fig. 4.6b).

IV-1.16. Effects of PTX on the expression of angiogenesis-related proteins in macrophage

The expression of angiogenesis-related proteins such as hypoxia inducible factor (HIF, 108.6%), angiogenin (107.3%), and vascular endothelial growth factor-C (VEGF-C, 107.4%) were increased in the 48-hour-treated sample. MMP-2 (109.2%) was up-regulated in the 24-hour-treated sample; however, it was down-regulated in the 48 hours treated sample. The expression levels of vascular endothelial growth factor-A (VEGF-A), von Willebrand factor (vWF), endothelin-1 (ET-1), CD31, MMP-10, and vascular cell adhesion molecule (VCAM) showed a minimal change within 5%, which was similar to that of the housekeeping protein. Capillary morphogenic protein (CMG2, 85.8%) decreased significantly over time. These findings reveal that PTX had weak angiogenic properties (Fig. 4.6c).

IV-1.17. Effects of PTX on the expression of oncogenic proteins in macrophage

RAW 264.7 cells treated with PTX demonstrated a slight decrease in the expression level of the tumorigenic proteins, telomerase reverse transcriptase (TERT, 93.7%) and 14-3-3 (94.3%) compared with the untreated control groups. The expression of yes-associated protein 1 (YAP, 97.4%) and mTOR (94.0-105.7%) did not show significant changes and were similar to those of the housekeeping protein. These results suggest that PTX treatment did not upregulate tumorigenic protein expression in RAW 264.7 cells (Fig. 4.7a).

IV-1.18. Effects of PTX on the expression of osteogenesis-related proteins in macrophages

RAW 264.7 cells treated with PTX showed slightly increased expression of osteoprotegerin (OPG, 108.4%), osteopontin (115.8%), and osterix (110.5%) compared with untreated controls. The expression level of receptor activator of nuclear factor kappa-B ligand (RANKL) was obviously increased to 117.1% after PTX treatment. The level of expression of cathepsin K was down-regulated to 92.7%, and the level of HSP-90 expression was reduced to 93.2% in the 24-hour-treated sample. The expression levels of bone morphogenic protein-2 (BMP-2), osteonectin, and alkaline phosphatase (ALP) demonstrated a little change similar to the control protein.

These results implied that PTX slightly increased a part of osteogenesis-related proteins in RAW 264.7 cells compared with the untreated control. However, RAW 264.7 cells are a macrophage cell line, which have the potential to become osteoclasts; after PTX treatment, the cells showed a slight osteogenic effect compared with the untreated control. Thus, RAW 264.7 cells treated with PTX may have an effect on bone formation (Fig. 4.7b).

IV-1.19. Effects of PTX on the global protein expressions in macrophage

The results of this *in vitro* study are summarized in Fig. 4.8. PTX was shown to inhibit cellular proliferation, apoptosis, and inflammation in RAW 264.7 cells. Conversely, angiogenesis and antioxidant activity were not significantly affected. Although RAW 264.7 cells are a macrophage cell line, PTX was expected to have an osteogenesis promoting effect, which is expected to provide an advantage in the treatment of inflammatory osteolytic lesion with anti-inflammatory effects (Table 4.1).

IV-2. Animal study: the effects of PTX on the bone healing in a rat ORN model

IV-2-1. Establishment of an ORN rat model

IV-2-1.1 Clinical evaluation of ORN model

In all groups, after a mean follow-up of two weeks, visible radiation-induced side effects such as local alopecia in the right mandible were noticeable. The progression of the skin alopecia was different depending on the irradiation dose; specifically, it could be found two or three weeks after 16 Gy (group 2), 18 Gy (group 3), and 20 Gy (group 4) of irradiation (Fig. 4.9). The length of the hair shaft was short and hair loss was serious. Exposure of the epidermis, erythema, and ulcers were absent. Moreover, there were no differences between presentation two weeks and three weeks after irradiation in the same radiation dosage group. We also detected changes in the body weight of the rats after irradiation (Table 4.2).

IV-2-1.2 Micro CT analysis of ORN model

No significant difference was found between the parameters, such as BV, BV/TV, and BMD depending on the dose of radiation and the time of follow-up. A standardized method of quantification was achieved in all samples. However, BV/TV showed a tendency to decrease with increasing irradiation dose at 2 weeks samples, and BV/TV was slightly lower in 3 weeks than 2 weeks. BMD shows decreased at 20 Gy in the 3 weeks sample. Trabecular spaces were increased at 20 Gy in the 3 weeks sample (Fig. 4.10).

IV-2-1.3. Histologic findings of ORN model

Morphological changes of the right mandible at the coronal level of first molar extraction site were detected. In the H&E staining sections, an increased number of osteoclast and inflammation cells were found at two weeks after 14 Gy irradiation. Additionally, fibrosis could be observed in the same sections at three weeks after 14 Gy irradiation. In group 2 (16 Gy), increased fibrosis was not present at two and three weeks after irradiation and resorption lines with microabscess and dead bone were found (Fig. 4.11).

Either increased osteoclast cells or fibrosis as well as the presence of necrotic bone could be observed in group 3 and 4. Increased fibrosis and decreased bone volume were observed in these two groups at three weeks after irradiation as compared with at two weeks. Histological findings with 18 Gy irradiation showing more dead bone than that seen with 16 Gy dose and the presence of resorption with osteoclast cells. There are numerous osteoclast cells observed in the radionecrotic lesion borderlines (Fig. 4.12). The histological features with 20 Gy irradiation showed the presence of resorption line with osteoclast cells, inflammatory infiltrate and empty osteocyte lacunae (Fig. 4.13). These results may explain the progression of ORN along with that of inflammation, fibrosis, and bone resorption.

There were increases in the number of osteoclasts and fibrosis, decreases in the number of osteoblasts, and the presence of bony space in the radiated samples. Notably, as the radiation dose increased, the number of osteoblasts tended to decrease and the number of osteoclasts tended to increase. There was statistically significant difference in Osteoblast/ HPF between 14 Gy and 18, 20 Gy (p <0.05). There was a significant difference in Osteoclast/ HPF

between 14 Gy and 16, 18 and 20 Gy, and there was a significant difference between 16 and 18 Gy and 20 Gy ($p < 0.05$) (Table 4.3). These results suggest that osteoblast is affected by radiation and that osteoblasts are degraded more than 18 Gy and that bone resorption changes more sensitively to dose changes.

IV-2-2. The effects of PTX on the bone healing in a rat ORN model

IV-2-2.1. Clinical evaluation

After irradiation, weight loss was observed in all experimental groups. The body weight decreased for two weeks after irradiation and recovered at three weeks. After the extraction, three weeks after the irradiation, no significant decrease in the body weight occurred. No statistically significant difference emerged in the body weight changes of the experimental groups ($p > 0.05$) (Fig. 4.14, Table 4.4). Three weeks after irradiation, the area of skin alopecia was quantitatively measured. There were no statistically significant differences between the experimental groups ($p > 0.05$). Seven weeks after irradiation (four weeks after extraction), the area of bone exposed in the oral cavity was measured. There were no statistically significant differences between the experimental groups ($p > 0.05$) (Table 4.5).

IV-2-2.2. Laboratory analysis

Blood analysis was performed before and three and seven weeks after irradiation. Seven weeks after irradiation, the white blood cell (WBC) showed statistically significant differences ($p = 0.025$) between T2 and T1 and between T2 and T4. Hb levels were also significantly different 7 weeks after irradiation ($p = 0.015$). Hb levels in the T4 group, which received normal saline instead of drugs, were lower than those in the other groups. The neutrophil count exhibited statistically significant differences between T2 and T3 ($p = 0.001$) and T2 and T4 ($p = 0.004$). Lymphocyte counts showed significant differences between T1 and T4 ($p = 0.027$). We evaluated the monocyte count and found significant

differences between T1 and T2 (p = 0.029), T2 and T3 (p = 0.007), and T2 and T4 (p = 0.016). Significant differences emerged in the NLR between T1 and T3 (p = 0.003), T1 and T4 (p = 0.027), and T2 and T3 (p = 0.019). There were no statistically significant differences in the eosinophil or basophil counts (Table 4.6, Fig. 4.15). Serum CRP did not change after irradiation or extraction.

IV-2-2.3 Micro- CT analysis

In the reconstructed 3D images, more bone healing was observed in the group that received both PTX and tocopherol (T3) than in the other groups. In the irradiated jaws, bone healing was delayed even four weeks after extraction, and multiple porosity was observed on the surface of the irradiated site. In our quantitative analysis, we evaluated TV, BV, BV/TV, Tb.Th., Tb. N., Tb. Sp., and BMD. For every parameter except Tb. Sp., bone formation in the test groups (T1, T2, T3, T4) was significantly reduced compared to the control groups (C1, C2, C3, C4), which did not receive radiation.

Using the method that defined a whole defect as an ROI, we found significant differences between the irradiation groups in the BT/TV (p = 0.025), Tb. N. (p = 0.021), Tb. Sp. (p = 0.019), and BMD (p = 0.012). In the BV/TV, T3 showed a mean value of 19.62%, indicating higher bone regeneration volume than found in T1, T2, and T4. In T3, the number of trabeculae was higher, and the trabecular space was smaller than in the other radiation groups, indicating that the bone was relatively closed. Also, in T3, the mean BMD was 0.314 g/cm^3, which is higher than that in the other groups (Table 4.7, Fig. 4.16).

Using the method that defined each ROI as a constant condition, we found significant differences in the BV/TV (p = 0.028), Tb.N. (p = 0.008), BMD (p = 0.013). Between groups T1 and T3, we found differences in the

BV/TV, Tb.N., and BMD; between groups T3 and T4, we found a significant difference in only the BMD. We found no significant differences between T2 and T4 (Table 4.8, Fig. 4.17). The method used to define each ROI can influence the experimental results, however, the similar results were obtained from the different method of specifying each ROI.

IV-2-2.4. Histological analysis

The control groups that did not receive radiation therapy showed progressive wound healing and bony replacement with no sequelae of an inflammatory lesion. With the active bony remodeling of the extraction socket, the pharmacological effects of PTX and tocopherol were not significant in the histological observation. Only a small increase in osteophytic new bone deposition was found in rats treated with both PTX and tocopherol (C3) (Fig. 4.18).

On the other hand, the experimental groups that received radiation therapy (35 Gy) showed unhealed extraction sockets filled with fibrous granulation tissue, indicating retarded bony remodeling and a mild inflammatory reaction. The experimental group treated with normal saline as a control (T4) showed granulomatous extraction sockets covered with disorganized blood clots in which the stromal connective tissue contained few collagen fibers indicating active osteolytic bony resorption. The rats treated with PTX (T1) showed marked shrinkage of the extraction socket, with intensive proliferation of capillaries via *de novo* angiogenesis, and the rats treated with tocopherol (T2) showed a small decrease in the number of inflammatory cells in their extraction sockets, which were still covered with disorganized blood clots. The rats treated with both PTX and tocopherol (T3)

showed marked new bone deposition up to the surface of the extraction socket and few inflammatory cell infiltrations. The T3 rats also appeared to have osteoclastic bone resorption followed by osteoblastic bony deposition (Fig. 4.19).

As a quantitative analysis, we counted the viable osteocytes and the number of empty lacunae without cells among all the lacunae within a certain area (Fig. 4.20). The results show a statistically significant difference between T1 and T4 ($p = 0.001$) and T3 and T4 ($p = 0.005$). The ratio of empty lacunae was the highest in the control group T4 ($p = 0.004$).

IV-2-2.5. Immunohistochemical analysis

We found statistically significant differences in the negative percentile of TNF-α expression between T2 and T3 and between T3 and T4; the expression of TNF-α was relatively low in the group taking PTX and tocopherol together (Fig. 4.21). Other inflammatory markers, such as IL-6, TGF-β1, and CD31 (platelet endothelial cell adhesion molecule, PECAM-1) did not show significant differences (Fig. 4.22).

IV-2-2.6. RT-qPCR

In a control experiment, PECAM-1 (CD31), RANKL/OPG, and TNF-α showed decreased mRNA expression over time. On the other hand, osteocalcin showed a tendency to increase over time, indicating that osteogenesis was achieved. After extraction, bone regeneration occurs during the prophase of inflammatory reaction and angiogenesis. Four weeks after tooth extraction in a rat, the extracted socket undergoes bony maturation. Osteoclast activity is likely to depend on the relative balance of the RANKL/OPG ratio.

The RANKL/OPG mRNA expression showed the lowest value four weeks after extraction. This result suggests that osteoclast activity diminished over time (Fig. 4.23).

PECAM-1, VEGF-A, OPG, RANKL, osteocalcin, and TNF-α were evaluated for angiogenesis, inflammation and osteogenesis. In CD31 and VEGF-A, mRNA expressions were increased in the group supplemented with PTX and tocopherol than in the other group. In the TNF-α expression, group with PTX and tocopherol showed lower expression level than the control group, but only PTX and tocopherol group showed higher expression level than the control group. RANKL was lower in the PTX and tocopherol combination groups and osteocalcin also increased in the PTX and tocopherol combination groups (Fig. 4.24)

V. Discussion

Established radiation induced bony damage is known to be irreversible. The reversibility of radiation fibrosis in humans is evidenced by regression of clinical disease after therapeutic intervention. The reversible component of fibrotic disease may be explained by a shift in the process of extracellular matrix remodeling towards degradation (57). Delanian and Lefaix (15) suggested that radiation induced fibrosis could be reversed by antioxidant therapy with PTX, tocopherol, and clodronate. Delanian et al. (58) published a prospective clinical trial of 18 patients diagnosed with mandibular refractory ORN, who had failed to improve after at least two months of conventional treatment. Sixteen of the 18 patients with ORN had complete mucosal healing with a median time to recovery of six months. Delanian et al. (43) developed an impressive regimen (PENTOCLO −PENtoxifylline − TOcopherol − CLOdronate) in a refractory group of 54 patients. The amount of exposed bone was reduced by 42% (2 months), 62% (4 months), 77% (6 months), 92% (12 months), and 96% (18 months). McLeod et al. (59) reported a retrospective study of 12 patients who received PTX and tocopherol with improvement in five patients, no change in five patients, and worsening in two patients. However, three patients whose final score improved after operations despite progression of ORN while on PTX and tocopherol underwent radical resection and reconstruction. In a retrospective study of 71 patients treated for ORN of the mandible, after medical management composed of PTX, tocopherol and doxycycline, the patients who required resection and free flap reconstruction declined from 51% (20/39) to 25% (8/32) (60).

Pathologic osteolytic lesions can be stabilized or gradually worsen and

can often be enlarged to such an extent that management becomes difficult. PTX has been reported to reduce radiation induced fibrosis. The mechanism of inhibiting fibrosis or reversing fibrosis has yet to be elucidated (39). PTX has been shown to enhance microvascular blood flow and reduce platelet aggregation to maintain perfusion in radiated tissue. PTX also down-regulates the production of proinflammatory cytokines, particularly TNF-α, in response to noxious stimuli and inhibits granulocyte-mediated cytotoxicity after TNF-α exposure and provides protection against radiation-induced, cytokine-mediated cellular damage (29). In a study by Delanian et al., two-thirds of patients responded to a maximal response after an average of two years. They recommended that long term treatment of more than three years in the presence of severe radiation induced fibrosis because of the risk of rebound effects (61).

In this study, we performed *in vitro* and animal studies to determine the efficacy of PTX, which was reported to be effective in ORN treatment.

IP-HPLC is used to determine protein expression levels versus reference controls. Generally, IP-HPLC is comparable to ELISA; the former uses protein A/G agarose beads in buffer solution and UV spectroscopy to determine whole area of protein peaks, and the latter uses fluorescence-conjugated antibody fixed plastic wells and fluoroscopy to measure the highest intensity of fluorescence excitation (53, 56, 62). Multiple trials have shown that IP-HPLC can detect protein expression changes accurately and reproducibly (± 5% standard deviation). When the IP-HPLC results were compared with the western blot data of cytoplasmic housekeeping protein (β-actin); the IP-HPLC exhibited a small error range of less than ± 5% that could be analyzed statistically, while the western blot showed a large error range (56).

IP-HPLC was used to analyze the cellular effect of PTX on murine macrophage cell line in this study. PTX seemed to suppress proliferation-related proteins in RAW 264.7 cells. PTX up-regulated cMyc/MAX signaling in 12- and 24-hour samples; however, decreased 48 hours sample and is thought to promote cellular proliferation up to 24 hours and suppress it more. Results of this study suggested that PTX inhibited the p53/Rb/E2F signaling pathway leading to cell proliferation.

PTX reduced expression of KRAS, NRAS, HRAS, and pAKT. The expression of ERK-1 was slightly up-regulated, while JNK-1, Rab, PKC levels were changed less than 5% in response to PTX. These results suggest that PTX slightly reduced RAS signaling compare to non-treated controls.

RAW 264.7 cells treated with PTX showed gradual decreases in the expression of NFkB signaling proteins. The expression of TNF-α was not significantly affected by PTX treatment. This is in contrast to results of previous studies; PTX is known to inhibit the synthesis of TNF-α and other pro-inflammatory cytokines (63). Inhibition of NFκB may be related to the reduction of pro-inflammatory cytokines (64).

RAW 264.7 cells treated with PTX showed slight up-regulation in the expression of IGF1, HER1, and HER2 in growth factor-related proteins expressions. The expression levels of FGF-1 and FGF-2 were significantly reduced after PTX treatment. When PTX was applied to a renal fibroblast cell line, it inhibited the proliferation of the fibroblasts in dose-dependent and time-dependent manners and suppressed FGF-2 synthesis (65). Clinical studies on radiation induced fibrosis have also shown that circulating FGF-2 level were reduced after eight weeks of PTX treatment (66). Tissue hypoxia can induce macrophage infiltration, which is a source of pro-fibrotic mediators, including

TGF-β1(67). In this study, TGF-β1 expression was not significantly affected by treatment with PTX in RAW 264.7 cells.

The expression levels of IL-1, IL-6, CD3, CD28, M-CSF, MCP-1, MMP-10, hepcidin, cathepsin K, LTA4H, CXCR4, and COX-2 were all down-regulated by PTX treatment. In this study, immune-related markers were increased, and matrix inflammation associated markers were decreased.

PTX down-regulated the expression of p53, MDM2, and PARP. However, the expression of BAX was increased at the 12- and 24-hour PTX treatment group and decreased slightly at the 48-hour PTX treatment group to 98.8% of baseline. The expression of BAK was decreased in the 48-hour sample, APAF-1 increase at 24 hours and decrease at 48 hours. The expression of caspase 9 decreased with time; however, the changes were not significant. This result suggests that PTX seems to down-regulate p53, but down-stream proteins associated with the intrinsic apoptotic pathway require further study. PTX also down-regulated FAS-mediated apoptosis-related proteins in RAW 264.7 cells. FASL, FAS, FADD, PARP, and caspase 8 were down-regulated by PTX treatment. PTX inhibited the extrinsic apoptotic pathway, which is in contrast to a previous study that showed that PTX is pro-apoptotic by activating caspases and matrix metalloproteinases (MMPs) and enhancing tumor necrosis factor apoptosis induce ligand (TRAIL) and reducing anti-apoptotic regulator expression (68).

The expression levels of antioxidant related proteins, NOS1, SOD-1, GST, and LC3 were down regulated by PTX in contrast with the control group. This suggests that the antioxidant effect of PTX in RAW 264.7 cells is unclear. Luo et al. (69) studied protective effects of PTX on acute liver injury; the levels of SOD and glutathione (GSH) in liver tissue were elevated by PTX treatment

compared with that of control group. In a study of methotrexate-induced damage in the livers and kidneys of rats, immunostaining of iNOS and TNF-α were decreased in the PTX administered group, while SOD levels decreased in liver tissue. These results are similar to result of our *in vitro* study (70).

The oncogenic protein expressions, TERT and 14-3-3 were down-regulated; PTX did not elevate tumorigenic protein expression in RAW 264.7 cells but actually showed some anti-cancer effects by up-regulating the expression of MBD4, which has some function in DNA repair. PTX not only has anti-tumor activity, it also increases the susceptibility of cancer cells to radiation therapy (71).

RAW 264.7 cells treated with PTX showed slight increases in the expression of OPG, osteopontin, and osterix. The expression of RANKL was markedly up-regulated by PTX treatment, which was not surprising because RAW 264.7 cells are derived from murine macrophages and are likely to differentiate into osteoclasts. Very few studies have been published on PTX and osteogenesis; Horiuchi et al (72, 73), reported that PTX promotes rh-BMP induced bone formation.

The expression levels of angiogenesis-related proteins, VEGF-A, vWF, ET-1, and CD31 did not show significant changes compare with the house keeping proteins. The expression of HIF (108.6%), angiogenin (107.3%), and MMP-2 (109.1%) were slightly elevated by PTX treatment. PTX showed a weak angiogenic effect in RAW 264.7 cells. The effect of PTX on angiogenesis is controversial. In a study of segmental cortical bone defects of the radius in a rat model, PTX appeared to improve angiogenesis (74). Conversely, PTX treatment significantly inhibited angiogenesis in a melanoma model (75).

The results of this study are summarized in Table 4.1. PTX was shown to inhibit cellular proliferation, apoptosis, and inflammation in RAW 264.7 cells. Conversely, angiogenesis and antioxidant activity were not significantly affected. Although RAW 264.7 cells are a macrophage cell line, PTX was expected to have an osteogenesis promoting effect, which is expected to provide an advantage in the treatment of osteonecrosis with anti-inflammatory effects (Fig. 4.8).

Radiation therapy to treat cancer inevitable affect normal tissue. The most sensitive cells to radiation therapy are those that divide rapidly, such as skin, bone marrow and gastrointestinal tract cells (76). By the third week after exposure, erythema is localized to the radiation field and the skin is noticeably red, edematous, with dry and moist desquamation, with loss of keratinized layers and depletion of the basal and stem cell population, scaly, hyper or hypopigmented (77). Late effects include alopecia, pigmentation changes, telangiectasis, atrophy, retraction, fibrosis, and ulceration (78). Hair loss is an effect of acute radiation syndrome (ARS) that is caused by exposure to high dose of ionizing radiation within several months (79). In some studies, PTX has decreased the rate of late radiation reaction, but no proven effect has been observed for acute radiation reactions (80). In the early inflammatory change after irradiation, PTX differentially modulated the expression of different inflammatory markers in the mouse tongue model. The mucoprotective effect of PTX does not appear to be based on modulation of NFκB associated inflammation (81). The pathological features of radiation fibrosis within the stroma include deposition of collagen and other extracellular matrix components, accompanied by appearance of atypical fibroblasts (82). Both

endothelial cell injury and tissue hypoxia after radiation are thought to stimulate the recruitment of inflammatory cells (83).

In this animal study to evaluate effects of PTX on ORN, we focused the radiation beam on a 2 x 1-cm^2- sized surface of the mandible. The prominent activation of osteoclasts and the attenuation of osteoblastic function during ORN result in the rarefying appearance with loss of cortical outlines and trabecular density (84). Mineral bone is not considered to be radiosensitive. The incidence of osteopenia varies between 8% and 23% of irradiated bone, and after single dose of > 20Gy changes in bone mineral content have found (85). In this study, we applied a single dose of 35 Gy and all the radiation groups showed delayed bone healing in the extraction socket compared with the control groups. Impaired bone healing was observed in histological and radiographic findings.

Skin changes were not confined to the irradiated area; hair loss occurred on the opposite side, and systemic erythema also occurred in some animals. We quantitatively measured the dimensions of alopecia. Radiation, the emission or transmission of energy in the form of waves and particles through a material medium, damages the DNA of the various cells in the skin that control cell growth. Alopecia, a common side effects of radiation treatment, is caused by an insufficient supply of nutrients due to the reduction of blood vessels in the dermis layer of skin. We found no statistically significant differences in alopecia between the groups receiving different drugs. Hair loss progressed until three or four weeks after irradiation and then recovered. Hair regrowth was observed seven weeks after irradiation.

Seven weeks after irradiation (four weeks after the tooth extractions), the animals were sacrificed, and the presence of intraoral bony exposure was

observed. Acute inflammatory symptoms such as pus, swelling, and erythema were not observed. The degree of intraoral bone exposure did not differ significantly among the experimental groups.

CBC and CRP analysis were performed before and three and seven weeks after irradiation. CRP did not differ between the experimental groups before or after irradiation. WBC, neutrophil, lymphocyte, and monocyte counts, and hemoglobin all changed over time in each experimental group, as determined by the Friedmann test ($p < 0.05$). We found no statistically significant difference between the experimental groups before and three weeks after irradiation ($p > 0.05$). The WBC, neutrophil count, lymphocyte count, monocyte count, and hemoglobin measurements differed significantly in the CBCs seven weeks after irradiation. In the WBC, significant differences occurred between T1 and T2 and between T2 and T3, with T2 having the lowest counts. In the neutrophil count, the lowest group was T2, and significant differences occurred between T2 and T4 and between T2 and T3. In the lymphocyte count, there was a significant difference between T1 and T4. The NLR differed significantly between T1 and T3, T1 and T4, and T2 and T3. Hb values were lower in the control group than in the PTX or tocopherol groups ($p < 0.05$). Similar to the normal saline control group, inflammatory markers, including WBC, neutrophil count, and NLR were elevated in the PTX and tocopherol combination group.

In the BV/TV in the micro-CT analyses, T3 showed a mean value of 19.62%, indicating higher bone regeneration volume than we found in T1, T2, and T4. In T3, the number of trabeculae was higher, and the trabecular space was smaller than in the other radiation groups, indicating that the bone was relatively closed. Also, in T3, the mean BMD was 0.314 g/cm^3, which is higher

than that in the other groups. When the ROI was defined as a constant condition, significant differences emerged in the BV/TV ($p = 0.028$), Tb. N. ($p = 0.008$), and BMD ($p = 0.013$). Between groups T1 and T3, differences emerged in the BV/TV, Tb. N., and BMD. Between T3 and T4, significant differences occurred in only the BMD. We found no significant differences between T2 and T4. However, osteogenesis in all the radiation groups was reduced compared with the control groups that did not receive radiation, as reflected in all the micro-CT parameter. In immunohistochemical staining, the expression of TNF-α decreased significantly in the group using both PTX and tocopherol compared with the groups given only tocopherol or normal saline. In this study, the expression of antibodies associated with inflammation, such as TNF-α and IL-6, had decreased four weeks after extraction. The angiogenesis marker PECAM did not differ between the experimental groups in the immunohistochemistry.

In the group using PTX and tocopherol, the inflammatory markers in the blood samples were somewhat elevated, but the micro-CT results showed more bone formation than in the other experimental groups. In the PTX only (T1) and tocopherol only (T2) groups, the neutrophil count and NLR were low, and the BV, BV/TV, and BMD were lower than in the PTX and tocopherol group (T3). In our correlation analysis, the inflammatory markers and bone formation did not show a significant relationship ($p > 0.05$). When PTX and tocopherol are used together, a synergistic effect on bone formation can be predicted.

In a study of the effects of maternal LPS exposure on intra-uterine fetal growth and skeletal development, PTX reversed LPS-induced skeletal ossification retardation in the caudal vertebrae, anterior and posterior phalanges, and supraoccipital bone (86). PTX has been shown to enhance bone forming

potential *in vivo* through cyclic adenosine monophosphate in osteoblasts and by enhancing the responsiveness of young mesenchymal cells to BMP-2 and BMP-4 (72, 87). Horiuch et al. studied new bone formation in recombinant human BMP-2 using parathyroid hormone and PTX. Ossicles from the PTX-treated group were significantly larger than those in the control group, with unchanged BMD (72).

Free radicals suppress osteoblast differentiation (87, 88) and facilitate bone resorption by activating osteoclasts (89). Oxidative stress has been suggested to create an imbalance between osteogenesis and bone resorption (89, 90). In a study of rabbit distraction osteogenesis, alpha tocopherol showed favorable effects on the quality of new bone formation in mature bone (91). High levels of alpha tocopherol are reported to decrease bone mass in rodents; however, Tennant et al. exhibited that high intake levels of the vitamin do affect the rat skeleton (92). These results are in contrast with our experimental results. We found that osteogenesis increased when PTX and tocopherol were used, through the rats received PTX or tocopherol alone did not differ significantly from the control group. More viable osteocytes were observed in the PTX and tocopherol could in the histopathological findings. The rats treated with both PTX and tocopherol showed marked new bone deposition up to the surface of the extraction socket and few inflammatory cell infiltrations. They also showed evidence of osteoclastic bone resorption followed by osteoblastic bony deposition.

In the result of qPCR, mRNA expressions of PECAM and VEGF-A were increased in PTX and tocopherol combination groups compared to other groups. Expression of RANKL was decreased in the group treated with PTX and tocopherol, and osteocalcin was increased in comparison with the other

group. expression of PECAM in immunohistochemistry was not different between groups. In the RT-qPCR results, when PTX and tocopherol were used together, there was synergistic effect on bone formation and angiogenesis.

In the animal study, we first considered oral route of administration for PTX and tocopherol. PTX is also licensed for intravenous (IV) administration. Clinically, PTX 50 mg is generally diluted in normal saline, and then the patient is placed on their back, and to receive slow administration over five minutes. However, we excluded IV administration from our experimental procedure. Gel-based PTX topical application was reported in a clinical patch test study in nickel-sensitive patients. Those researchers used 5, 10, and 15% PTX in neutral gel, but those the concentrations might not be sufficiently high to provide an inhibitory effect (93). Another trial used a microemulsion containing PTX as a topical treatment for skin disorders (94). Although topical application of PTX has been reported in the dermatology literature, we ruled out local application for this study because of difficulty in application in applying it to bone, maintaining proper concentration and release control.

The efficacy of PTX appeared within 2-4 weeks, and it is recommended that this drug be used for at least 8 weeks in the clinical situation. Efficacy has been demonstrated in a double-blind trial for 6 months (95). The animal experiment was designed so that the effect of the drug could be obtained by taking the drug for 3 weeks from the day after irradiation and taking it for 4 weeks after the extraction. However, it is not known exactly in this experiment whether PTX has a protective effect of radiation. PTX increased osteogenesis related markers such as OPG, osteopontin, RUNX2, and osterix in RAW 264.7 cells, but *in vivo* study, osteocalcin was expressed lower than control at the mRNA level. In the angiogenesis, there was no significant effect in CD31 in

VEGF expression levels *in vitro* study, but slightly increased at mRNA level compared to control *in vivo* study. In terms of osteogenesis and angiogenesis, it was shown that the use of PTX in combination with tocopherol was more effective than PTX or tocopherol alone.

In this *in vitro* study, PTX inhibited inflammation and cellular apoptosis, and promoted bone healing. However, when using PTX alone, there was no difference in bone healing compared to control group in the rat ORN model. The cellular effect of tocopherol has not been investigated in this study, but it is known to have a strong antioxidant effect. PTX inhibited apoptosis of osteocytes and reduces proinflammatory cytokines when radiation is applied to the jaw. In addition, tocopherol plays a role of complementing PTX by removing free radicals and protect cells from lipid peroxidation. The cytoprotective effect of both drugs is added, and it is thought that the cells with bone forming ability survive from the radiation induced free radical attack and the osteogenesis is increased compared to the control. The mRNA expressions of RANKL was decreased when PTX and tocopherol combined. In addition to osteogenesis, angiogenesis was also increased when PTX and tocopherol used together. The mechanism of this increase should be further investigated. Additional experiments are needed to understand the interaction of the PTX and tocopherol, and more extensive studies are needed. Also, prospective clinical study should be added to know the clinical effect of PTX.

VI. Conclusion

In this study, the effects of the PTX were evaluated *in vitro* and *in vivo* studies. In *in vitro* study using IP-HPLC, we determined that PTX treated RAW 264.7 cells showed decreased expressions of proliferation-, extrinsic apoptosis-, and inflammation-related proteins and increased expressions of osteogenesis-related proteins (Fig. 6.1). The anti-inflammatory effect, anti-apoptotic effect and osteogenesis promoting effect are thought to be helpful in the treatment of osteoradionecrosis.

In the animal study, acute inflammation at the early stage of irradiation was assessed at three weeks after irradiation by degree of skin alopecia or laboratory examination, but there was no difference according to experimental group. The inhibitory effect of PTX on TNF-α was observed in the immunohistochemistry. When the PTX and tocopherol were applied together in the rat ORN model, the bone healing was promoted in the irradiated jaw. In the result of qPCR, the increase in CD31 and VEGF-A levels in the PTX and tocopherol combination groups may suggest a synergistic effect on angiogenesis. However, since the number of samples is small, additional experiments are required.

This study suggests that PTX can be effective in the treatment of ORN of the jaw because it has anti-inflammation, suppression of cellular apoptosis, and promoting effect on the osteogenesis. When PTX was used with tocopherol, it could promote bone healing in a rat ORN model. PTX could be effective for the treatment for ORN, and further prospective clinical study should be performed.

References

1. Nabil S, Samman N. Incidence and prevention of osteoradionecrosis after dental extraction in irradiated patients: a systematic review. Int J Oral Maxillofac Surg. 2011;40(3):229-43.

2. Jacobson G. Pentoxifylline, Vitamin E, and Modification of Radiation-Induced Fibrosis. Oxidative Stress in Cancer Biology and Therapy 2012. p. 357-72.

3. Chan KC, Perschbacher SE, Lam EW, Hope AJ, McNiven A, Atenafu EG, Lee L, Pharoah MJ. Mandibular changes on panoramic imaging after head and neck radiotherapy. Oral Surg Oral Med Oral Pathol Oral Radiol. 2016;121(6):666-72.

4. Vissink A BF, Spijkervet KF, Jansma J, Coppes RP. Prevention and treatment of the consequences of head and neck radiotherapy. Crit Rev Oral Biol Med. 2003;14(3):213-25.

5. Costa DA, Costa TP, Netto EC, Joaquim N, Ventura I, Pratas AC, Winckler P, Silva IP, Pinho AC, Sargento IG, Guerreiro FG, Moreira AR. New perspectives on the conservative management of osteoradionecrosis of the mandible: A literature review. Head Neck. 2016;38(11):1708-16.

6. Chopra S, Kamdar D, Ugur OE, Chen G, Peshek B, Marunick M, Kim H, Lin HS, Jacobs J. Factors predictive of severity of osteoradionecrosis of the mandible. Head Neck. 2011;33(11):1600-5.

7. Madrid C, Abarca M, Bouferrache K. Osteoradionecrosis: an update. Oral Oncol. 2010;46(6):471-4.

8. Gevorgyan A WK, Poon I, Blanas N, Enepekides DJ, Higgins KM. Osteoradionecrosis of the mandible - a case series at a single institution. J Otolaryngol Head Neck Surg. 2013;42:1-7.

9. Rivero JA, Shamji O, Kolokythas A. Osteoradionecrosis: a review of pathophysiology, prevention and pharmacologic management using pentoxifylline, alpha-tocopherol, and clodronate. Oral Surg Oral Med Oral Pathol Oral Radiol. 2017;124(5):464-71.

10. Jacobson AS, Buchbinder D, Hu K, Urken ML. Paradigm shifts in the management of osteoradionecrosis of the mandible. Oral Oncol. 2010;46(11):795-801.

11. Meyer I. Infectious diseases of the jaws. J Oral Surg. 1970;28(1):17-26.

12. Marx RE. Osteoradionecrosis: a new concept of its pathophysiology. J Oral Maxillofac Surg. 1983;41(5):283-8.

13. O'Dell K, Sinha U. Osteoradionecrosis. Oral Maxillofac Surg Clin North Am. 2011;23(3):455-64.

14. Jegoux F, Malard O, Goyenvalle E, Aguado E, Daculsi G. Radiation effects on bone healing and reconstruction: interpretation of the literature. Oral Surg Oral Med Oral Pathol Oral Radiol Endod. 2010;109(2):173-84.

15. Delanian S, Lefaix JL. The radiation-induced fibroatrophic process: therapeutic perspective via the antioxidant pathway. Radiother Oncol. 2004;73(2):119-31.

16. Lyons AJ, Brennan PA. Pentoxifylline - a review of its use in osteoradionecrosis. Br J Oral Maxillofac Surg. 2017;55(3):230-4.

17. Wynn TA. Fibrotic disease and the T(H)1/T(H)2 paradigm. Nat Rev Immunol. 2004;4(8):583-94.

18. Martin M, Lefaix J, Delanian S. TGF-beta1 and radiation fibrosis: a master switch and a specific therapeutic target? Int J Radiat Oncol Biol Phys. 2000;47(2):277-90.

19. Coffin F. The incidence and management of osteoradionecrosis of the jaws following head and neck radiotherapy. Br J Radiol. 1983;56(671):851-7.

20. Morton ME, Simpson W. The management of osteoradionecrosis of the jaws. Br J Oral Maxillofac Surg. 1986;24(5):332-41.
21. Glanzmann C, Gratz KW. Radionecrosis of the mandibula: a retrospective analysis of the incidence and risk factors. Radiother Oncol. 1995;36(2):94-100.
22. Clayman L. Clinical controversies in oral and maxillofacial surgery: Part two. Management of dental extractions in irradiated jaws: a protocol without hyperbaric oxygen therapy. J Oral Maxillofac Surg. 1997;55(3):275-81.
23. Schwartz HC, Kagan AR. Osteoradionecrosis of the mandible: scientific basis for clinical staging. Am J Clin Oncol. 2002;25(2):168-71.
24. Notani K, Yamazaki Y, Kitada H, Sakakibara N, Fukuda H, Omori K, Nakamura M. Management of mandibular osteoradionecrosis corresponding to the severity of osteoradionecrosis and the method of radiotherapy. Head Neck. 2003;25(3):181-6.
25. Ward A CS. Pentoxifylline. a review of its pharmacodynamic and pharmacokinetic properties, and its therapeutic efficacy. Drugs. 1987;34:50-97.
26. Zhang M, Xu YJ, Mengi SA, Arneja AS, Dhalla NS. Therapeutic potentials of pentoxifylline for treatment of cardiovascular diseases. Exp Clin Cardiol. 2004;9(2):103-11.
27. Magnusson M, Gunnarsson M, Berntorp E, Bjorkman S, Hoglund P. Effects of pentoxifylline and its metabolites on platelet aggregation in whole blood from healthy humans. Eur J Pharmacol. 2008;581(3):290-5.
28. Neuner P KG, Schauder E, Pourmojib M, Macheiner W, Grunwald C, Knobler R, Schwartz A, Luger TA, Schwarz T. Pentoxifylline in vivo down-regulates the release of IL-1 beta, IL-6, IL-8 and tumour necrosis factor-alpha by human peripheral blood mononuclear cells. Immunology. 1994;83(2):262-7.
29. Rube CE, Wilfert F, Uthe D, Schmid KW, Knoop R, Willich N, Schuck A, Rübe C. Modulation of radiation-induced tumour necrosis factor alpha (TNF-

alpha) expression in the lung tissue by pentoxifylline. Radiother Oncol. 2002;64(2):177-87.

30. Zein CO, Yerian LM, Gogate P, Lopez R, Kirwan JP, Feldstein AE, McCullough AJ. Pentoxifylline improves nonalcoholic steatohepatitis: a randomized placebo-controlled trial. Hepatology. 2011;54(5):1610-9.

31. Speer EM, Diago-Navarro E, Ozog LS, Dowling DJ, Hou W, Raheel M, Fries BC, Levy O. Pentoxifylline alone or in combination with gentamicin or vancomycin inhibits live microbe-induced pro-inflammatory cytokine production in human cord blood and cord blood monocytes in vitro. Antimicrob Agents Chemother. 2018.

32. Shabaan AE, Nasef N, Shouman B, Nour I, Mesbah A, Abdel-Hady H. Pentoxifylline therapy for late-onset sepsis in preterm infants: a randomized controlled trial. Pediatr Infect Dis J. 2015;34(6):e143-8.

33. Akdag A, Dilmen U, Haque K, Dilli D, Erdeve O, Goekmen T. Role of pentoxifylline and/or IgM-enriched intravenous immunoglobulin in the management of neonatal sepsis. Am J Perinatol. 2014;31(10):905-12.

34. Poggi C, Dani C. Sepsis and Oxidative Stress in the Newborn: From Pathogenesis to Novel Therapeutic Targets. Oxid Med Cell Longev. 2018;2018:9390140.

35. Berman B DM. Pentoxifylline inhibits the proliferation of human fibroblasts derived from keloid, scleroderma and morphoea skin and their production of collagen, glycosaminoglycans and fibronectin. Br J Dermatol. 1990;123:339-46.

36. Duncan MR HA, Berman B. Pentoxifylline, pentifylline, and interferons decrease type I and III procollagen mRNA levels in dermal fibroblasts: evedence for mediation by nuclear factor 1 down-regulation. J Invest Dermatol. 1995;104:282-6.

37. Horvath B, Marton Z, Halmosi R, Alexy T, Szapary L, Vekasi J, Biro Z, Habon T, Kesmarky G, Toth K. In vitro antioxidant properties of pentoxifylline, piracetam, and vinpocetine. Clin Neuropharmacol. 2002;25(1):37-42.

38. Lin SL, Chen RH, Chen YM, Chiang WC, Lai CF, Wu KD, Tsai TJ. Pentoxifylline attenuates tubulointerstitial fibrosis by blocking Smad3/4-activated transcription and profibrogenic effects of connective tissue growth factor. J Am Soc Nephrol. 2005;16(9):2702-13.

39. Boerma M, Roberto KA, Hauer-Jensen M. Prevention and treatment of functional and structural radiation injury in the rat heart by pentoxifylline and alpha-tocopherol. Int J Radiat Oncol Biol Phys. 2008;72(1):170-7.

40. Yang YL, Lee MG, Lee CC, Su PI, Chi CY, Liu CH, Wu MC, Yen ZS, Chen SC. Pentoxifylline decreases post-operative intra-abdominal adhesion formation in an animal model. PeerJ. 2018;6:e5434.

41. Lee JG, Shim S, Kim MJ, Myung JK, Jang WS, Bae CH, Lee SJ, Kim KM, Jin YW, Lee SS, Park S. Pentoxifylline Regulates Plasminogen Activator Inhibitor-1 Expression and Protein Kinase A Phosphorylation in Radiation-Induced Lung Fibrosis. Biomed Res Int. 2017;2017:1279280.

42. Delanian S, Porcher R, Balla-Mekias S, Lefaix JL. Randomized, placebo-controlled trial of combined pentoxifylline and tocopherol for regression of superficial radiation-induced fibrosis. J Clin Oncol. 2003;21(13):2545-50.

43. Delanian S, Chatel C, Porcher R, Depondt J, Lefaix JL. Complete restoration of refractory mandibular osteoradionecrosis by prolonged treatment with a pentoxifylline-tocopherol-clodronate combination (PENTOCLO): a phase II trial. Int J Radiat Oncol Biol Phys. 2011;80(3):832-9.

44. Peh HY, Tan WS, Liao W, Wong WS. Vitamin E therapy beyond cancer: Tocopherol versus tocotrienol. Pharmacol Ther. 2016;162:152-69.

45. Das Gupta S, Suh N. Tocopherols in cancer: An update. Mol Nutr Food Res.

2016;60(6):1354-63.

46. Constantinou C, Papas A, Constantinou AI. Vitamin E and cancer: An insight into the anticancer activities of vitamin E isomers and analogs. Int J Cancer. 2008;123(4):739-52.

47. Chin KY, Ima-Nirwana S. The effects of alpha-tocopherol on bone: a double-edged sword? Nutrients. 2014;6(4):1424-41.

48. Arjmandi B, Juma S, Beharka A, Bapna M, Akhter M, Meydani S. Vitamin E improves bone quality in the aged but not in young adult male mice. J Nutr Biochem. 2002;13(9):543.

49. Hampson G, Edwards S, Sankaralingam A, Harrington DJ, Voong K, Fogelman I, et al. Circulating concentrations of vitamin E isomers: Association with bone turnover and arterial stiffness in post-menopausal women. Bone. 2015;81:407-12.

50. Fujita K, Iwasaki M, Ochi H, Fukuda T, Ma C, Miyamoto T, Takitani K, Negishi-Koga T, Sunamura S, Kodama T, Takayanagi H, Tamai H, Kato S, Arai H, Shinomiya K, Itoh H, Okawa A, Takeda S. Vitamin E decreases bone mass by stimulating osteoclast fusion. Nature Medicine. 2012;18:589.

51. Hamama S, Delanian S, Monceau V, Vozenin MC. Therapeutic management of intestinal fibrosis induced by radiation therapy: from molecular profiling to new intervention strategies et vice et versa. Fibrogenesis Tissue Repair. 2012;5(Suppl 1):S13.

52. Kim YS, Lee SK. IP-HPLC Analysis of Human Salivary Protein Complexes. The Korean Journal of Oral and Maxillofacial Pathology. 2015;39(5):615-22.

53. Kim YS. Protein expression changes induced by cisplatin in an oral cancer cell line as determined by immunoprecipitation-based high performance liquid chromatography. Kor J Oral Maxillofac Pathol 2015;39:567-82.

54. Kim SM, Eo MY, Cho YJ, Kim YS, Lee SK. Immunoprecipitation high

performance liquid chromatographic analysis of healing process in chronic suppurative osteomyelitis of the jaw. J Craniomaxillofac Surg. 2018;46(1):119-27.

55. Yoon CS, Lee SK. Preliminary study on the Cell Biological Effect of Dialyzed Coffee Extract in RAW 264.7 Cells. The Korean Journal of Oral and Maxillofacial Pathology. 2016;40(6):911-20.

56. Yoon CS, Kim MK, Kim YS, Lee SK. In vitro protein expression changes in RAW 264.7 cells and HUVECs treated with dialyzed coffee extract by immunoprecipitation high performance liquid chromatography. Sci Rep. 2018;8(1):13841.

57. Iredale J. Defining therapeutic targets for liver fibrosis: exploiting the biology of inflammation and repair. Pharmacol Res. 2008;58(2):129-36.

58. Delanian S, Depondt J, Lefaix JL. Major healing of refractory mandible osteoradionecrosis after treatment combining pentoxifylline and tocopherol: a phase II trial. Head Neck. 2005;27(2):114-23.

59. McLeod NM, Pratt CA, Mellor TK, Brennan PA. Pentoxifylline and tocopherol in the management of patients with osteoradionecrosis, the Portsmouth experience. Br J Oral Maxillofac Surg. 2012;50(1):41-4.

60. D'Souza J, Lowe D, Rogers SN. Changing trends and the role of medical management on the outcome of patients treated for osteoradionecrosis of the mandible: experience from a regional head and neck unit. Br J Oral Maxillofac Surg. 2014;52(4):356-62.

61. Delanian S, Porcher R, Rudant J, Lefaix JL. Kinetics of response to long-term treatment combining pentoxifylline and tocopherol in patients with superficial radiation-induced fibrosis. J Clin Oncol. 2005;23(34):8570-9.

62. Kim SM, Eo MY, Cho YJ, Kim YS, Lee SK. Differential protein expression in the secretory fluids of maxillary sinusitis and maxillary retention cyst. Eur

Arch Otorhinolaryngol. 2017;274(1):215-22.

63. Zhang R, Bharadwaj U, Li M, Chen C, Yao Q. Effects of pentoxifylline on differentiation, maturation, and function of human CD14+ monocyte-derived dendritic cells. J Immunother. 2007;30(1):89-95.

64. Wang W, Tam WF, Hughes CC, Rath S, Sen R. c-Rel is a target of pentoxifylline-mediated inhibition of T lymphocyte activation. Immunity. 1997;6(2):165-74.

65. Strutz F, Heeg M, Kochsiek T, Siemers G, Zeisberg M, Muller GA. Effects of pentoxifylline, pentifylline and gamma-interferon on proliferation, differentiation, and matrix synthesis of human renal fibroblasts. Nephrol Dial Transplant. 2000;15(10):1535-46.

66. Okunieff P, Augustine E, Hicks JE, Cornelison TL, Altemus RM, Naydich BG, Ding I, Huser AK, Abraham EH, Smith JJ, Coleman N, Gerber LH. Pentoxifylline in the treatment of radiation-induced fibrosis. J Clin Oncol. 2004;22(11):2207-13.

67. Rabbani ZN, Mi J, Zhang Y, Delong M, Jackson IL, Fleckenstein K, Salahuddin FK, Zhang X, Clary B, Anscher MS, Vujaskovic Z. Hypoxia inducible factor 1alpha signaling in fractionated radiation-induced lung injury: role of oxidative stress and tissue hypoxia. Radiat Res. 2010;173(2):165-74.

68. Wang Y, Dong L, Li J, Luo M, Shang B. Pentoxifylline induces apoptosis of HepG2 cells by reducing reactive oxygen species production and activating the MAPK signaling. Life Sci. 2017;183:60-8.

69. Luo M, Dong L, Li J, Wang Y, Shang B. Protective effects of pentoxifylline on acute liver injury induced by thioacetamide in rats. Int J Clin Exp Pathol. 2015;8(8):8990-6.

70. Armagan I, Bayram D, Candan IA, Yigit A, Celik E, Armagan HH, Uğuz AC. Effects of pentoxifylline and alpha lipoic acid on methotrexate-induced

damage in liver and kidney of rats. Environ Toxicol Pharmacol. 2015;39(3):1122-31.

71. Golunski G, Woziwodzka A, Piosik J. Potential Use of Pentoxifylline in Cancer Therapy. Curr Pharm Biotechnol. 2018;19(3):206-16.

72. Horiuchi H, Saito N, Kinoshita T, Wakabayashi S, Tsutsumimoto T, Otsuru S, Takaoka K. Enhancement of recombinant human bone morphogenetic protein-2 (rhBMP-2)-induced new bone formation by concurrent treatment with parathyroid hormone and a phosphodiesterase inhibitor, pentoxifylline. J Bone Miner Metab. 2004;22(4):329-34.

73. Horiuchi H, Saito N, Kinoshita T, Wakabayashi S, Tsutsumimoto T, Takaoka K. Enhancement of bone morphogenetic protein-2-induced new bone formation in mice by the phosphodiesterase inhibitor pentoxifylline. Bone. 2001;28(3):290-4.

74. Cakmak G, Sahin MS, OzdemIr BH, KaradenIz E. Effect of pentoxifylline on healing of segmental bone defects and angiogenesis. Acta Orthop Traumatol Turc. 2015;49(6):676-82.

75. Kamran MZ, Gude RP. Pentoxifylline inhibits melanoma tumor growth and angiogenesis by targeting STAT3 signaling pathway. Biomed Pharmacother. 2013;67(5):399-405.

76. Olascoaga A, Vilar-Compte D, Poitevin-Chacon A, Contreras-Ruiz J. Wound healing in radiated skin: pathophysiology and treatment options. Int Wound J. 2008;5(2):246-57.

77. Miller MB, Koltai PJ. Treatment of experimental frostbite with pentoxifylline and aloe vera cream. Arch Otolaryngol Head Neck Surg. 1995;121(6):678-80.

78. Stone HB, Coleman CN, Anscher MS, McBride WH. Effects of radiation on normal tissue: consequences and mechanisms. The Lancet Oncology.

2003;4(9):529-36.

79. Nanashima N, Ito K, Ishikawa T, Nakano M, Nakamura T. Damage of hair follicle stem cells and alteration of keratin expression in external radiation-induced acute alopecia. Int J Mol Med. 2012;30(3):579-84.

80. Aygenc E, Celikkanat S, Bilgili H, Aksaray F, Orhun S, Kaymakci M, Ozdem C. Pentoxifylline effects on acute and late complications after radiotherapy in rabbit. Otolaryngol Head Neck Surg. 2001;124(6):669-73.

81. Gruber S, Bozsaky E, Roitinger E, Schwarz K, Schmidt M, Dorr W. Early inflammatory changes in radiation-induced oral mucositis : Effect of pentoxifylline in a mouse model. Strahlenther Onkol. 2017;193(6):499-507.

82. Westbury CB, Yarnold JR. Radiation fibrosis-current clinical and therapeutic perspectives. Clin Oncol (R Coll Radiol). 2012;24(10):657-72.

83. Wang J, Boerma M, Fu Q, Hauer-Jensen M. Significance of endothelial dysfunction in the pathogenesis of early and delayed radiation enteropathy. World J Gastroenterol. 2007;13(22):3047-55.

84. Mallya SM, Tetradis S. Imaging of Radiation- and Medication-Related Osteonecrosis. Radiol Clin North Am. 2018;56(1):77-89.

85. Hopewell JW. Radiation-therapy effects on bone density. Med Pediatr Oncol. 2003;41(3):208-11.

86. Xu DX, Chen YH, Wang H, Zhao L, Wang JP, Wei W. Tumor necrosis factor alpha partially contributes to lipopolysaccharide-induced intra-uterine fetal growth restriction and skeletal development retardation in mice. Toxicol Lett. 2006;163(1):20-9.

87. Wakabayashi S, Tsutsumimoto T, Kawasaki S, Kinoshita T, Horiuchi H, Takaoka K. Involvement of phosphodiesterase isozymes in osteoblastic differentiation. J Bone Miner Res. 2002;17(2):249-56.

88. Mody N, Parhami F, Sarafian TA, Demer LL. Oxidative stress modulates

osteoblastic differentiation of vascular and bone cells. Free Radic Biol Med. 2001;31(4):509-19.

89. Suda N, Morita I, Kuroda T, Murota S. Participation of oxidative stress in the process of osteoclast differentiation. Biochim Biophys Acta. 1993;1157(3):318-23.

90. Kasai S, Ito A, Shindo K, Toyoshi T, Bando M. High-Dose alpha-Tocopherol Supplementation Does Not Induce Bone Loss in Normal Rats. PLoS One. 2015;10(7):e0132059.

91. Kurklu M, Yildiz C, Kose O, Yurttas Y, Karacalioglu O, Serdar M, Deveci S. Effect of alpha-tocopherol on bone formation during distraction osteogenesis: a rabbit model. J Orthop Traumatol. 2011;12(3):153-8.

92. Tennant KG, Leonard SW, Wong CP, Iwaniec UT, Turner RT, Traber MG. High-Dietary Alpha-Tocopherol or Mixed Tocotrienols Have No Effect on Bone Mass, Density, or Turnover in Male Rats During Skeletal Maturation. J Med Food. 2017;20(7):700-8.

93. Saricaoglu H, Baskan EB, Tunali S. The effect of the topical application of different pentoxifylline concentrations on the patch test results of nickel-sensitive patients. Int J Dermatol. 2004;43(4):315-6.

94. Cavalcanti AL, Reis MY, Silva GC, Ramalho IM, Guimaraes GP, Silva JA, Saraiva KL, Damasceno BP. Microemulsion for topical application of pentoxifylline: In vitro release and in vivo evaluation. Int J Pharm. 2016;506(1-2):351-60.

95. Futran ND, Trotti A, Gwede C. Pentoxifylline in the treatment of radiation-related soft tissue injury: preliminary observations. Laryngoscope. 1997;107(3):391-5.

Tables

Table 3.1. Experimental groups according to radiation dose

Group	Radiation total dose (Gy)	Evaluation (weeks)	Number
Group 1	14	2	2
		3	2
Group 2	16	2	2
		3	2
Group 3	18	2	2
		3	2
Group 4	20	2	2
		3	2
			16

Table 3.2. Classification of animal study groups

	Medication	N
Irradiation group	Pentoxifylline (T1)	10
	Tocopherol (T2)	10
	Pentoxifylline + tocopherol (T3)	10
	Normal saline (T4)	10
Control group	Pentoxifylline (C1)	2
(no-irradiation)	Tocopherol (C2)	2
	Pentoxifylline + tocopherol (C3)	2
	Normal saline (C4)	2

Table 3.3. Rat primers used in RT-qPCR

Primer	Forward	Reverse
Osterix	GCTCACTATGGCTCCAGTCC	TTTCCCAGGGCTGTTGAGTC
Osteocalcin	GAATAGACTCCGGCGCTACC	AGCTCGTCACAATTGGGGTT
RANKL	CAGGTTTGCAGGACTCGACT	GAGCCACGAACCTTCCATCA
OPG	AACCGAGTGTGCGAATGTGA	ACCTGAGAAGAACCCATCCG
TNF-α	GGCTCCCTCTCATCAGTTCC	CGCTTGGTGGTTTGCTACG
CD31	CTGGGAGGTATCGAATGGGC	GTGCATTTGTACTTCCCGGC
VEFG-A	GGCTCACTTCCAGAAACACG	AGGCTCCCCAAAAACGTCTG

Abbreviation: RANKL; receptor activator of nuclear kappa-B ligand, OPG; osteoprotegerin, TNF- α; tumor necrosis factor- α, CD31; cluster of differentiation 31, VEGF-A, vascular endothelial growth factor-A

Table 4.1. Representative cellular signaling affected by pentoxifylline in RAW 264.7cells

Signaling	Up-regulated	Unchanged	Down-regulated
Proliferation ↓		PCNA	Ki-67, CDK4, PLK4, MPM2, cyclin D2, Rb-1, E2F-1, MDM2
Apoptosis ↓	BAX, APAF-1	BAK, caspase 9	p53, PARP, FASL, FADD, caspase 8
Antioxidant and cellular protection	AP-1, SP-1, AMPK-1		NOS-1, SOD-1, GST
Angiogenesis	HIF, angiogenin, VEGF-C	VEGF-A, vWF, ET-1, CD31	CMG2
Osteogenesis↑	OPG, RANKL, osteopontin, RUNX2, osterix	Osteonectin, ALP	Cathepsin K
Inflammation ↓	CD4, IL-10, MMP-1, MMP-2, MMP-3, MMP-9,	TLR3, CD31, CD68, lysozyme, TNF-α	IL-1, IL-6, CD3, CD20, CD28, M-CSF, cathepsin K, LTA4H, CXCR4, COX-2
Growth factor	IGF-1, HER1, HER2	TGF-β1	FGF-1, FGF-2, ERβ

Abbreviation: PCNA: proliferating cell nuclear antigen, Ki-67, CDK4: cyclin dependent kinase 4, PLK4: polo-like kinase 4, MPM2: mitotic protein monoclonal 2, Rb-1: retinoblastoma-1, MDM2: mouse double minute 2 homolog, BAX: Bcl-2 associated X, APAF: apoptotic protease activating factor 1, BAK: Bcl-2 homologous antagonist killer, PARP: poly-ADP ribose polymerase, FASL: FAS ligand, FADD: FAS-associated via death domain, AP-1: activating factor-1, SP-1: specific protein-1, AMPK-1: AMP-activated protein kinase, NOS1: nitric oxide synthase 1, SOD-1: superoxide dismutase-1, GST: glutathione S-transferase, HIF: hypoxia inducible factor, VEGF-A: vascular endothelial growth factor-A, VEGF-C: vascular endothelial growth factor-C, vWF: von Willebrand factor, ET-1: endothelin-1, CD31: cluster of differentiation 31, CMG2: capillary morphogenic protein 2, OPG: osteoprotegerin, RANKL:

receptor activator of nuclear factor kappa-B ligand, RUNX2: RUNT-related transcription factor 2, ALP: alkaline phosphatase, CD4: cluster of differentiation, IL-10: interleukin-1, MMP-1: matrix metalloproteinase-1, MMP-2: matrix metalloproteinase-2, MMP-3: matrix metalloproteinase-3, MMP-9: matrix metalloproteinase-9, TLR3: Toll like receptor 3, CD68: cluster of differentiation 68, TNF-α: tumor necrosis factor-α, IL-1: interleukin-1, IL-6: interleukin-10, CD3: cluster of differentiation 3, CD30: cluster of differentiation 30, CD28: cluster of differentiation, M-CSF: macrophage-colony stimulating factor, LTA4H: leukotriene-A4 hydrolase, CXCR4: C-X-C chemokine receptor 4, COX-2: cyclooxygenase-2, IGF-1: insulin growth factor-1, HER1: human epidermal growth factor receptor 1, HER2: human epidermal growth factor receptor 2, TGF-β1: transforming growth factor-β1, ERβ: estrogen receptor β, ↑: upregulation, ↓: downregulation

Table 4.2. Changes in body weight after irradiation.

Dose	No	Pre-irradiation (g)	Two weeks after irradiation (g)	Three weeks after irradiation (g)
0 Gy		265.52	292.59	325.16
(no irradiation)	2	270.24	325.88	357.51
Mean ± SD		267.88 ± 3.34	324.24 ± 2.33	356.33 ± 1.66
		269.34	363.74	
		249.35	328.28	
14 Gy	4	265.68	331.87	366.04
		272.17	367.95	367.36
Mean ± SD		264.14 ± 10.21	347.96 ± 20.78	366.70 ± 0.93
		280.6	372.25	
		263.77	347.49	
16 Gy	4	267.65	354.3	269.91
		269.12	350.94	362.21
Mean ± SD		270.29 ± 7.24	356.25 ± 11.03	316.06 ± 65.27
		262.83	321.85	
		271.17	375.5	
18Gy	4	280.04	377.36	410.81
		264.41	354.91	389.92
Mean ± SD		269.61 ± 7.84	357.41 ± 25.79	400.37 ± 14.77
		275.5	374.08	
		272.75	321.3	
20Gy	4	272.95	363.44	397.58
		243.6	307.36	385.81
Mean ± SD		266.20 ± 15.12	341.55 ± 32.23	391.70 ± 8.32

SD: standard deviation

Table 4.3. Counts of osteoblasts and osteoclasts in the high power field (HPF) following irradiation dose and timing.

	Osteoblast/HPF		Osteoclast/HPF	
Dose / time	2 weeks	3 weeks	2 weeks	3 weeks
14Gy	11.0 ± 1.0	5.50 ± 0.50*	1.0 ± 0.0	0.5 ± 0.5*
16Gy	6.0 ± 1.0	5.0 ± 3.0	7.5 ± 1.5	9.0 ± 1.0*
18Gy	2.5 ± 1.5	0.5 ± 0.5*	10.5 ± 1.5	9.5 ± 4.5*
20Gy	1.5 ± 0.5	0.5 ± 0.5*	19.0 ± 1.0	19.5 ± 3.5*

The data is presented as mean ± standard deviation (SD).

*: $p < 0.05$

Table 4.4. Weight changes after irradiation in the experimental group.

Group	0w (g)	1w (g)	2w (g)	3w (g)	4w (g)	5w (g)	6w (g)	7w (g)
T1	317.66 ± 41.56	315.96 ± 45.20	344.83 ± 54.48	378.32 ± 32.86	387.52 ± 39.26	400.03 ± 34.65	392.76 ± 45.57	380.49 ± 55.32
T2	342.49 ± 28.96	328.46 ± 35.22	317.92 ± 57.06	367.37 ± 59.26	393.94 ± 37.73	412.34 ± 31.49	413.82 ± 29.71	399.54 ± 45.42
T3	335.17 ± 16.40	308.70 ± 24.79	294.15 ± 66.70	343.33 ± 51.20	363.55 ± 44.20	376.01 ± 55.93	386.86 ± 53.71	385.88 ± 51.86
T4	339.46 ± 35.95	315.31 ± 35.95	286.36 ± 61.03	328.36 ± 55.87	360.15 ± 42.45	377.90 ± 37.76	386.00 ± 46.05	386.90 ± 63.21
C1	365.81 ± 2.60	382.08 ± 1.05	428.27 ± 6.72	451.69 ± 7.36	453.1 ± 5.20	474.02 ± 3.33	491.42 ± 4.07	495.90 ± 3.96
C2	387.01 ± 31.84	414.81 ± 7.17	444.09 ± 14.75	493.61 ± 51.05	473.18 ± 21.92	494.74 ± 17.98	518.85 ± 12.64	524.53 ± 24.82
C3	389.91 ± 2.74	418.06 ± 8.85	465.16 ± 9.29	496.50 ± 5.83	503.94 ± 12.01	527.45 ± 13.79	561.47 ± 18.78	573.52 ± 20.58
C4	346.63 ± 26.11	390.29 ± 3.25	418.84 ± 8.94	434.27 ± 14.69	438.43 ± 23.33	459.76 ± 25.89	474.75 ± 31.03	484.42 ± 24.06

The data is displayed as mean ± standard deviation (SD). w: week(s)

Table 4.5. Measurement of skin alopecia three weeks after irradiation and bone exposure seven weeks after irradiation

Group	Alopecia (mm^2)	Bone exposure (mm^2)
T1	243.16 ± 486.69	5.86 ± 2.80
T2	604.61 ± 771.29	5.40 ± 1.95
T3	373.66 ± 529.08	3.29 ± 3.95
T4	819.58 ± 1118.98	3.00 ± 3.35

The data is displayed as mean ± standard deviation (SD).

Table 4.6. Comparisons of blood analysis in the pre-irradiation, 3 weeks, and 7 weeks after irradiation.

Group	WBC (x10^3)			Neutrophil			Lumphocyte		
	Pre	3wk	7wk	Pre	3wk	7wk	Pre	3wk	7wk
T1	10.44 ± 2.36	17.07 ± 3.98	12.41 ± 2.27	1.53 ± 0.83	5.61 ± 2.99	2.60 ± 0.74	8.57 ± 1.55	10.76 ±1.84	9.29 ± 1.89
T2	9.97 ± 1.84	16.23 ± 4.64	9.25 ± 1.81	1.38 ± 1.00	7.00 ± 3.77	1.83 ± 0.50	8.27 ± 1.11	8.49 ± 2.18	7.07 ± 1.83
T3	11.06 ± 1.93	15.73 ± 3.14	12.27 ± 2.91	1.48 ± 0.68	5.53 ± 2.54	3.75 ± 1.00	9.17 ± 1.44	10.36 ± 2.00	7.99 ± 1.39
T4	10.10 ± 2.26	16.62 ± 3.68	10.95 ± 1.85	1.77 ± 0.96	5.97 ± 1.74	3.35 ± 1.31	7.96 ± 1.69	8.85 ± 1.68	7.10 ± 1.63
C1	11.93 ±2.38	11.49 ± 0.76	10.84 ± 0.78	1.63 ± 0.17	1.35 ± 0.34	1.96 ± 0.96	9.90 ± 2.14	9.80 ± 1.07	8.27 ± 1.28
C2	10.6	13.09 ± 1.13	12.17 ± 0.97	1.08	3.29 ± 0.68	1.86 ± 0.64	9.11	9.75 ± 0.35	9.75± 1.09
C3	10.1	11.29 ± 4.36	10.23 ± 3.61	1.7	2.1 ± 1.80	1.99 ± 1.04	8.03	8.76 ± 2.27	7.91 ± 2.38
C4	12.89	14.76	12.56 ± 1.04	2.92	1.59	2.32 ± 0.01	9.23	12.80	9.87 ± 1.89

Group	Monocyte			NLR		
	Pre	3wk	7wk	Pre	3wk	7wk
T1	0.13 ± 0.07	0.41 ± 0.20	0.28 ± 0.18	0.17 ± 0.07	0.54 ± 0.30	0.28 ± 0.08
T2	0.17 ± 0.05	0.47 ± 0.26	0.13 ± 0.06	0.16 ± 0.11	0.91 ± 0.64	0.28 ± 0.12
T3	0.22 ± 0.07	0.44 ± 0.03	0.22 ± 0.05	0.16 ± 0.07	0.54 ± 0.25	0.49 ± 0.20
T4	0.20 ± 0.09	0.59 ± 0.25	0.26 ± 0.09	0.22 ± 0.11	0.68 ± 0.17	0.51 ± 0.28
C1	0.12 ± 0.01	0.15 ± 0.04	0.20 ± 0.11	0.17 ± 0.02	0.14 ± 0.05	0.24 ± 0.15

C2	0.15	0.32 ± 0.03	0.23 ± 0.01	0.12	0.28 ± 0.06	0.19 ± 0.03
C3	0.18	0.24 ± 0.23	0.20 ± 0.16	0.21	0.22 ± 0.15	0.24 ± 0.06
C4	0.21	0.19	0.16 ± 0.02	0.32	0.12	0.24 ± 0.03

The data is presented as mean ± standard deviation (SD). Abbreviation: WBC: white blood cell count, NLR: neutrophil to lymphocyte ratio, Pre: pre-irradiation, 3wk: three weeks after irradiation, 7wk: seven weeks after irradiation

Table 4.7. Trabecular microstructure measured by micro-CT in the whole extraction socket

Group	TV (mm^3)	BV (mm^3)	BV/TV (%)	Tb.Th. (mm)	Tb.N. (1/mm)	Tb. Sp. (mm)	BMD (g/cm^3)
T1	13.31 ± 1.30	0.82 ± 0.22	6.13 ± 1.32	0.11 ± 0.01	0.54 ± 0.08	0.73 ± 0.09	0.15 ± 0.03
T2	12.96 ± 2.50	0.88 ± 0.43	7.08 ± 4.15	0.12 ± 0.01	0.58 ± 0.28	0.68 ± 0.10	0.18 ± 0.05
T3	12.76 ± 1.71	2.51 ± 2.51	19.62 ± 16.03	0.14 ± 0.03	1.37 ± 1.10	0.50 ± 0.17	0.31 ± 0.16
T4	11.52 ± 1.78	0.09 ± 0.29	7.30 ± 2.18	0.11 ± 0.01	0.65 ± 0.19	0.64 ± 0.09	0.18 ± 0.03
C1	7.53 ± 0.77	3.79 ± 0.84	50.04 ± 6.07	0.15 ± 0.03	3.30 ± 0.34	0.19 ± 0.02	0.58 ± 0.05
C2	11.20 ± 2.33	6.94 ± 0.89	62.45 ± 5.04	0.16 ± 0.02	3.90 ± 0.11	0.15 ± 0.00	0.66 ± 0.03
C3	11.76 ± 0.15	8.75 ± 0.65	74.39 ± 4.53	0.22 ± 0.03	3.45 ± 0.24	0.14 ± 0.02	0.78 ± 0.06
C4	12.18 ± 1.77	6.49 ± 1.59	52.91 ± 5.38	0.13 ± 0.00	3.98 ± 0.45	0.17 ± 0.01	0.60 ± 0.03

The data is displayed as mean ± standard deviation (SD). Abbreviation: TV: tissue volume, BV: bone volume, BV/TV: bone volume/tissue volume, Tb.Th.: trabecular thickness, Tb.N.: trabecular number, Tb.Sp.: trabecular spaces, BMD: bone mineral density

Table 4.8. Trabecular microstructure measured by micro CT in the same volume of interests.

Group	TV (mm^3)	BV (mm^3)	BV/TV (%)	Tb.Th. (mm)	Tb.N. (1/mm)	Tb. Sp. (mm)	BMD (g/cm^3)
T1	3.69 ± 0.47	0.23 ± 0.10	6.07 ± 2.45	0.12 ± 0.04	0.49 ± 0.18	0.57 ± 0.05	0.16 ± 0.03
T2	3.84 ± 0.15	0.37 ± 0.24	9.60 ± 6.08	0.13 ± 0.03	0.75 ± 0.42	0.54 ± 0.08	0.21 ± 0.06
T3	3.58 ± 0.41	0.75 ± 0.69	19.08 ± 15.24	0.13 ± 0.03	1.42 ± 1.06	0.42 ± 0.17	0.31 ± 0.17
T4	3.47 ± 0.53	0.37 ± 0.20	10.38 ± 4.54	0.12 ± 0.01	0.88 ± 0.30	0.49 ± 0.09	0.21 ± 0.05
C1	3.51 ± 0.58	1.71 ± 0.55	47.97 ± 7.80	0.14 ± 0.02	3.56 ± 0.04	0.19 ± 0.02	0.56 ± 0.06
C2	3.88 ± 0.06	2.28 ± 0.26	58.74 ± 5.80	0.13 ± 0.02	4.39 ± 0.24	0.15 ± 0.01	0.63 ± 0.03
C3	3.52 ± 0.57	2.66 ± 0.27	76.00 ± 4.52	0.20 ± 0.02	3.89 ± 0.16	0.12 ± 0.02	0.78 ± 0.05
C4	3.60 ± 0.30	1.90 ± 0.47	52.57 ± 8.66	0.12 ± 0.01	4.39 ± 0.32	0.19 ± 0.04	0.58 ± 0.06

The data is presented as mean ± standard deviation (SD). Abbreviation: TV: tissue volume, BV: bone volume, BV/TV: bone volume/tissue volume, Tb.Th.: trabecular thickness, Tb.N.: trabecular number, Tb.Sp.: trabecular spaces, BMD: bone mineral density

Figure legends and Figures

Figure 2.1. PTX is a methylxanthine derivatives that inhibits phosphodiesterases, (a) chemical structure of PTX; (b) 3D conformer image of PTX

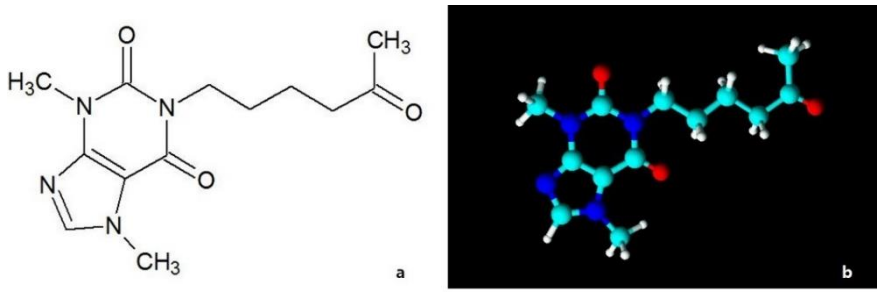

Figure 2.2. Structure of α-tocopherol, (a) chemical structure; (b) 3D conformer image

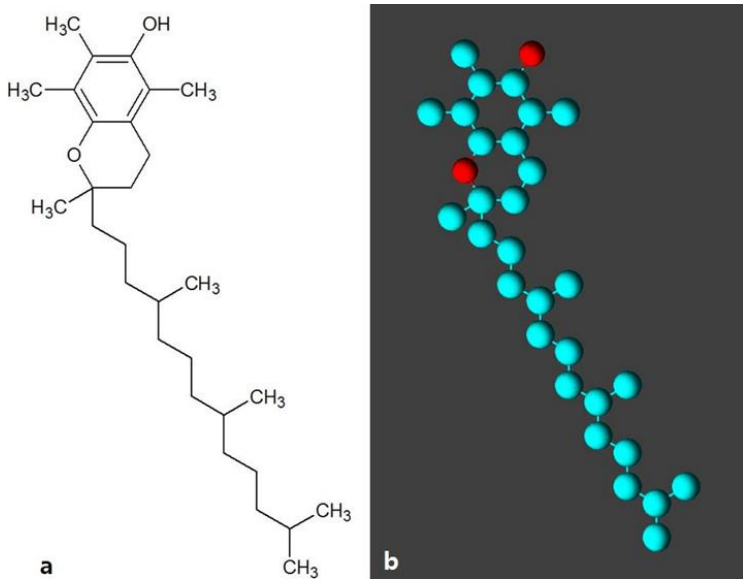

Figure 2.3. Procedures in immunoprecipitation-high performance liquid chromatography (IP-HPLC). The mixture of protein sample and antibody-bound A/G agarose beads are incubated by stirring (a), and after multiple washes of agarose beads (b), the target protein is eluted (c) and analyzed by automatic HPLC system (d) using UV spectroscopy.

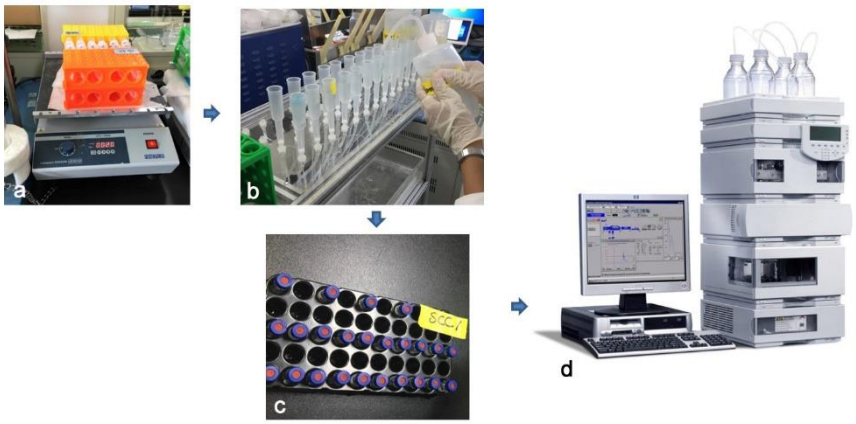

Figure 3.1. Time table of radiation-induced mucositis and osteonecrosis animal model design.

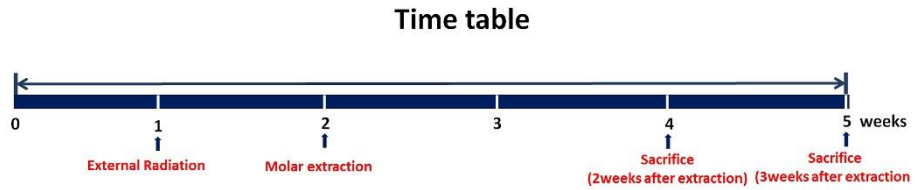

Figure 3.2. (a) Animal receiving irradiation, (b) Experimental radiological setting used in this study, 260 kV, 10 mA, 2 mL Al filter, (c) Specimens for evaluation after harvesting of the lower jaw including soft tissue.

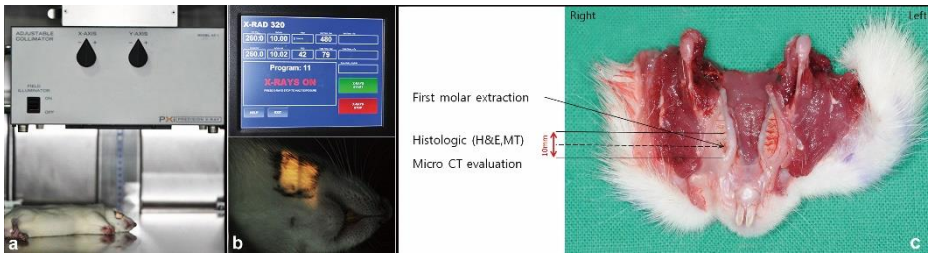

Figure 3.3. Radiation delivery procedures, (a) 2x1-cm skin marking on the left mandible; (b) X-RAD 320 Irradiator® (Precision X-ray Inc., North Branford, USA) settings; (c) beam focused on the planned surface for testing

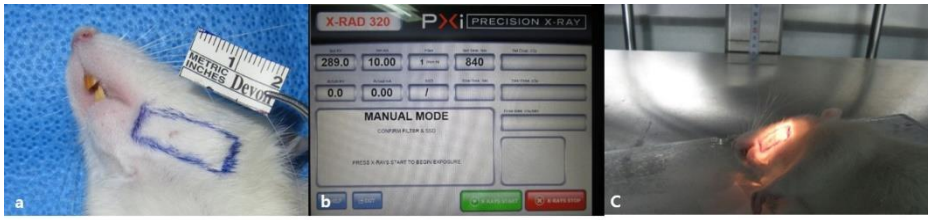

Figure 3.4. Timeline of experimental procedure. The next day after irradiation the drug was administered according to the experimental drug. Three weeks after irradiation, left mandibular molars were extracted. The animals were sacrificed seven weeks after irradiation

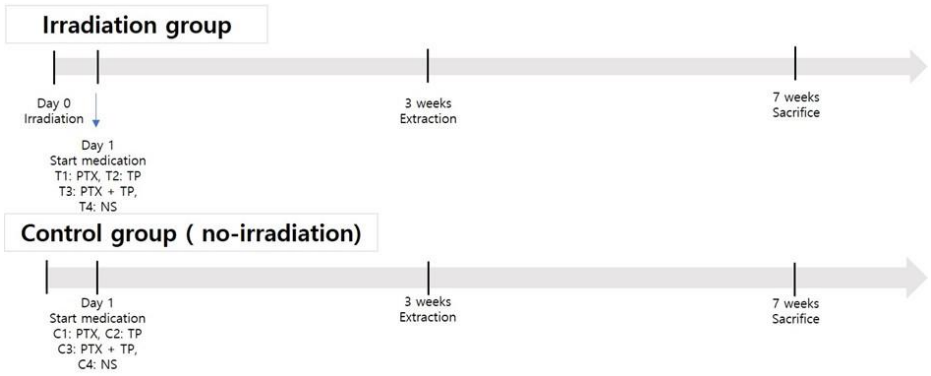

Figure 3.5. Measurement of dimension of alopecia using Image J software® (NIH, Bethesda, Maryland, USA)

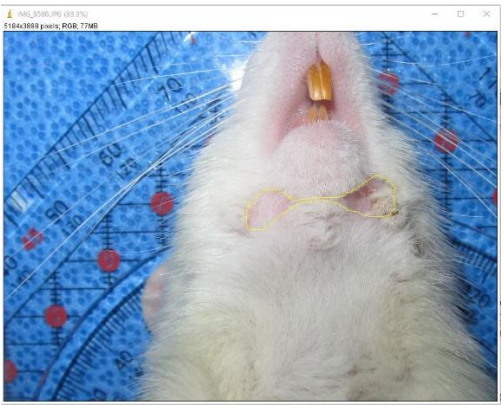

Figure 3.6. Description of the two methods of ROI designation for the micro-CT analysis; (a) original coronal CT image; (b) the area in red is the ROI, and the entire extraction socket is selected as the ROI in the CT image; (c) a 50 x 80-pixels rectangular ROI image

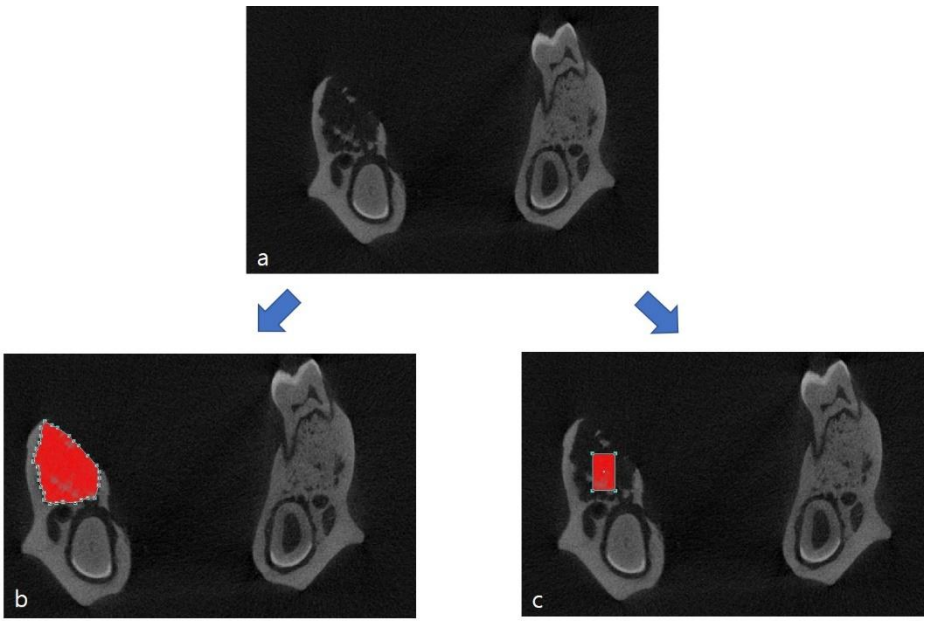

Figure 3.7. Counting of empty lacunae in the extraction socket in the histologic photographs; (a) x40 image; (b) x400 magnification of inner surface of alveolar socket, 500 x 500 pixels were selected for cell counting

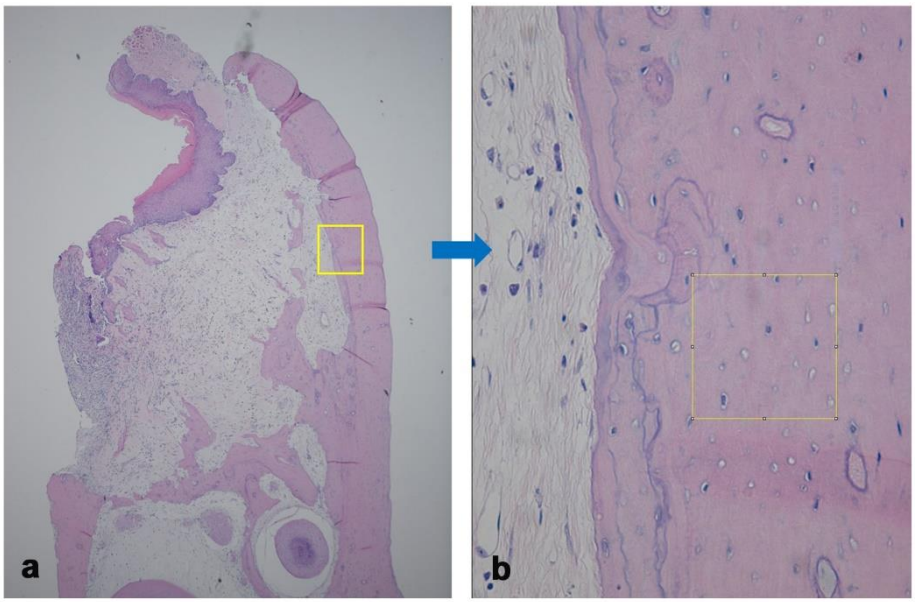

Figure 4.1. (a) Expression of proliferation-related proteins after PTX treatment in macrophage, (b) Expression of cMyc/MAX/MAD signaling-related proteins after PTX treatment in macrophage, (c) Expression of p53/Rb/E2F signaling-related proteins after PTX treatment in macrophage, (left) changes in protein expression over time, (right) protein expression patterns in the sample treated with PTX for 12 hours.

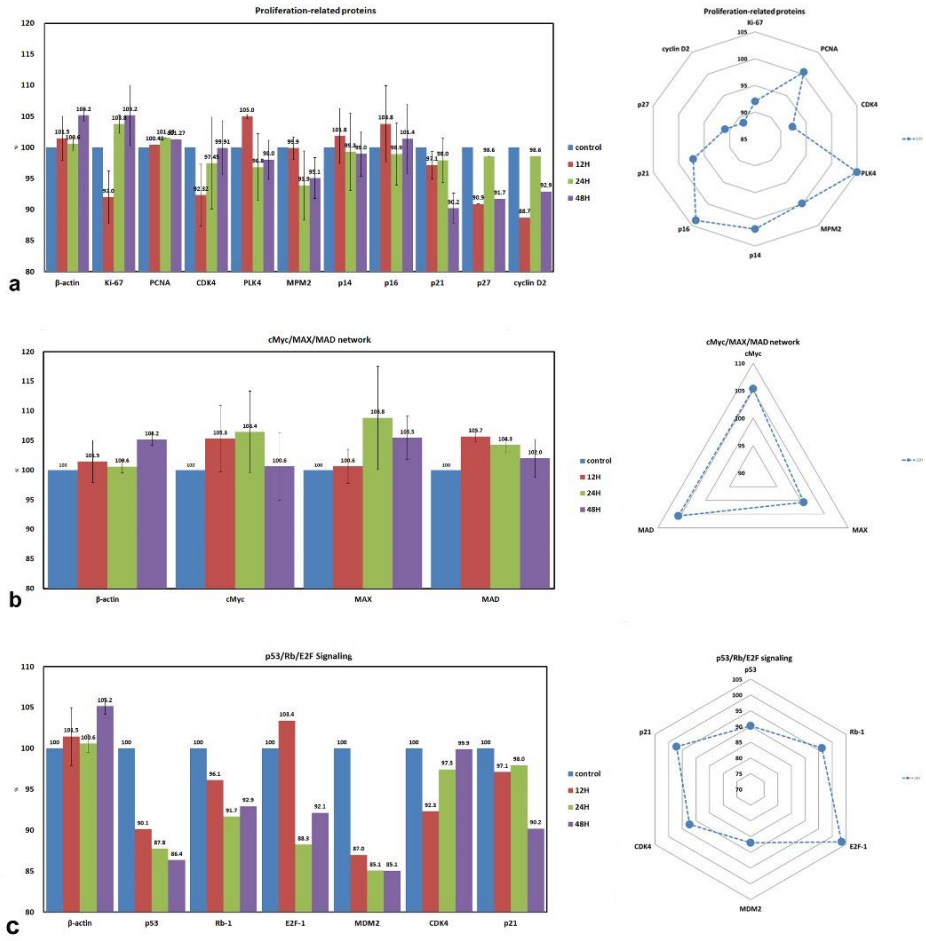

Figure 4.2. (a) Expression of epigenetic modification-related proteins after PTX treatment in macrophage, (b) Expression of protein translation-related proteins after PTX treatment in macrophage, (c) Expression of cellular differentiation-related proteins after PTX treatment in macrophage, (left) changes in protein expression over time, (right) protein expression patterns in the sample treated with PTX for 12 hours.

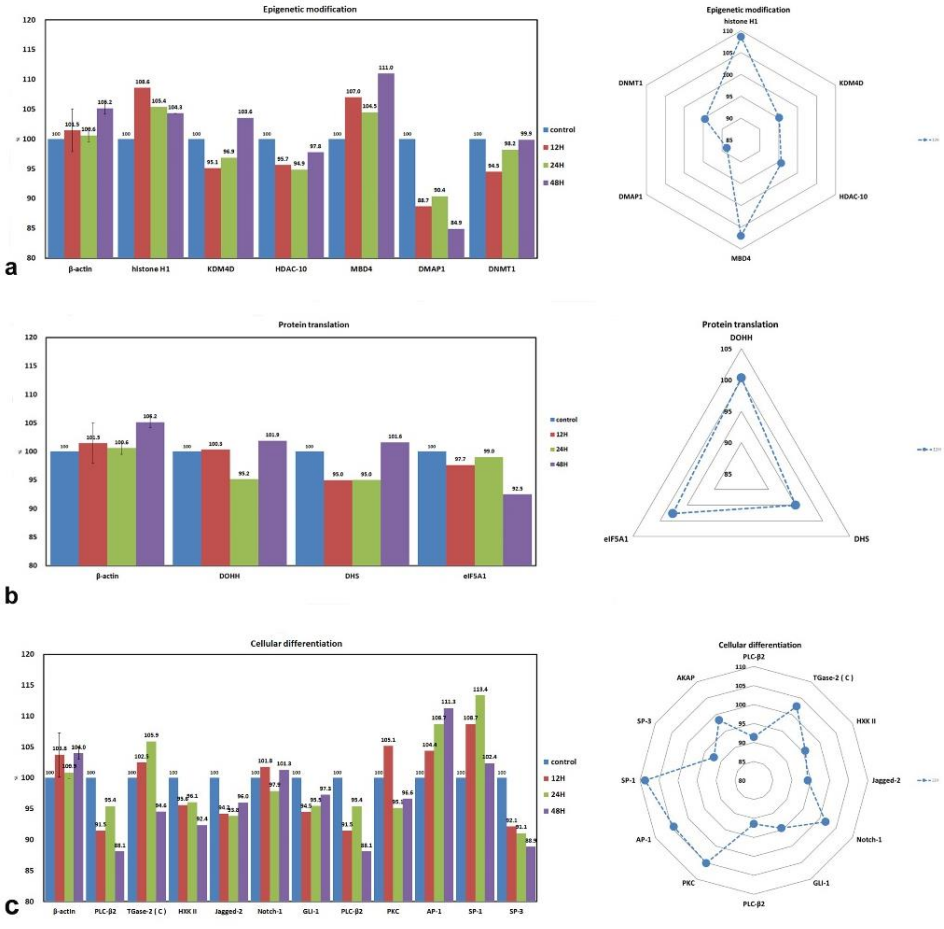

Figure 4.3. (a) Expression of RAS signaling-related proteins after PTX treatment in macrophage, (b) Expression of NFκB signaling-related proteins after PTX treatment in macrophage, (c) Expression of growth factor-related proteins after PTX treatment in macrophage, (left) changes in protein expression over time, (right) protein expression patterns in the sample treated with PTX for 12 hours.

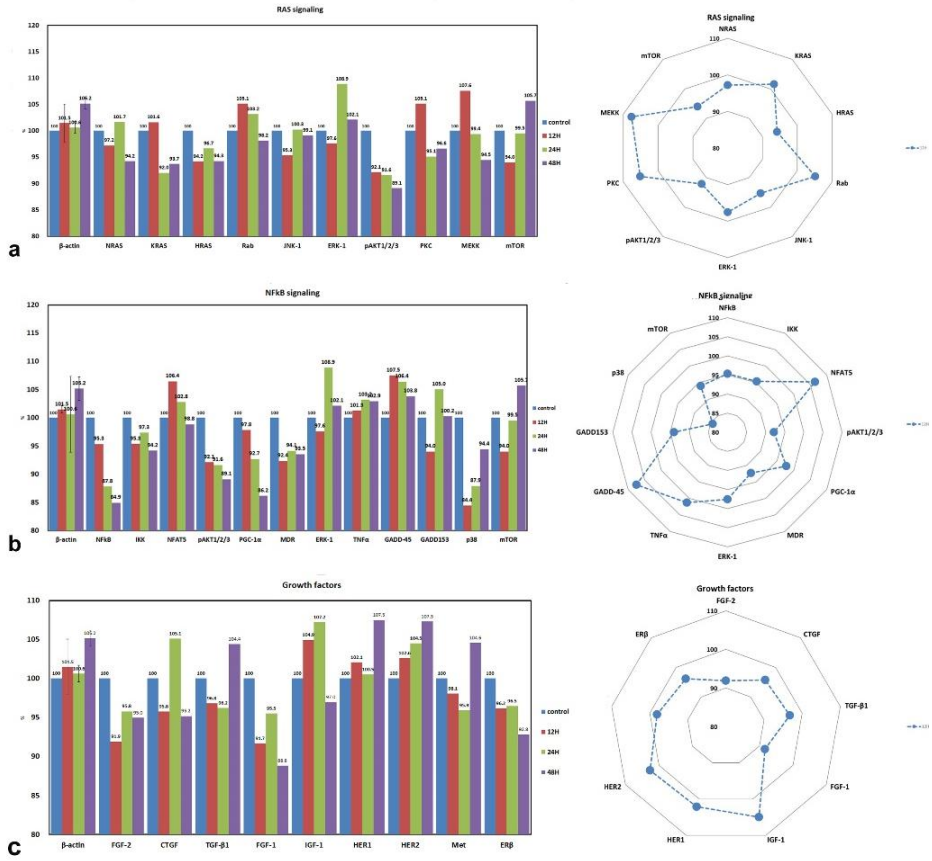

Figure 4.4. (a) Expression of inflammation-upregulated proteins after PTX treatment in macrophage, (b) Expression of inflammation down-regulated proteins after PTX treatment in macrophage, (left) changes in protein expression over time, (right) protein expression patterns in the sample treated with PTX for 12 hours.

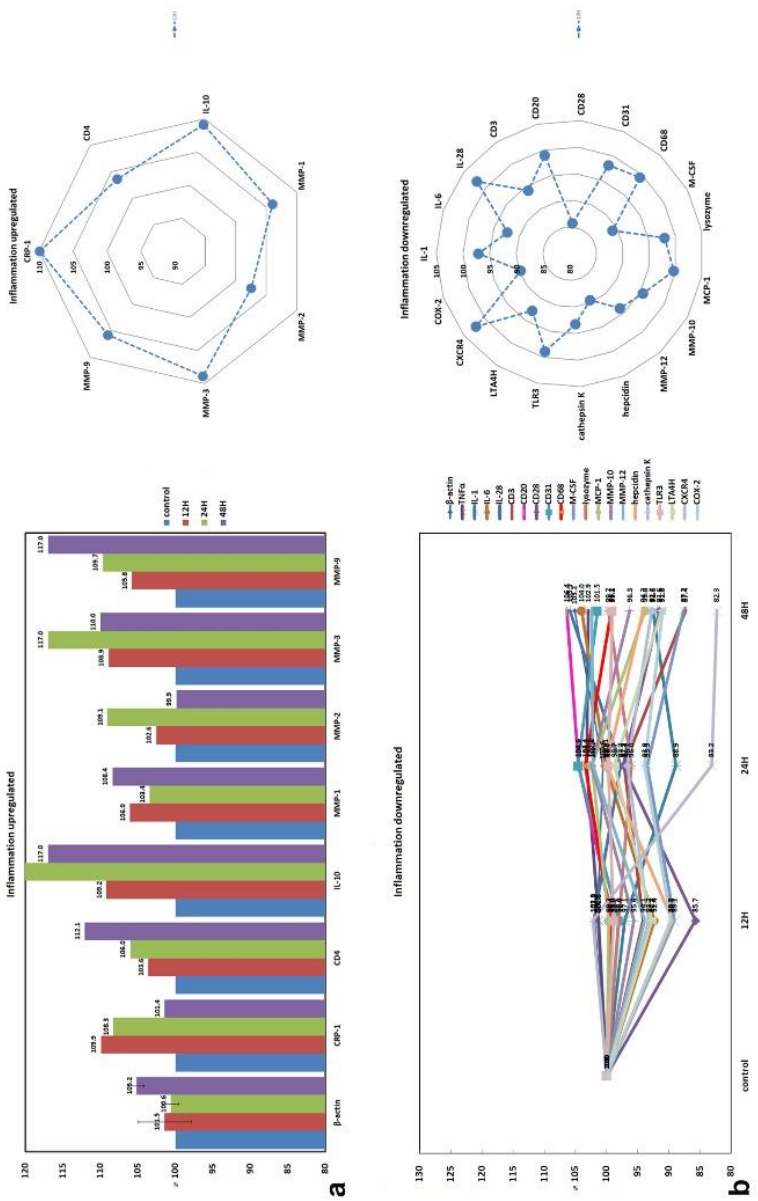

Figure 4.5. (a) Expression of p53 mediated apoptosis-related proteins after PTX treatment in macrophage, (b) Expression of FAS-mediated apoptosis-related proteins after PTX treatment in macrophage, (left) changes in protein expression over time, (right) protein expression patterns in the sample treated with PTX for 12 hours.

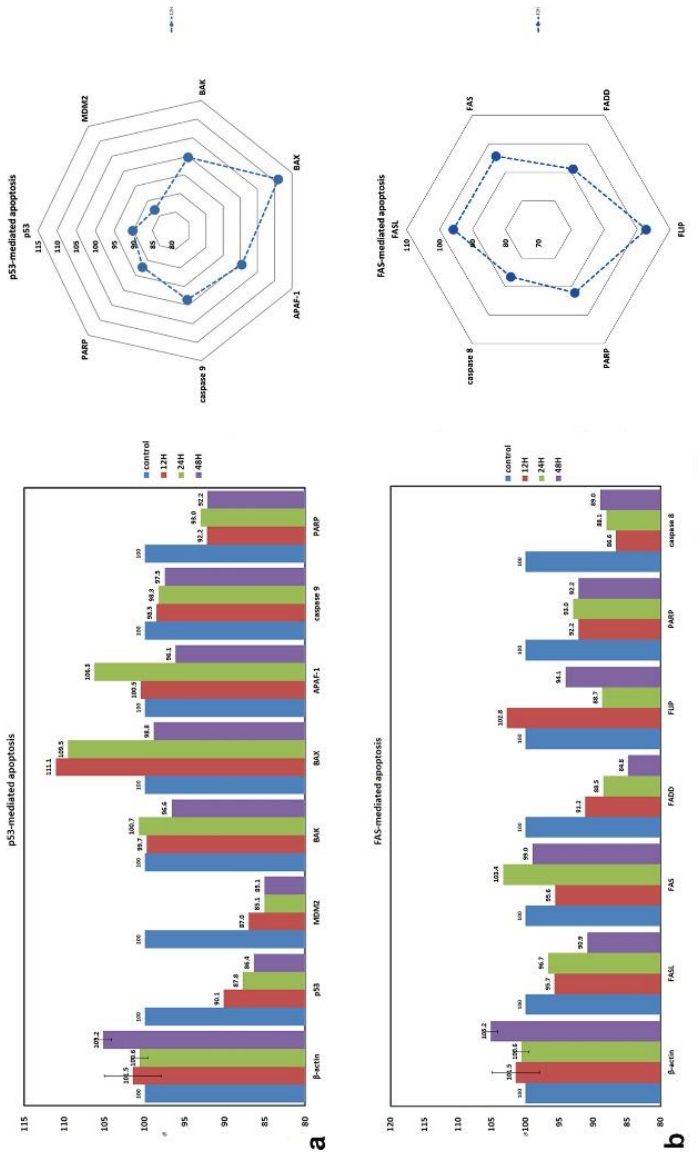

Figure 4.6. (a) Expression of cellular protection and survival-related proteins after PTX treatment in macrophage, (b) Expression of antioxidant-related proteins after PTX treatment in macrophage, (c) Expression of angiogenesis-related proteins in after PTX treatment in macrophage, (left) changes in protein expression over time, (right) protein expression patterns in the sample treated with PTX for 12 hours.

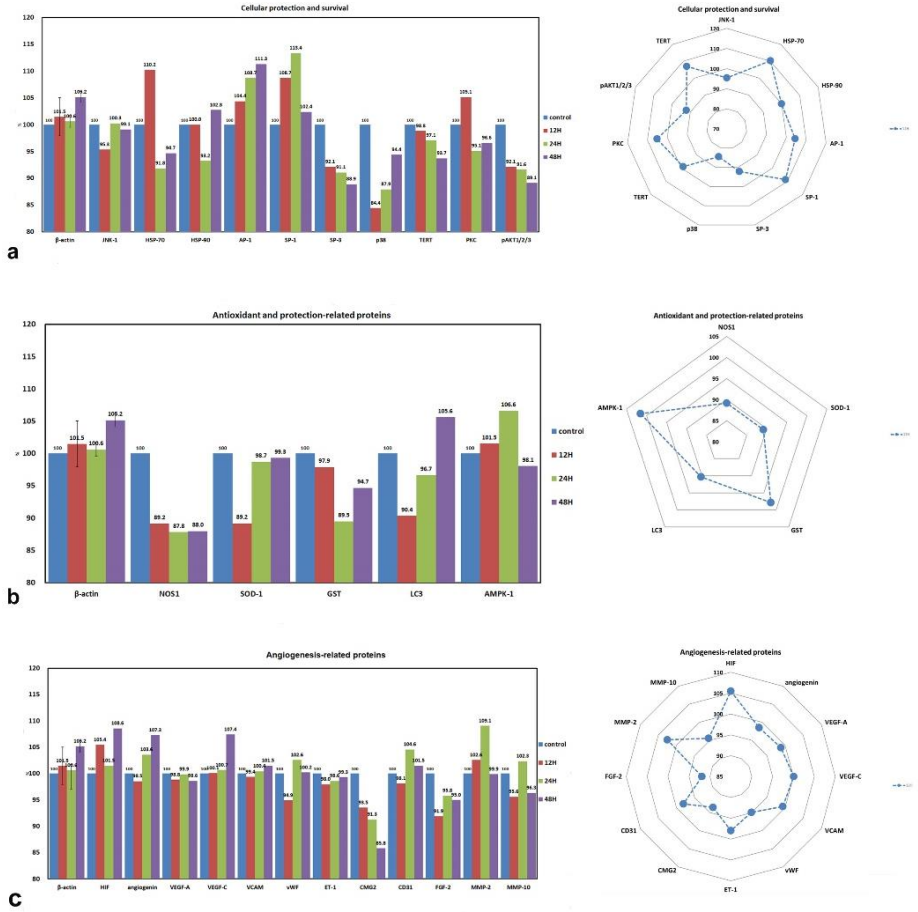

Figure 4.7. (a) Expression of oncogenic proteins after PTX treatment in macrophage, (b) Expression of osteogenesis-related proteins after PTX treatment in macrophage, (left) changes in protein expression over time, (right) protein expression patterns in the sample treated with PTX for 12 hours.

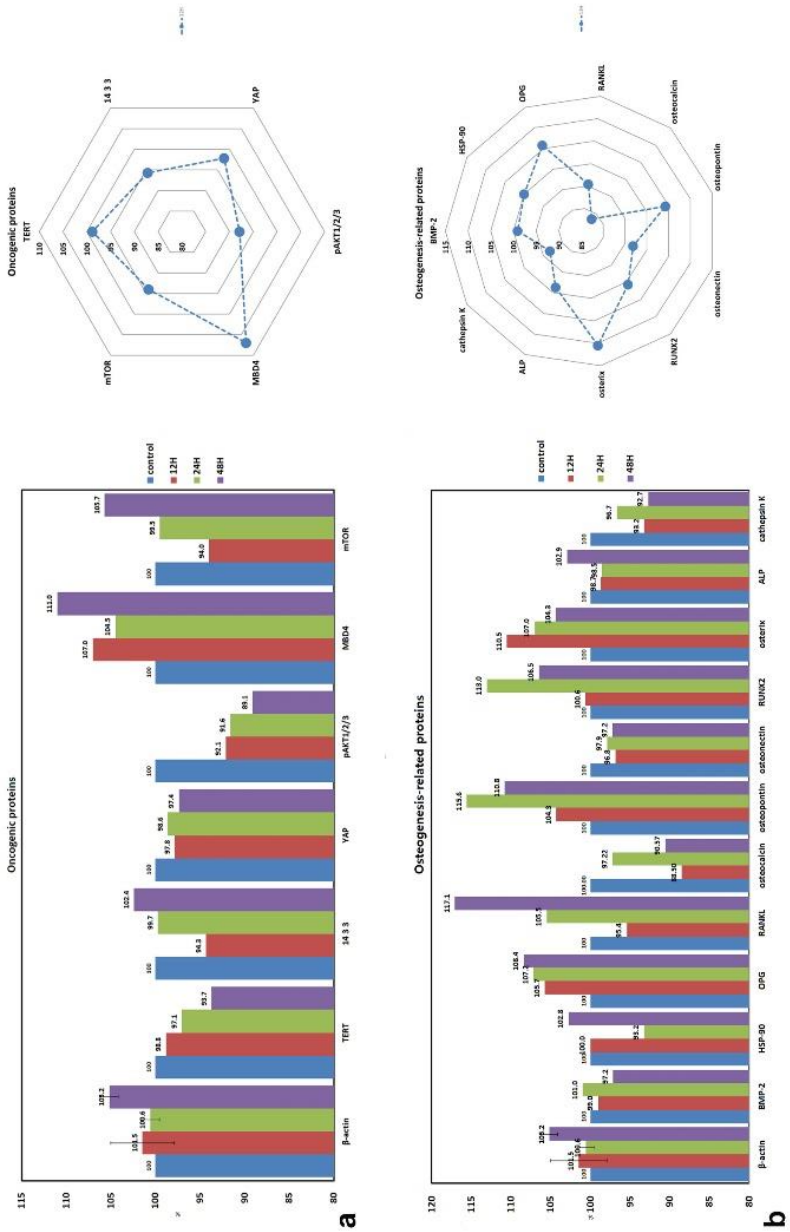

Figure 4.8. Global protein expression diagrams showing the effects of PTX on RAW 264.7 cells after 12-hour treatment. Up-regulating (red dots) and down-regulating (blue dots) proteins were displayed in this diagram. PTX down-regulated the proliferation-, apoptosis-, inflammation-, oncogenic-related proteins and up-regulated the osteogenesis-related proteins.

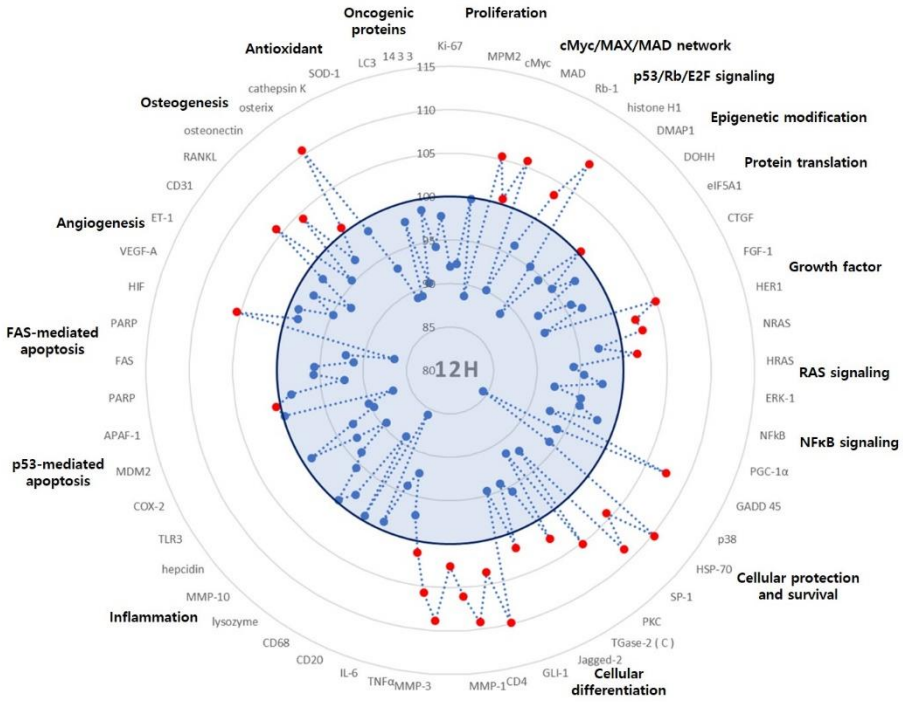

Figure 4.9. Progression of hair loss in the clinical photo, (a) Control group, (b) Two weeks after irradiation, (c) Two weeks after irradiation (contralateral side).

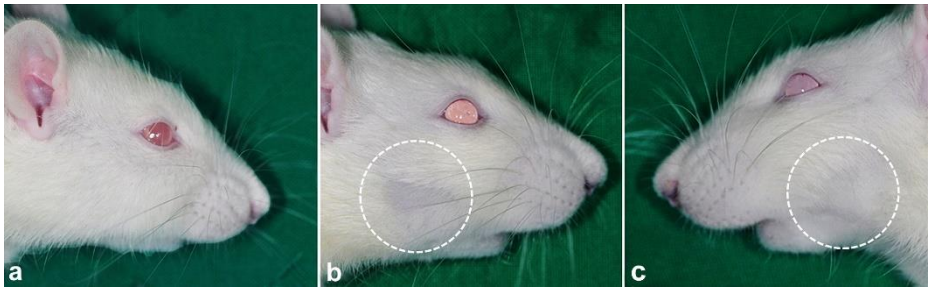

Figure 4.10. Differences in bone mineral densities (BMD), bone volume/tissue volume (BV/TV), and trabecular spaces (Tb.Sp.) between radiation doses and period.

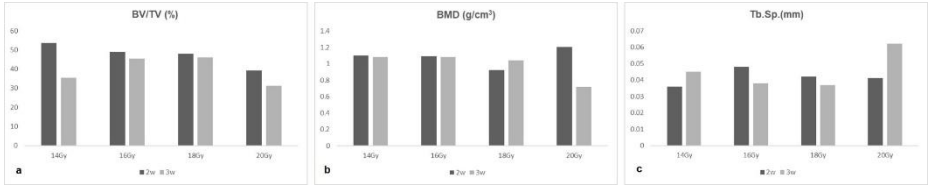

Figure 4.11. Histological findings with 16 Gy irradiation showing resorption line (a1; arrow), microabscess (a2, a3; arrow), and dead bone (c1, c2, e1, e2; arrow), with empty osteocyte lacunae (b, d, e1; arrowhead) in the defect site. a1 arrow: resorption line, a2 arrow, a3: abscess border line and abscess area; b arrowhead: empty osteocyte lacunae; c1, c2 arrow: dead bone borderline; d, e1 arrowhead: empty osteocyte lacunae; e1, e2 arrow: dead bone borderline (a1: original magnification, × 100; a2: original magnification, × 200, a3, b: original magnification, × 400; c1, c2: original magnification, × 200 and polarized view in c2, d, e1, e2: original magnification, × 1,000 and polarized view in e2)

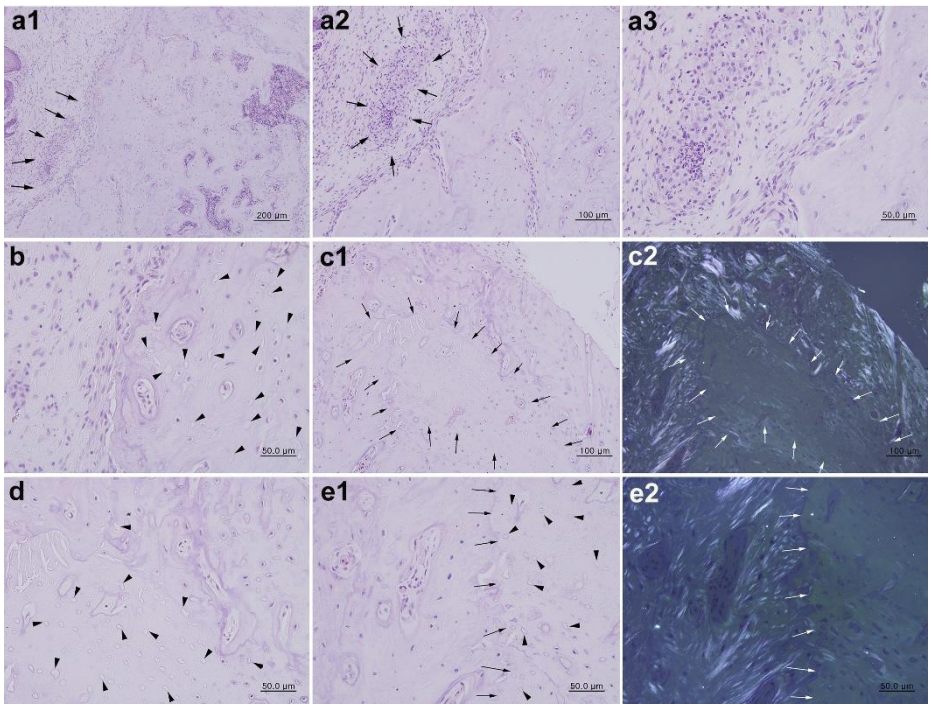

Figure 4.12. Histological findings with 18 Gy irradiation showing more dead bone than that seen with 16 Gy dose and the presence of resorption with osteoclast cells. Abscess (a1, a2, a3; arrow), inflammatory infiltrate (b1; arrow), and empty osteocyte lacunae (b2, b3; arrow head) were observed. The close-up of the box in c1 is c2. There are numerous osteoclast cells observed in the radionecrotic lesion borderlines. a1, a2 arrow, a3: abscess and abscess borderline; b1 arrow: inflammatory cell; b2, b3 arrowhead: empty osteocyte lacunae; c1, c2 arrow: osteoclast cells; c3: internal osteoclast cells. a1, a2: resorption line; a3 arrow: inflammatory cell; b1, b2, b3 arrowhead: empty osteocyte lacunae; c1, c2, c3 arrow: osteoclast cells; c3 arrowhead: dead bone borderline. (a1: original magnification, × 100; a2: original magnification, × 400, a3: original magnification, × 1,000, b1: original magnification, × 200, b2, b3: original magnification, × 400; c1: original magnification, × 200; c2, c3: original magnification, × 1,000)

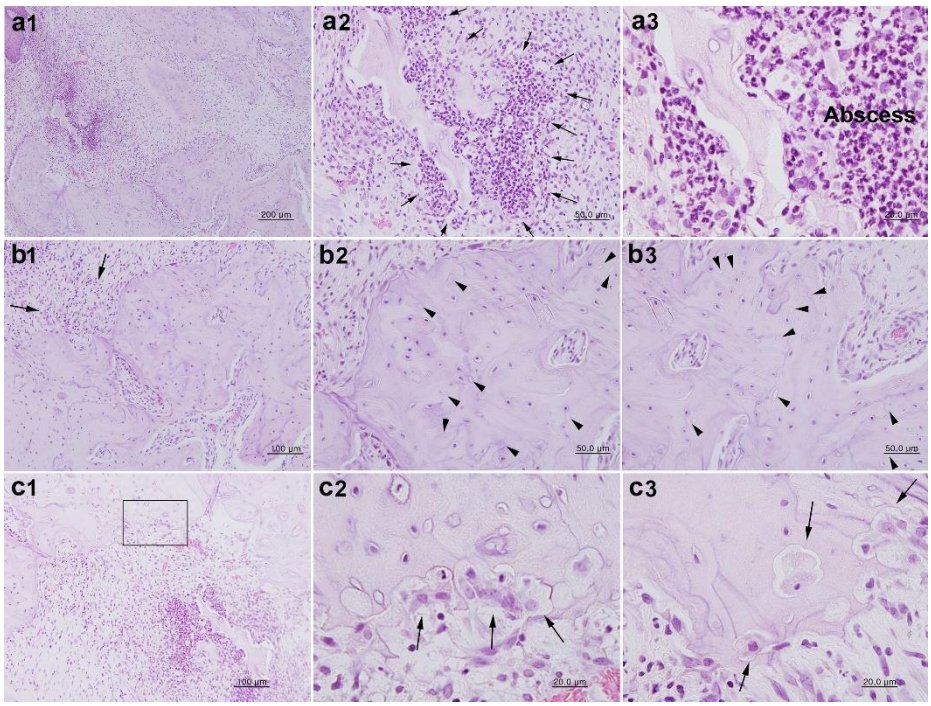

Figure 4.13. Histological findings with 20 Gy irradiation. The histological features with 20 Gy irradiation showed the presence of resorption line (a1, a2) with osteoclast cells (c1, c2, c3; arrow), inflammatory infiltrate (a3) and empty osteocyte lacunae (b1, b2, b3; arrow head). a1, a2: resorption line; a3 arrow: inflammatory cell; b1, b2, b3 arrow head: empty osteocyte lacunae; c1, c2, c3 arrow: osteoclast cells; c3 arrow head: dead bone border line (a1: original magnification, ×100; a2: original magnification, ×200, a3, b1, b2, b3, c1: original magnification, ×400; c2, c3: original magnification, ×1000)

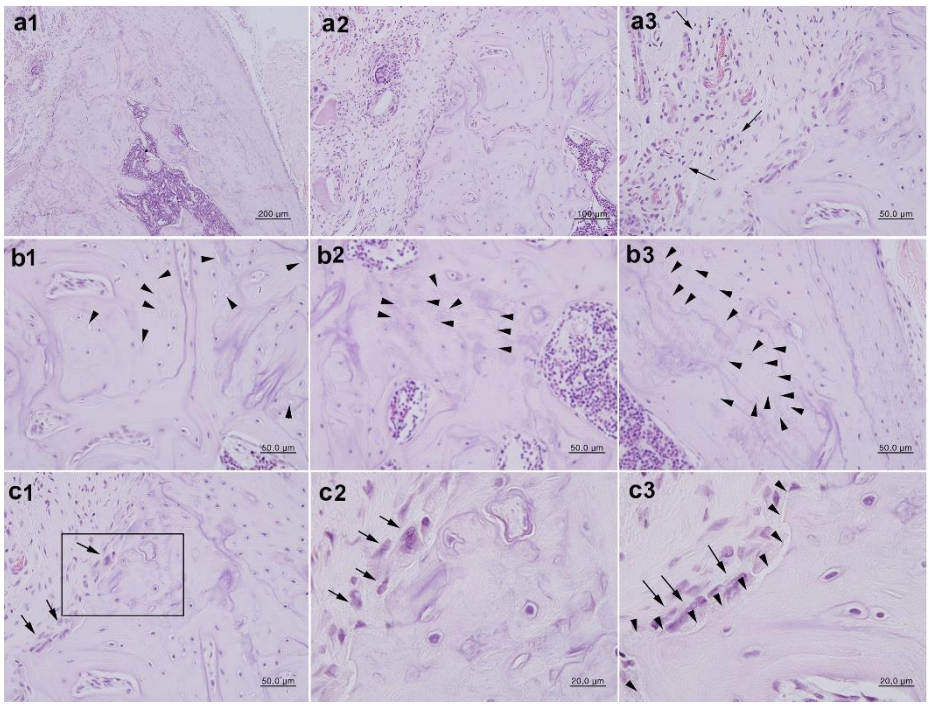

Figure 4.14. Weight changes of the experimental animals

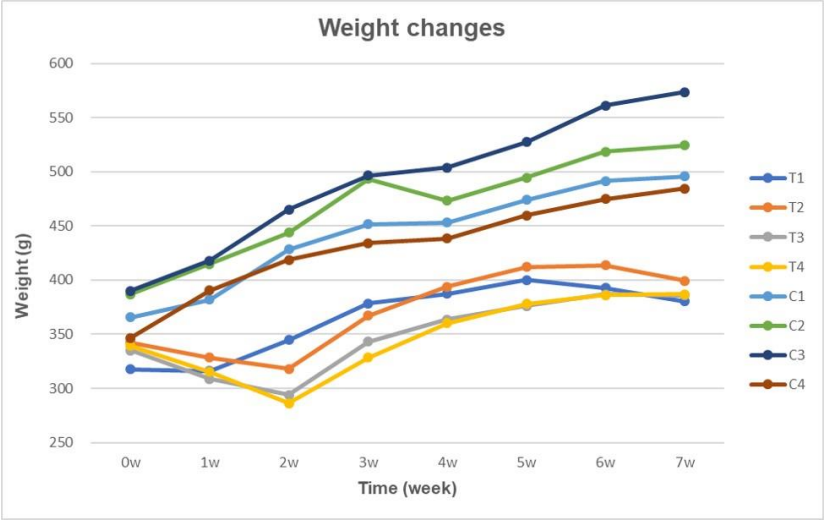

Figure 4.15. Comparisons between experimental groups in blood analysis including (a) WBC, (b) neutrophil, (c) lymphocyte, and (d) monocyte counts, (e) neutrophil to lymphocyte ratio (NLR), and (f) hemoglobin (Hb), *: $p < 0.05$, T1; group treated with pentoxifylline, T2; group treated with tocopherol, T3; group treated with pentoxifylline and tocopherol, T4; group treated with normal saline.

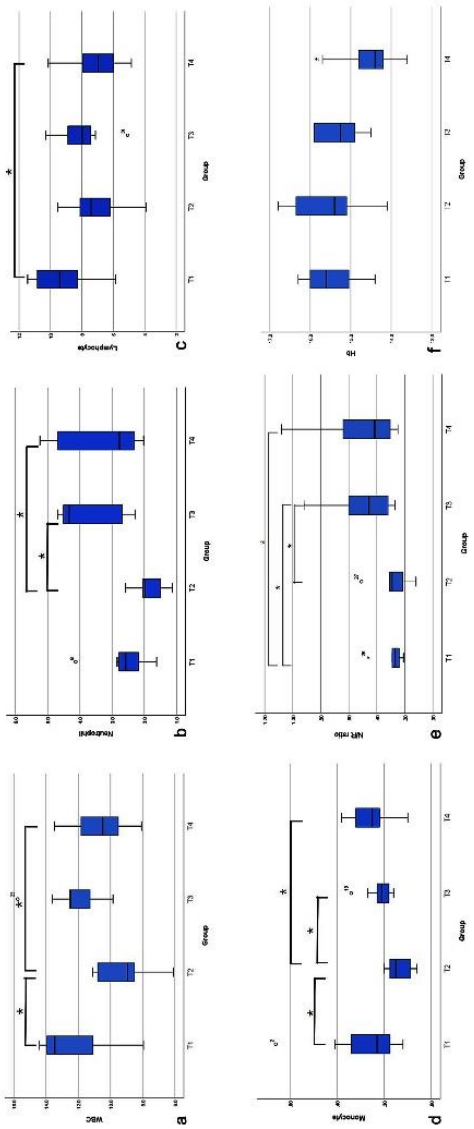

Figure 4.16. Reconstructed 3D images of an irradiated mandible (a,b,c,d) and comparisons of CT parameters between test groups (d,e,f,g) in the whole defect as a ROI (a) T1, PTX administration group; (b) T2, tocopherol administration group; (c) T3, PTX and tocopherol combination group; (d) control group; (e) bone volume/tissue volume (BV/TV); (f) trabecular number (Tb.N.); (g) trabecular spaces (Tb.sp.); (h) bone mineral density (BMD). *: $p < 0.05$

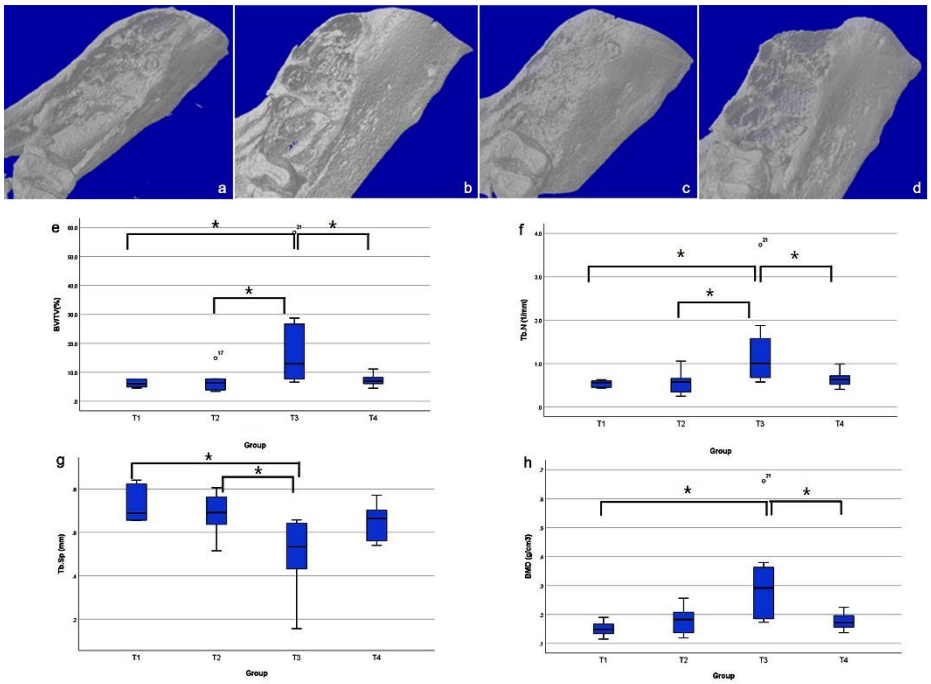

Figure 4.17. Reconstructed 3D images of an irradiated mandible (a,b,c,d) and comparisons of CT parameters between test groups (d,e,f,g) in the same ROI (a) T1, PTX administration group; (b) T2, tocopherol administration group; (c) T3, PTX and tocopherol combination group; (d) control group; (e) bone volume/tissue volume (BV/TV); (f) trabecular number (Tb.N.); (g) trabecular spaces (Tb.sp.); (h) bone mineral density (BMD). *: $p < 0.05$

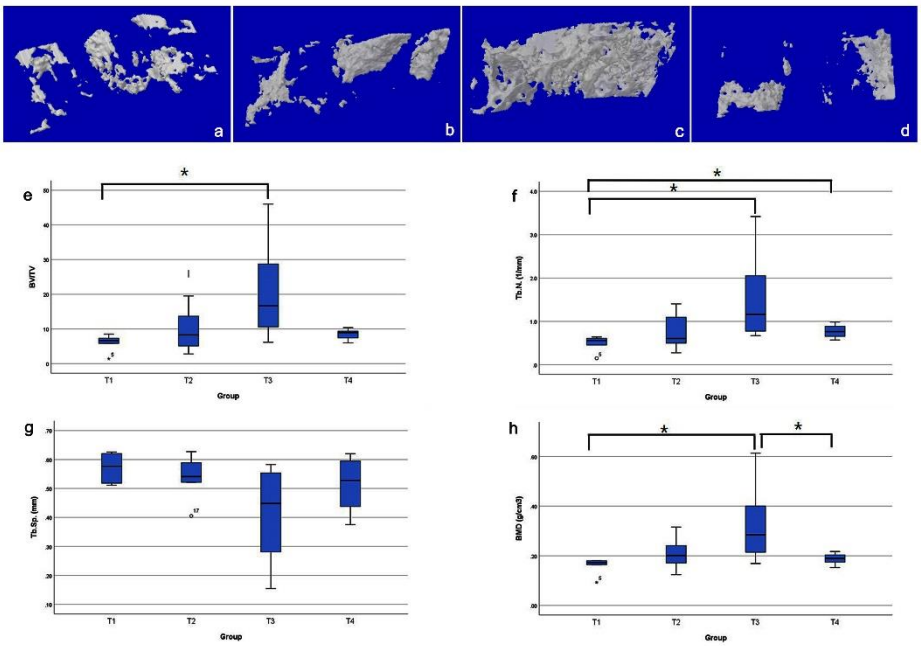

Figure 4.18. Histologic findings in the control group without radiation effect. (a) PTX administration group, a1; H&E staining with original magnification, x40, a2; MT staining with original magnification, x40, a3; H&E staining with original magnification, x200, a4: H&E staining with original magnification, x400, (b) tocopherol administration group, b1;H&E staining with original magnification, x40, b2; MT staining with original magnification, x40, b3; H&E staining with original magnification, x200, b4: H&E staining with original magnification, x400, (c) PTX and tocopherol administration group, c1; H&E staining with original magnification, x40, c2; MT staining with original magnification, x40, c3; H&E staining with original magnification, x200, c4: H&E staining with original magnification, x400, (d) normal saline administration group, d1; H&E staining with original magnification, x40, d2; MT staining with original magnification, x40, d3; H&E staining with original magnification, x200, d4: H&E staining with original magnification, x400.

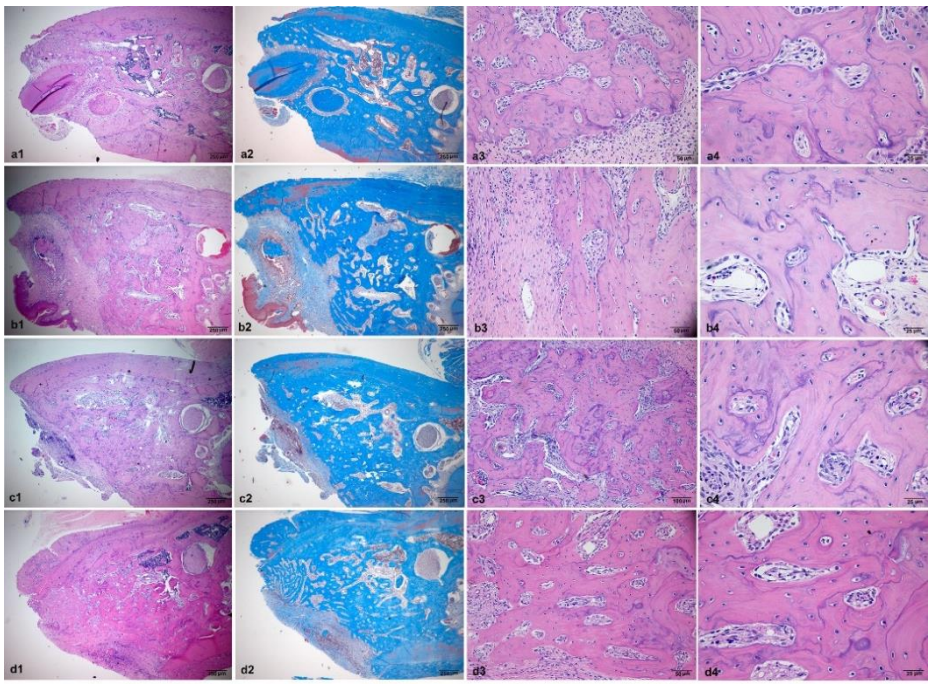

Figure 4.19. Histologic findings in the irradiation group, (a) PTX administration group, a1: H&E staining with original magnification, x40; a2: MT staining with original magnification, x40, arrow: newly formed bone; a3: H&E staining with original magnification, x100, arrow: newly capillary formation; a4: H&E staining with original magnification, x400, arrow head: empty lacunae; (b) tocopherol administration group, b1: H&E staining with original magnification, x40, arrow: newly formed bone; b2: MT staining with original magnification, x40, arrow: newly formed bone; b3: H&E staining with original magnification, x100, arrow: newly formed bone; b4: H&E staining with original magnification, x400, arrow head: empty lacunae; (c) PTX and tocopherol administration group, c1: H&E staining with original magnification, x40, arrow: newly formed bone; c2: MT staining with original magnification, x40, arrow: newly formed bone; c3: H&E staining with original magnification, x100; c4: H&E staining with original magnification, x400, arrow head: empty lacunae; (d) normal saline administration group, d1: H&E staining with original magnification, x40, arrow: newly formed bone; d2: MT staining with original magnification, x40, arrow: newly formed bone; d3; H&E staining with original magnification, x100; arrow: newly formed bone, large arrow: granulomatous lesion; d4: H&E staining with original magnification, x400, arrow head: empty lacunae.

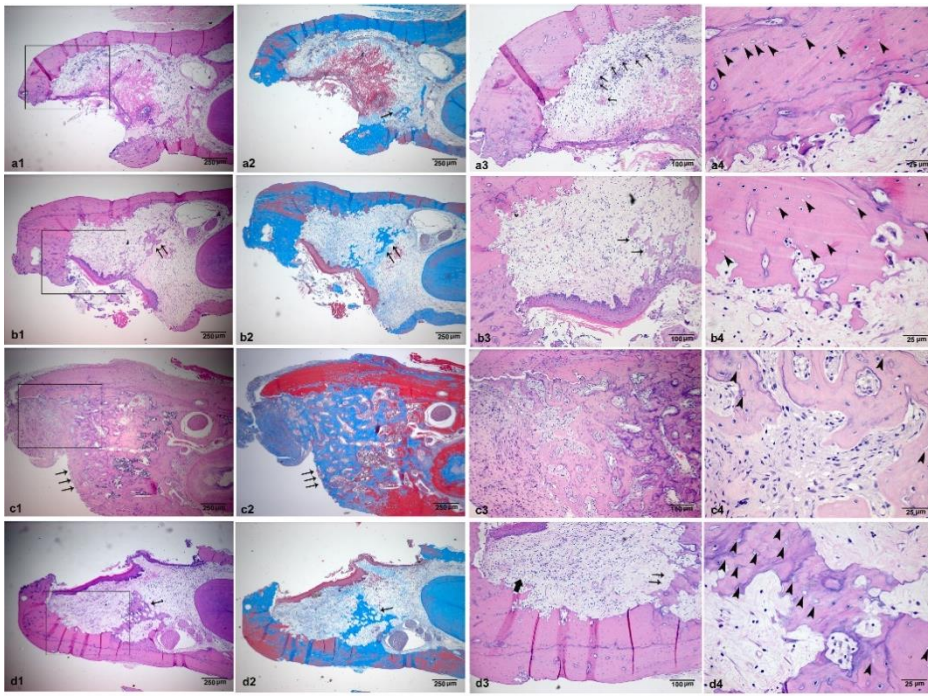

Figure 4.20. Comparisons of the ratio of empty lacunae between the experimental group. *: $p < 0.05$.

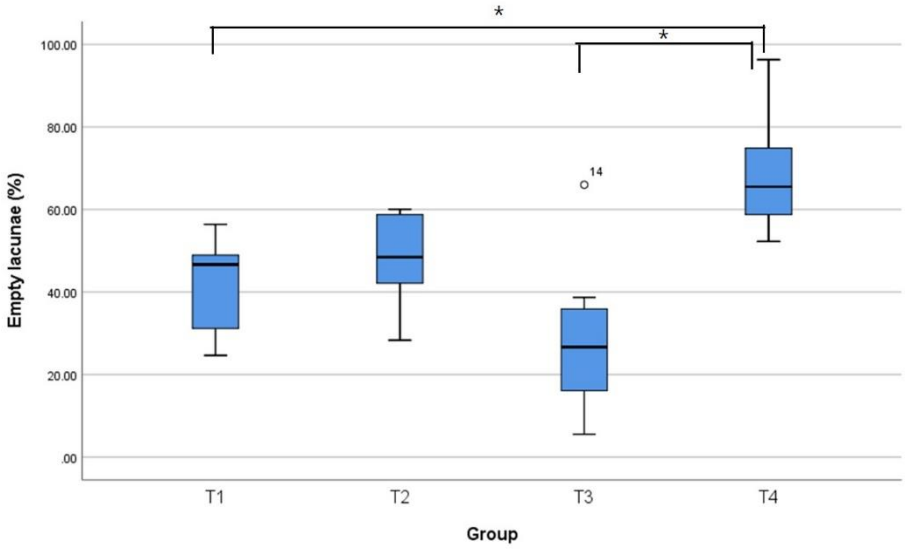

Figure 4.21. Comparison of expression of TNF-α, red arrowhead: TNF-α positive cell, (a) PTX administration group, a1: original magnification, x40; a2: H&E staining with original magnification, x400: a3: MT staining with original magnification, x400; a4: original magnification, x400; (b) tocopherol administration group, b1: original magnification, x40; b2: H&E staining with original magnification, x400; b3: MT staining with original magnification, x400; b4: original magnification, x400; (c) PTX and tocopherol administration group, c1: original magnification, x40; c2: H&E staining with original magnification, x400; c3: MT staining with original magnification, x400; c4: original magnification, x400; (d) normal saline administration group, d1: original magnification, x40; d2: H&E staining with original magnification, x400; d3: MT staining with original magnification, x400; d4: original magnification, x400.

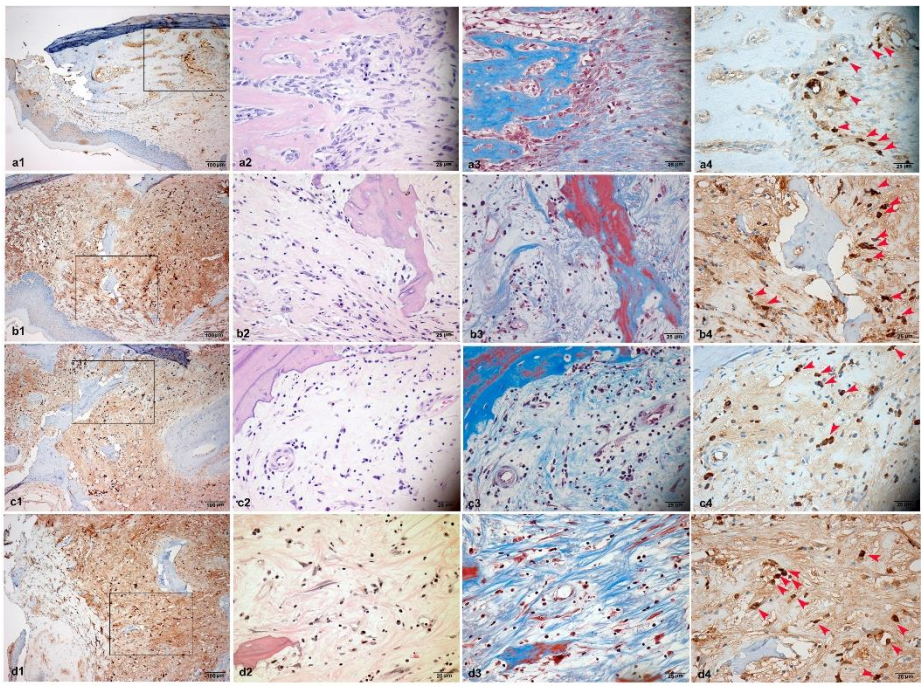

Figure 4.22. Comparison of immunohistochemistry in the irradiated group. Original magnification, x200.

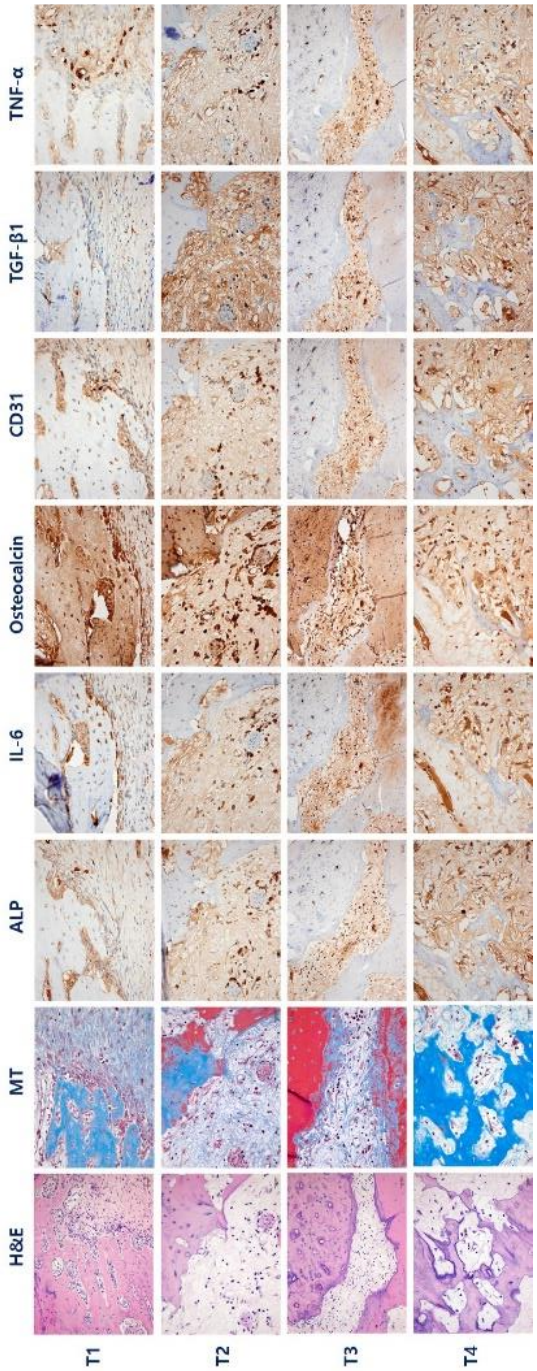

Figure 4.23. Relative mRNA expression in the alveolar bone healing after tooth extraction. PECAM1; platelet endothelial cell adhesion molecule1, TNF-α; tumor necrosis factor-α, RANKL/OPG; receptor activator of nuclear factor kappa-B ligand/osteoprotegerin ratio, OCN; osteocalcin, OSX; osterix.

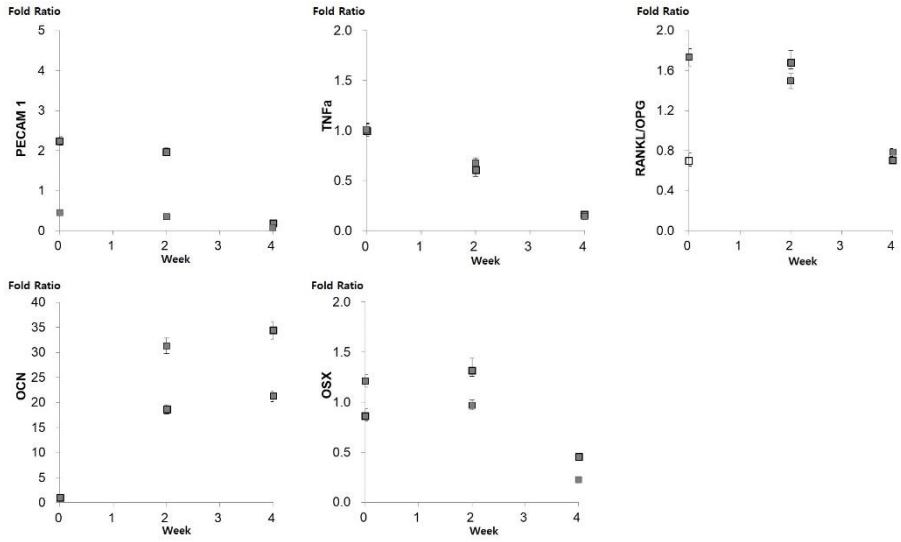

Figure 4.24. Comparisons of relative mRNA expressions between treatment groups, PECAM1, platelet endothelial cell adhesion molecule1; VEGF-A, vascular endothelial growth factor-A; TNF-α, tumor necrosis factor-α; RANKL, receptor activator of nuclear factor kappa-B ligand; OCN, osteocalcin; PTX, pentoxifylline treated group; TP, tocopherol treated group; PTX/TP, pentoxifylline and tocopherol combination group; control, normal saline treated group.

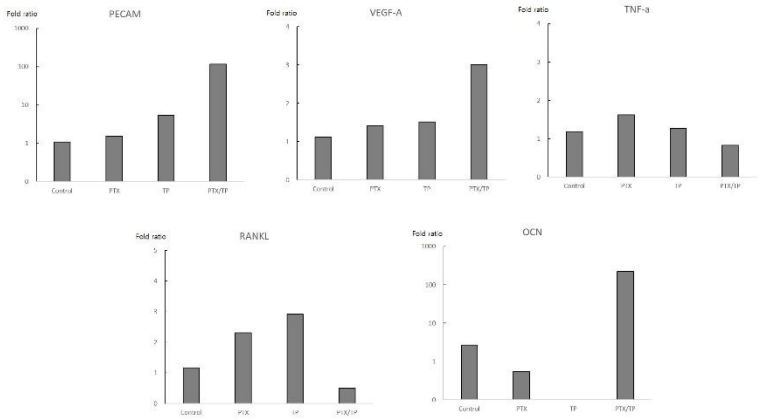

Figure 6.1. Summary of differential protein expressions in RAW 264.7 cells treated with PTX focused on the proliferation, inflammation, angiogenesis, and osteogenesis, CDK4: cyclin dependent kinase 4, PLK4: polo-like kinase 4, MPM2: mitotic protein monoclonal 2, Rb-1: retinoblastoma-1, PARP: poly-ADP ribose polymerase, FASL: FAS ligand, FADD: FAS-associated via death domain, OPG: osteoprotegerin, RANKL: receptor activator of nuclear factor kappa-B ligand, RUNX2: RUNT-related transcription factor 2, IL-10: interleukin-1, MMP-1: matrix metalloproteinase-1, MMP-2: matrix metalloproteinase-2, MMP-3: matrix metalloproteinase-3, MMP-9: matrix metalloproteinase-9, IL-1: interleukin-1, IL-6: interleukin-10, CD28: cluster of differentiation, M-CSF: macrophage-colony stimulating factor, LTA4H: leukotriene-A4 hydrolase, CXCR4: C-X-C chemokine receptor 4, COX-2: cyclooxygenase-2, ↑: upregulation, ↓: downregulation

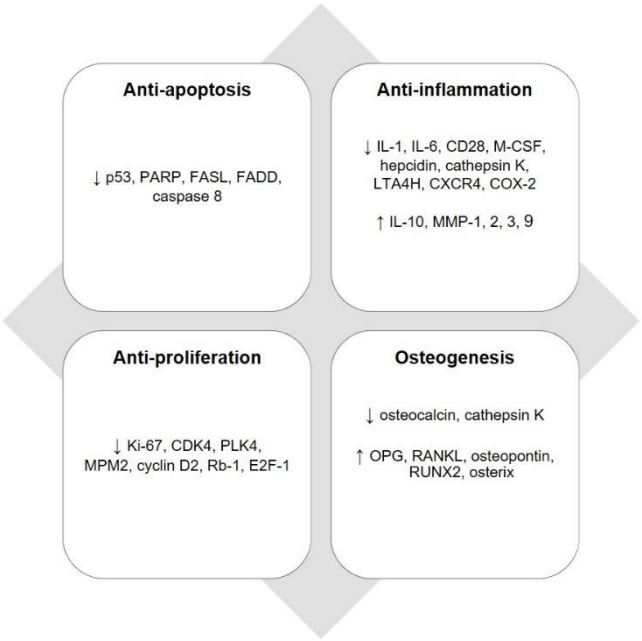

Supplement

Supplement 1. Antibodies used in immunoprecipitation-high performance liquid chromatography analyses.

Signaling proteins	No.	Antibodies
Cellular proliferation	10	Ki-67*, PCNA*, CDK4*, PLK4*, MPM2*, p14*, p16*, p21*, p27*, cyclin D2*
cMyc/MAX/MAD signaling	3	cMyc*, MAX*, MAD*
p53/Rb/E2F signaling	4 (2)	p53, Rb-1#, E2F-1*, MDM2*, CDK4*, p21*
Epigenetic modification	7	DMAP1, histone H1*, KDM4D $, HDAC-10$, MBD4, DNMT1
Protein translation signaling	3	DOHH*, DHS*, elF5A-1$
RAS signaling	7 (3)	NRAS$, KRAS$, HRAS, Rab, JNK-1*, ERK-1*, MEKK, (pAKT1/2/3*, mTOR, PKC)
Growth factor signaling	9	TGF-β1#, IGF-1*, HER1*, HER2*, ERβ,* FGF-1, FGF-2, Met, CTGF

NFkB signaling	9(3)	NFkB*, IKK*, NFATS*, PGC-1α, GADD45*, GADD153*, mTOR@, p38*, MDR*, (ERK-1*, pAKT1/2/3*, TNFα*)
Immunity signaling	7	CD3*, CD4, CD20*, CD28*, CD31*, CD68*, cathepsin K*
Inflammatory signaling	20	TNFα@, IL-1*, IL-6*,IL-10*,IL-28*, COX-2*, lysozyme*, M-CSF*, MMP-1*, MMP-2*, MMP-3*, MMP-9*, MMP-10*, MMP-12, MCP-1, LTA4H, CXCR4, TLR3, hepcidin, CRP-1*
Cell protection	8 (3)	HSP-70*, HSP-90*, AP-1*, SP-1*, SP-3*, p38*, PKC*, pAKT1/2/3*, (p38, JNK-1, TERT)
Cellular differentiation	6(4)	PLC-β2, TGase-2, HXKII*, Jagged-2, Notch-1, GLI-1, (PKC, AP-1, SP-1, SP-3)
Antioxidant-related proteins	5	SOD-1*, GST*, LC3*, AMPK*, NOS-1,
p53-mediated cellular apoptosis	6 (1)	p53*, MDM2*, BAX*, BAK*, APAF-1*, caspase 9*, (PARP)
FAS-mediated cellular apoptosis	6	FASL*, FAS*, FADD*, FLIP*, caspase 8*, PARP*

Oncogenic proteins	3(3)	14-3-3[*], TERT[*], YAP, (pAKT1/2/3, MBD4, mTOR)
Angiogenesis-related proteins	8(4)	HIF[&], VEGF-A[*], VEGF-C[*], VCAM, angiogenin[*], CMG2[$], vWF[$], ET-1[*](CD31, MMP-2, MMP-10, FGF-2)
Osteogenesis-related proteins	9 (2)	RANKL, OPG[*], osteonectin, osteopontin, osteocalcin, RUNX2, ALP[*], osterix[*], BMP-2[*] (cathepsin K, HSP-90)
Control cytoplasmic proteins	1	β-actin[*]
Total	131(25)	

[*] Santa Cruz Biotechnology, USA; [#] DAKO, Denmark; [$] Neomarkers, CA, USA; [@] ZYMED, CA, USA; [&]Abcam, Cambridge, UK

Abbreviations: ALP: alkaline phosphatase, AMPK: AMP-activated protein kinase, APAF-1: apoptotic protease-activating factor 1, AP-1: activating protein-1, BAK: BCL2 antagonist/killer, BAX: BCL2 associated X, BMP-2: bone morphogenic protein-2, CASP 3: caspase 3, CASP 8: caspase 8, CASP 9: caspase 9, c-CASP 9: cleaved-caspase 9, CD3: cluster of differentiation 3, CDK4: cyclin dependent kinase 4, CEA: carcinoembryonic antigen, cMyc: V-myc myelocytomatosis viral oncogene homolog, CMG2: capillary morphogenesis protein 2, COX-2: cyclooxygenase-2, CRP-1: C-reactive protein-1, CXCR4: C-X-C chemokine receptor type 4, DMAP1: DNA methytransferase 1 associated protein, DNMT1: DNA (cytosine-5)-methyltransferase1, DOHH: deoxyhypusine hydroxylase, DHS: deoxyhypusine synthase, E2F-1: transcription factor, elF5A-1: eukaryotic translation initiation factor 5A-1, ERβ: estrogen

receptor beta, ERK: extracellular signal-regulated protein kinases, ET-1: endothelin-1, FAS: CD95/Apo1, FASL: FAS ligand, FADD: FAS associated via death domain, FGF-1: fibroblast growth factor-1, FLIP: FLICE-like inhibitory protein, vascular endothelial growth factor receptor 3 precursor (FLT4), GADD45: growth arrest and DNA-damage-inducible 45, GST: glutathione S-transferase, HDAC-10: histone deacetylase-10, HIF: hypoxia inducible factor-1α, Histone H1, HER1: human epidermal growth factor receptor 1, hTERT: human telomerase reverse transcriptase, HSP-70: heat shock protein-70, HSP-90: heat shock protein-90, HXKII: hexokinase II, IKK: ikappaB kinase, IGF-1, IL-1: interleukin-1, JNK-1: Jun N-terminal protein kinase, KDM4D: Lysine-Specific Demethylase 4D, KRAS: V-Ki-ras2 Kirsten rat sarcoma viral oncogene homolog, LC3: microtubule-associated protein 1A/1B-light chain 3, LTA4H: Leukotriene A4 hydrolase, MAX: myc-associated factor X, MBD4: methyl-CpG-binding domain protein 4, MCP-1: monocyte chemoattractant protein 1, M-CSF: macrophage colony-stimulating factor, MDM2: mouse double minute 2 homolog, MEKK: MAP kinase kinase kinase, MPM2: mitotic protein monoclonal 2, MDR: Monoclonal Anti-P-Glycoprotein, Met: tyrosine-protein kinase Met, MMP-1: matrix metalloprotease-1, MMP-2: matrix metalloproteinase-2, mTOR: mammalian target of rapamycin, NFATS: nuclear factor of activated T-cells, NFkB: nuclear factor kappa-light-chain-enhancer of activated B cells, NOS-1: NRAS: neuroblastoma RAS Viral Oncogene homolog, OPG: osteoprotegerin, OPN: osteopontin, OSX: osterix, pAKT: v-akt murine thymoma viral oncogene homolog, p-Akt1/2/3 phosphorylated (p-Akt, Thr 308), PARP: poly-ADP ribose polymerase, PCNA: proliferating cell nuclear antigen, PGC-1α: Peroxisome Proliferator-Activated Receptor-γ-Coactivator1α, PKC: protein kinase C, PLC-β2: 1-phosphoatidylinositol-4,5-bisphosphate phosphodiesterase beta-2, Rb-1: retinoblastoma-1, RANKL: receptor activator of nuclear factor kappa-B ligand, RUNX2: Runt-related transcription factor 2, SOD-1: superoxide dismutase-1, SP-1: specificity protein 1, SP-3: specificity protein 3, TGase-2: transglutaminase-2, TGF-β1: transforming growth factor-β1, TLR3: Toll like receptor 3, TNF-α: tumor necrosis factor-α, β-actin, 14-3-3, VEGF vascular endothelial growth factor, vWF: von Willebrand factor. The number of antibodies overlapped; ( ).

-국문 초록-

펜톡시필린의 대식세포에서 단백질 발현 양상과 백서 방사선골괴사증 모델에서 골 치유에 대한 효과

서 미 현

서울대학교 대학원 치의과학과 구강악안면외과학전공

(지도교수 김 성 민)

연구 배경 및 연구 목적

방사선 치료는 두경부 암의 치료에 있어, 오랫동안 확립되어 온 치료 방법이다. 악골의 방사선 골괴사증 (osteoradionecrosis, ORN)은 방사선 치료의 심각한 부작용 중의 하나이다. 최근에, 방사선 유발 섬유화 이론이 악골의 방사선 골괴사증에 적용됨에 따라, 펜톡시필린 (pentoxifylline, PTX)이 방사선 골괴사증의 치료 및 예방에 사용됨이 보고된 바 있다. 이 연구의 목적은, 마우스 대식 세포 계열인 RAW 264.7 세포에서 펜톡시필린의 효과를 면역침전 고성능 액체 크로마토그래피 (immunoprecipitation-high performance liquid chromatography, IP-HPLC)를 사용하여

분석하고, 방사선 골괴사증 백서 동물 모델에 펜톡시필린을 적용하여 그 효과에 대해서 알아보는 것이다.

연구 방법

1. PTX를 처리한 대식 세포의 단백질 발현 양상에 대한 연구

펜톡시필린의 세포에 대한 효과를 알아보기 위하여, RAW 264.7 세포에 펜톡시필린을 10 μg/ml을 12시간, 24시간, 48시간 처리한 후 단백질 발현 양상을 IP-HPLC를 통하여 분석하였다.

2. PTX의 백서 방사선 골괴사증 모델에서 골 치유에 미치는 효과

총 48마리의 Spraque-Dawley 백서를 실험에 사용하였다. 40 마리는 하악의 좌측에 35 Gy로 방사선을 조사하였다. 8마리는 방사선 조사를 하지 않고 대조군으로 설정하였다. 백서는 실험군에 따라 펜톡시필린 (T1, C1), 토코페롤 (T2, C2), 펜톡시필린과 토코페롤의 병용 (T3, C3), 생리 식염수 (T4, C4)를 방사선 조사 다음날부터 투여하였다. 방사선 조사 3주 후, 하악 좌측의 대구치 2개를 발거하였고, 약제는 실험 종료일까지 투여하였다. 백서는 발치 4주 후 (방사선 조사 7주 후) 희생하였다. 매주 체중, 피부 변화 등의 임상적 평가를 시행하였으며, 방사선 조사 전, 3주 후, 7주 후에 일반 혈액 검사 (complete blood cell count, CBC)와 C 반응성 단백 (C-reactive protein, CRP)을 측정하였다. 희생 후 micro CT, 헤마톡실린-에오신 (hematoxylin and eosin, H&E)과 Masson's trichrome 염색을 사용한 조직학적 분석, 면역화학

분석, quantitative reverse transcription PCR (RT-qPCR) 분석을 시행하였다.

연구 결과

1. PTX를 처리한 대식 세포의 단백질 발현 양상에 대한 연구

펜톡시필린은 면역 관련, 골형성과 연관된 단백질은 증가시켰으며, 반면에 세포 증식, 염증, 세포 자멸사 연관된 단백질은 감소시켰다. 펜톡시필린은 RAW 264.7 세포에서 세포 증식, 면역, 항염증, 세포 자멸사, 골형성과 관련된 단백질의 전반적인 발현에 영향을 미치는 것으로 볼 수 있다.

2. PTX의 백서 방사선 골괴사증 모델에서 골 치유에 미치는 효과

체중, 피부 탈모, 희생 시 골 노출 정도는 실험군에 따른 차이는 관찰되지 않았다(p >0.05). 혈액 검사에서는 CRP는 방사선 조사에 따른 차이가 관찰되지 않았고, 방사선 조사 7주 후의 CBC에서실험군에 따른 차이가 있었다. 백혈구 수, 중성구 수, 림프구 수, 단핵구 후, 중성구 림프구 비율 (neutrophil to lymphocyte ratio, NLR)은 약제 복용에 따라, 통계학적으로 유의미한 차이가 있었다. 헤모글로빈 수치는 대조군인 T4에서 다른 실험군에 비하여 낮은 수치를 보였다 (p <0.05). Micro CT 분석에서 bone volume/tissue volume, 골 소주 수, 골 소주 공간, 골밀도 (bone mineral density, BMD)에서 실험군에 따른 차이가 관찰되었다 (p <0.05). 조직학적 분석에서 펜톡시필린과 토코페롤을

병용한 실험군 (T3)에서 골의 재형성이 가장 증가하여 나타났으며, 살아 있는 골세포 (osteocyte)의 수가 다른 실험군에 비하여 유의미하게 높게 나타났다 (p <0.05). 면역 화학 분석에서는 TNF-α의 발현이 펜톡시필린과 토코페롤을 함께 사용한 실험군 (T3)에서 대조군 (T4)과 토코페롤 복용군 (T2)에 비하여 낮게 나타났다. RT-qPCR에서는 PECAM, VEGF-A, osteocalcin의 mRNA 발현이 펜톡시필린과 토코페롤을 함께 복용시킨 그룹 (T3)에서 증가하였다.

결론

세포 실험에서 펜톡시필린은 항염증 효과, 세포 자멸사 억제 효과, 골형성 촉진 효과를 나타내었다. 동물 실험에서 펜톡시필린은 토코페롤과 함께 사용될 때 방사선 조사를 받은 발치와 결손부에서 골 형성을 촉진시키는 효과가 있었다. 따라서, 펜톡시필린은 토코페롤과 함께 사용할 때, 악골 방사선골괴사증의 치료에 유용하게 사용될 수 있으며, 추가적인 전향적 임상 연구가 진행되어야 할 것으로 사료된다.

.....

주요어: 방사선 골괴사증, 펜톡시필린, 면역 침전 고성능 액체 크로마토그래피

학번: 2011-31179